

AD-A034 027

ARMY MISSILE RESEARCH DEVELOPMENT AND ENGINEERING LAB--ETC F/8 9/4  
ANALYSIS AND DESIGN OF DIGITAL CONTROL SYSTEMS. PART II. PRINCI--ETC(U)  
OCT 76 R E YATES, Y T TSAY, C F CHEN

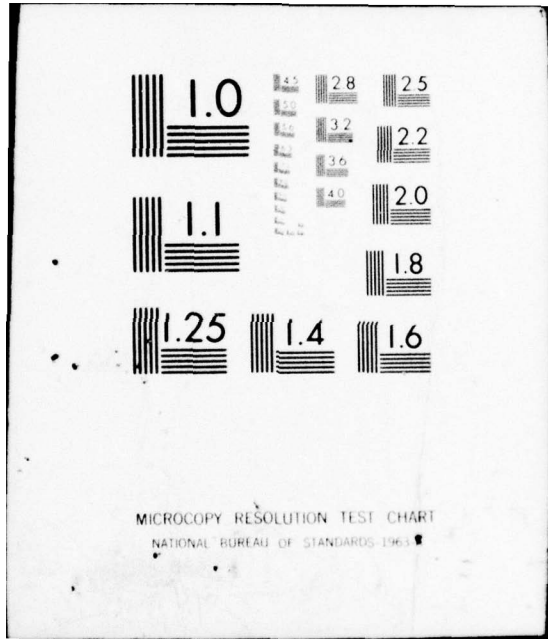
UNCLASSIFIED

R6-77-3

NL

1 OF 3  
AD  
A034027





MICROCOPY RESOLUTION TEST CHART  
NATIONAL BUREAU OF STANDARDS-1963-A

ADA034027



TECHNICAL REPORT RG-77-3

12

**ANALYSIS AND DESIGN OF DIGITAL CONTROL SYSTEMS  
PART II - PRINCIPLES AND TECHNIQUES**

R. E. Yates, Y. T. Tsay, and C. F. Chen  
Guidance and Control Directorate  
US Army Missile Research, Development  
and Engineering Laboratory  
US Army Missile Command  
Redstone Arsenal, Alabama 35809

29 October 1976

DDC  
FORM 1021  
JAN 6 1977  
REGULATORY  
C

APPROVED FOR PUBLIC RELEASE; DISTRIBUTION UNLIMITED.



**U.S. ARMY MISSILE COMMAND**

*Redstone Arsenal, Alabama 35809*

**DISPOSITION INSTRUCTIONS**

**DESTROY THIS REPORT WHEN IT IS NO LONGER NEEDED. DO NOT  
RETURN IT TO THE ORIGINATOR.**

**DISCLAIMER**

**THE FINDINGS IN THIS REPORT ARE NOT TO BE CONSTRUED AS AN  
OFFICIAL DEPARTMENT OF THE ARMY POSITION UNLESS SO DESIGNATED  
BY OTHER AUTHORIZED DOCUMENTS.**

**TRADE NAMES**

**USE OF TRADE NAMES OR MANUFACTURERS IN THIS REPORT DOES  
NOT CONSTITUTE AN OFFICIAL ENDORSEMENT OR APPROVAL OF  
THE USE OF SUCH COMMERCIAL HARDWARE OR SOFTWARE.**

UNCLASSIFIED

SECURITY CLASSIFICATION OF THIS PAGE (When Data Entered)

REPORT DOCUMENTATION PAGE		READ INSTRUCTIONS BEFORE COMPLETING FORM
1. REPORT NUMBER ⑨ Technical Report, RG-77-3	2. GOVT ACCESSION NO.	3. RECIPIENT'S CATALOG NUMBER ⑭ RG-77-3
4. TITLE (and Subtitle) ⑥ ANALYSIS AND DESIGN OF DIGITAL CONTROL SYSTEMS. PART II. PRINCIPLES AND TECHNIQUES.	5. TYPE OF REPORT & PERIOD COVERED	
7. AUTHOR(s) ⑩ R.E. Yates, Y.T. Tsay and C.F. Chen	6. PERFORMING ORG. REPORT NUMBER	
9. PERFORMING ORGANIZATION NAME AND ADDRESS Commander, US Army Missile Command Attn: DRSMI-RG Redstone Arsenal, Alabama 35809	8. CONTRACT OR GRANT NUMBER(s) ⑫ 212 p.	
11. CONTROLLING OFFICE NAME AND ADDRESS Commander, US Army Missile Command Attn: DRSMI-RPR Redstone Arsenal, Alabama 35809	10. PROGRAM ELEMENT, PROJECT, TASK AREA & WORK UNIT NUMBERS ⑮ (DA) 1M362303A214 AMC Management Structure Code No. 632303.11.21403	
14. MONITORING AGENCY NAME & ADDRESS (if different from Controlling Office)	12. REPORT DATE ⑪ 29 Oct 1976	
	13. NUMBER OF PAGES 203	
	15. SECURITY CLASS. (of this report) UNCLASSIFIED	
	15a. DECLASSIFICATION/DOWNGRADING SCHEDULE	
16. DISTRIBUTION STATEMENT (of this Report) Approved for public release: Distribution unlimited.		
17. DISTRIBUTION STATEMENT (of the abstract entered in Block 20, if different from Report)		
18. SUPPLEMENTARY NOTES		
19. KEY WORDS (Continue on reverse side if necessary and identify by block number) Discrete-Time Feedback Control Systems Nonrecursive Filters and Compensators Gibbs' Phenomenon Truncated Fourier Series		
20. ABSTRACT (Continue on reverse side if necessary and identify by block number) In discrete-time feedback control system design, the use of nonrecursive compensators has advantages. However, the existing methods for designing such compensators are difficult.  This report (1) lays the foundation necessary to understand window effects by investigating the basic properties of Gibbs' phenomena in both the time and		

UNCLASSIFIED

SECURITY CLASSIFICATION OF THIS PAGE(When Data Entered)

19. Key Words (Con't)

Windowing Techniques  
Trapezoidal Window  
Return Difference Stability Criteria

*could*

20. Abstract (Con't)

the frequency domains, (2) analyzes the stability and performance aspects of discrete-time feedback systems via the Fast Fourier Transform (FFT) algorithm, and (3) formulates a computer-oriented nonrecursive compensator design procedure.

Handwritten form with a checkmark and classification 'A'.

INTS	Info Section	<input type="checkbox"/>
1-0	Ref Section	<input type="checkbox"/>
CLASSIFICATION		
BY		
DISTRIBUTION/AVAILABILITY STATEMENTS		
Class	Ext	Use of Special
A		

UNCLASSIFIED

SECURITY CLASSIFICATION OF THIS PAGE(When Data Entered)

## CONTENTS

	<u>Page</u>
I INTRODUCTION	1
II THE GIBBS' PHENOMENON	4
2.0 Introduction	4
2.1 Truncated Fourier Series	4
2.2 Gibbs' Phenomenon in The Time Domain	8
2.3 Gibbs' Phenomenon in The Frequency Domain - Real Periodic Functions	12
2.4 Gibbs' Phenomenon in The Frequency Domain - Complex Periodic Functions	17
2.5 Demonstration of Gibbs' Phenomena with HP Fourier Analyzer	20
2.6 Remarks	24
III THE GENERALIZED GIBBS' PHENOMENON AND WINDOWS	28
3.0 Introduction	28
3.1 Windowing in the Time Domain	28
3.2 The Generalized Gibbs Phenomenon in The Time Domain	30
3.3 The Trapezoidal Window in The Time Domain	35
3.4 Windowing and The Generalized Gibbs' Phenomenon in The Frequency Domain	42
3.5 The Trapezoidal Window in the Frequency Domain	49
3.6 Remarks	56
IV DESIGN OF NONRECURSIVE FILTERS USING THE WINDOW METHOD	63
4.0 Introduction	63
4.1 Low-Pass Filter Design	64
4.2 Frequency Transformation I: Low-Pass to Low-Pass Transformation	72
4.3 Frequency Transformation II: Low-Pass to High-Pass Transformation	76
4.4 Design of A Nonrecursive Band-Pass Filter	84
4.5 Design of A Nonrecursive Band-Rejection Filter	91
4.6 Remarks	96

## CONTENTS (Continued)

	<u>Page</u>
<b>V ANALYSIS OF DISCRETE-TIME CONTROL SYSTEMS</b>	<b>98</b>
5.0 Introduction	98
5.1 Frequency Response of Discrete-Time Control Systems	98
5.2 Transient Response of Discrete-Time Control Systems	102
5.2.1 Unit Impulse Response	104
5.2.2 Unit Step Response	106
5.3 Block Diagram Operations for Discrete-Time Control Systems	113
5.4 Closed Loop Transfer Function	117
5.5 Stability of Discrete-Time Control System	121
5.6 Remarks	131
<b>VI DESIGN OF DISCRETE-TIME CONTROL SYSTEMS</b>	<b>133</b>
6.0 Introduction	133
6.1 Frequency Domain Approach for Discrete-Time Control System Design	133
6.2 Specifying The Frequency Response of Closed Loop Systems	136
6.3 The Steady State Error at The Sampling Instants	141
6.4 Calculation of The Frequency Response of Required Compensator	148
6.5 General Procedure for Designing Nonrecursive Compensators by The Window Method	151
6.6 Type "0" System Design	153
6.7 Type "1" System Design	162
6.8 Remarks	181
<b>VII CONCLUSIONS</b>	<b>183</b>

CONTENTS (Concluded)

	<u>Page</u>
<b>APPENDIX A - EVALUATION OF FOURIER COEFFICIENTS AND COMPUTATION OF THE FOURIER TRANSFORM VIA THE FFT ALGORITHM</b>	185
<b>A.0 Introduction</b>	185
<b>A.1 Evaluation of Fourier Coefficients</b>	185
<b>A.1.1 Fourier Analysis of Periodic Functions in The Time Domain</b>	185
<b>A.1.2 Fourier Analysis of Periodic Functions in The Frequency Domain</b>	187
<b>A.2 Computation of The Fourier Transform</b>	188
<b>APPENDIX B - THE INVERSE FOURIER TRANSFORM OF A PERIODIC FUNCTION IN THE FREQUENCY DOMAIN</b>	190
<b>APPENDIX C - KEYBOARD PROGRAMS</b>	191
<b>BIBLIOGRAPHY</b>	201

## ILLUSTRATIONS

<u>Figure</u>		<u>Page</u>
2-1	The Time Function $g_n(t)$ .....	11
2-2	Overshoots of Magnitude and Phase Relative to Those of Real and Imaginary Parts .....	20
2-3	Partial Sums of The Square Wave .....	22
2-4	Maximum Overshoot for Different Partial Sums of Example 1 .....	23
2-5	The Periodic Function $F(\omega)$ and The Magnitude and Phase of Various Partial Sums of $F(\omega)$ .....	25
2-6	The Jump-Up Spike of Different Partial Sums of Example 2 .....	27
3-1	Time and Step Responses of Trapezoidal Window with $b = 0$ .....	37
3-2	Time and Step Responses of Trapezoidal Window with $b = 0.1$ .....	37
3-3	Time and Step Responses of Trapezoidal Window with $b = 0.2$ .....	38
3-4	Time and Step Responses of Trapezoidal Window with $b = 0.3$ .....	38
3-5	Time and Step Responses of Trapezoidal Window with $b = 0.4$ .....	39
3-6	Time and Step Responses of Trapezoidal Window with $b = 0.5$ .....	39
3-7	Overshoot Ratio of The Trapezoidal Window with Respect to The Parameter $b$ .....	40
3-8	Width of The Main Lobe of The Trapezoidal Window with Respect to The Parameter $b$ .....	40
3-9	Effect of Trapezoidal Windowing on the 15th Partial Sum of The Truncated Fourier Series .....	43
3-10	Effect of Trapezoidal Windowing on The 255th Partial Sum of The Truncated Fourier Series .....	44

ILLUSTRATIONS (Continued)

<u>Figure</u>		<u>Page</u>
3-11	Trapezoidal Window in The Frequency Domain, b = 0 .....	51
3-12	Trapezoidal Window in The Frequency Domain, b = 0.1 .....	51
3-13	Trapezoidal Window in The Frequency Domain, b = 0.2 .....	52
3-14	Trapezoidal Window in The Frequency Domain, b = 0.3 .....	52
3-15	Trapezoidal Window in The Frequency Domain, b = 0.4 .....	53
3-16	Trapezoidal Window in The Frequency Domain, b = 0.5 .....	53
3-17	Trapezoidal Window in The Frequency Domain, b = 0.418 .....	54
3-18	The Peak of The Highest Side Lobe .....	54
3-19	The Hanning Window .....	58
3-20	The Hamming Window .....	58
3-21	The 16th Partial Sum of The Truncated Fourier Series .....	59
3-22	The 16h Partial Sum with The Trapezoidal Window, b = 11/32 .....	59
3-23	The 16th Partial Sum with The Trapezoidal Window, b = 13/32 .....	60
3-24	The 16th Partial Sum with the Trapezoidal Window, b = 1/2 .....	60
3-25	The 256th Partial Sum of The Truncated Fourier Series .....	61
3-26	The 256th Partial Sum with the Trapezoidal Window, b = 171/512 .....	61
3-27	The 256th Partial Sum with The Trapezoidal Window, b = 212/512 .....	62

ILLUSTRATIONS (Continued)

<u>Figure</u>		<u>Page</u>
3-28	The 256th Partial Sum with The Trapezoidal Window, $b = 1/2$ .....	62
4-1	Frequency Response of Low-Pass Filter with The Rectangular Window .....	68
4-2	Frequency Response of Low-Pass Filter with The Trapezoidal Window, $b = 0.375$ .....	69
4-3	Frequency Response of Low-Pass Filter with The Trapezoidal Window, $b = 0.438$ .....	70
4-4	Frequency Response of Low-Pass Filter with The Hanning Window .....	71
4-5	Frequency Responses of Two Low-Pass Filters .....	74
4-6	Frequency Response of Low-Pass Filter with Rectangu- lar Window .....	78
4-7	Frequency Response of Low-Pass Filter with Trapezoi- dal Window, $b = 0.438$ .....	79
4-8	Frequency Response of Low-Pass Filter with Hanning Window .....	80
4-9	The Amplitude Response of An Ideal High-Pass Fil- ter .....	81
4-10	Frequency Response of High-Pass Filter with Trapezoi- dal Window, $b = 0.438$ .....	85
4-11	Construction of The Band-Pass Filter from A Low-Pass and A High-Pass Filter .....	87
4-12	Frequency Response of Band-Pass Filter with Trape- zoidal Window, $b = 0.438$ .....	92
4-13	Construction of The Band-Rejection Filter from A Low- Pass and A High-Pass Filter .....	93
4-14	Frequency Response of Band-Pass Filter with Trapezoi- dal Window, $b = 0.438$ .....	97
5-1	Frequency Response of $G(z)$ , $N = 64$ .....	103

ILLUSTRATIONS (Continued)

<u>Figure</u>		<u>Page</u>
5-2	Frequency Response of $G(z)$ , $N = 1024$ .....	103
5-3	The Unit Impulse Response of Example 2 .....	105
5-4	The Unit Step Response of Example 3 .....	108
5-5	The Unit Impulse Response of Example 4 .....	110
5-6	The Unit Step Response of Example 4 .....	110
5-7	Frequency Response of Example 5 .....	112
5-8	The Unit Impulse Response of Example 5 .....	112
5-9	The Unit Step Response of Example 5 .....	112
5-10	Block Diagram Simplification .....	118
5-11	Missile Launching System with Digital Controller ...	119
5-12	The Nyquist Contour for Discrete-Time Control Systems .....	125
5-13	Phase Plot of The Return Difference of Example 6 ...	129
5-14	Phase Plot of The Return Difference of Example 7 ...	129
5-15	Phase Plot of The Return Difference of Example 8 ...	132
5-16	Phase Plot of The Return Difference of Example 9 ...	132
6-1	Basic Configuration of Direct Digital Control System .....	134
6-2	Simplified Block Diagram in The Z-Domain .....	134
6-3(a)	Required Unit Step Response .....	139
6-3(b)	Unit Impulse Response .....	139
6-3(c)	Frequency Response (Rectangular) .....	140
6-3(d)	Frequency Response (Polar) .....	140
6-4	The Unit Feedback System .....	141

ILLUSTRATIONS (Concluded)

<u>Figure</u>		<u>Page</u>
6-4(a)	Frequency Response of $D(z)$ .....	149
6-4(b)	Error Response of The Unit Ramp Input .....	149
6-5	A Type "0" Dynamic System .....	154
6-6	Open Loop Frequency Response .....	154
6-7	Design Models of Example 1 .....	155
6-8	Performance of The System Compensated with $D_1(z)$ ....	157
6-9	Performance of The System Compensated with $D_2(z)$ ....	159
6-10	Performance of The System Compensated with $D_3(z)$ ....	160
6-11	A Type "0" System with Digital Controller .....	161
6-12	Open Loop Frequency Response .....	161
6-13	Design Models for Example 2 .....	163
6-14	Performance of The System Compensated with $D_1(z)$ ....	165
6-15	Performance of The System Compensated with $D_2(z)$ ....	166
6-16	Performance of The System Compensated with $D_3(z)$ ....	167
6-17	Infrared Tracking System .....	168
6-18	Design Models of Example 3 .....	171
6-19	Performance of The System Compensated with $D_1(z)$ ....	173
6-20	Performance of The System Compensated with $D_2(z)$ ....	174
6-21	Performance of The System Compensated with $D_3(z)$ ....	175
6-22	Gun Drive Control System .....	177
6-23	Frequency Response of The Required Compensator .....	177
6-24	Performance of The System Compensated with $D_1(z)$ ....	179
6-25	Performance of The System Compensated with $D_2(z)$ ....	180
6-26	Performance of The System Compensated with $D_3(z)$ ....	182

TABLES

<u>Table</u>		<u>Page</u>
3-1	Overshoot Ratio $g_c$ and the Width of Main Lobe $T_w^*$ .....	41
3-2	Peak of The Highest Side Lobe .....	55
4-1	Coefficients of Low-Pass Filter Designed by Four Different Windows .....	72
4-2	Coefficients of Low-Pass Filter with A Cutoff Fre- quency of 200 Hz .....	77
6-1	Required Unit Step and Impulse Responses .....	138
6-2	Compensators for Example 1 .....	156
6-3	Compensators for Example 2 .....	164
6-4	Compensators for Example 3 .....	172
6-5	Compensators for Example 4 .....	178

## CHAPTER I INTRODUCTION

Most design techniques for sampled-data or discrete-time feedback systems are borrowed from those developed for continuous systems. For example, the w-transform or fictitious frequency method is simply an extension of the Bode approach<sup>[1]</sup>. Therefore, the compensators synthesized by this method are, in general, the recursive type.

It is known that the recursive type compensators have the following inherent shortcomings<sup>[2,3]</sup>: (1) stability problems; (2) phase characteristic problems; and (3) arbitrary approximation problems. In recent years, nonrecursive type compensators have become increasingly more important. By using the nonrecursive type filters, one can not only eliminate the disadvantages of the recursive filters but also have a simpler design procedure and an easier realization process.

This report is concerned with nonrecursive compensator design from fundamental principles to detailed design procedures. The method developed in this report utilizes the Fast Fourier Transform (FFT) algorithm and is minicomputer oriented. The simple FFT algorithm<sup>[4]</sup> and the availability of powerful minicomputers<sup>[5]</sup> enable us to deal with complicated systems quite easily and accurately.

There are three types<sup>[2,6,7]</sup> of design methods available for the design of nonrecursive compensators:

- (1) Window method - The main contributors are Kaiser<sup>[8]</sup>, Helms<sup>[9,10]</sup>, Gold and Rader<sup>[11]</sup>, Rabiner<sup>[6,7]</sup>, etc.
- (2) Analytic method - This method entails the use of analytic techniques analogous to the Butterworth and Chebyshev methods for designing recursive filters. Hermann<sup>[12]</sup> was mainly responsible for this development.

- (3) Successive approximation method - This efficient method is computer oriented. Parks and McClellan<sup>[13]</sup>, Rabiner, Gold and McGonegal<sup>[6]</sup> have developed a useful catalogue of compensator designs.

Since the window method is simple, straightforward and yet affords plenty of room for improvement, we will concentrate on the window method. The principle of the window method is based on reducing Gibbs' phenomenon<sup>[15,17]</sup> and improving the convergence of the truncated Fourier series in the frequency domain along with the interpretation of the generalized Gibbs' phenomenon. However, in the literature, Gibbs' phenomena in the time domain are considered in detail while only mentioned in the frequency domain. For clarity, we will derive the time domain Gibbs' phenomenon as a basis and develop its frequency domain counterpart in a systematic manner in Chapter II. The latter is necessary to understand the phenomena in both domains before firmly establishing window techniques.

In Chapter III, the generalized Gibbs' phenomenon is established. The trapezoidal window function is used as a basic unit from which a family of new windows are developed, and a thorough understanding and insight of windowing is obtained. Windows<sup>[18,19,20]</sup>, such as Hamming, Hanning, Kaiser etc., are empirical in nature; however, a theoretical base will be presented in this report. In the frequency domain, the main lobe and side lobes of a windowed Fourier series can be clearly seen. Both the derivation and interpretation presented here are believed to be new.

Chapter IV concentrates on nonrecursive filters<sup>[2,3,20]</sup>. The most common complaint in the nonrecursive filter field is that frequency transformations cannot be applied; since through their application the resulting filter becomes recursive. We will develop a complete, novel technique from which high-pass, band-pass, and band-rejection filters can be designed via frequency transformations.

Chapter V concentrates on the analysis of discrete-time control systems. The procedure for using the FFT and minicomputers to obtain the frequency response and transient response of discrete-time control systems will be presented logically utilizing block diagram transformations. Particular emphasis will be placed on the theorems associated with the z-transform. For example, the Ragazzini-Zadeh identity<sup>[21]</sup> is repeatedly applied to simplify and manipulate the system block diagram. A unique and novel stability study based completely on return difference is utilized to derive a stability criterion which is believed to be new.

The design of discrete-time control systems is investigated in Chapter VI. Specifications of example closed loop control systems are presented and analyzed using the FFT, Fourier Analyzer, and window techniques. The design procedure through which realizable nonrecursive compensators are designed utilizing the window method is presented in detail. Two frequently used examples of discrete-time control systems (type "0" and type "1") are discussed in detail. The resulting compensators are synthesized and their performance verified.

In summary, this report presents an FFT-oriented, minicomputer-aided, design procedure for nonrecursive compensator synthesis of discrete-time feedback systems. The method is simple, powerful, and more accurate than previously existing methods.

CHAPTER 11  
THE GIBBS' PHENOMENON

2.0 INTRODUCTION

It is well known<sup>[15]</sup> that for a periodic function with bounded variation, the Fourier series converges at every point, particularly at points of discontinuity. In 1899 Gibbs pointed out that convergence of the truncated Fourier series behaves in a quite different manner at points of discontinuity. Bôcher, in 1906, extended Gibbs' result and established a theorem commonly called the Gibbs' phenomenon.

In this report, the phenomenon originally discovered by Gibbs and Bôcher is referred to as the Gibbs' phenomenon in the time domain. However, the same phenomenon exists in the frequency domain and will be referred to as the Gibbs' phenomenon in the frequency domain. Gibbs' phenomenon is an important aspect associated with analysis and design of nonrecursive filters and compensators.

Let us start with analysis of the truncated Fourier series.

2.1 TRUNCATED FOURIER SERIES

Let  $f(t)$  be a real periodic function of time  $t$  with period  $T$  and bounded in  $(-\frac{T}{2}, \frac{T}{2})$ . The Fourier series expansion of  $f(t)$  is given by

$$f(t) = \sum_{k=-\infty}^{\infty} a_k e^{jk\omega_0 t} \quad (1)$$

where

$$a_k = \frac{1}{T} \int_{-\frac{T}{2}}^{\frac{T}{2}} f(\tau) e^{-jk\omega_0\tau} d\tau \quad (2)$$

and

$$\omega_0 = \frac{2\pi}{T} \quad (3)$$

For computing advantages and practical purposes, we often take only a finite number of terms of the Fourier series in Eq. (1). In other words, we calculate the partial sum instead of dealing with the entire infinite series. Consider the  $n$ th partial sum (which contains  $2n+1$  terms):

$$f_n(t) = \sum_{k=-n}^n a_k e^{jk\omega_0 t} \quad (4)$$

Substituting Eq. (2) into Eq. (4) yields

$$f_n(t) = \int_{-\frac{T}{2}}^{\frac{T}{2}} d_n(t-\tau) f(\tau) d\tau \quad (5)$$

where

$$d_n(t) = \frac{1}{T} \sum_{k=-n}^n e^{jk\omega_0 t} \quad (6)$$

Equation 6 is called the periodic Dirichlet kernel<sup>[17]</sup> or window function in the time domain. With some algebraic manipulations, it is easy to arrive at the following:

$$d_n(t) = \frac{\omega_0 \sin \left[ \left( n + \frac{1}{2} \right) \omega_0 t \right]}{2\pi \sin \left( \frac{\omega_0 t}{2} \right)} \quad (7)$$

According to Eq. (5), the partial sum of a Fourier series is given by the convolution of  $f(t)$  and  $d_n(t)$  over one period. The interpretation of Eq. (5) for the partial sum of Eq. (1) is straightforward; however it is not simple, since the window function [Eq. (7)] is complicated.

A second interpretation in terms of the Fourier Transform results if we let  $F(j\omega)$  be the Fourier Transform of  $f(t)$ , then

$$f(t) = \frac{1}{2\pi} \int_{-\infty}^{\infty} F(j\omega) e^{j\omega t} d\omega \quad (8)$$

From Eq. (1), we have

$$F(j\omega) = 2\pi \sum_{k=-\infty}^{\infty} a_k \delta(\omega - k\omega_0) \quad (9)$$

The  $n$ th partial sum of  $f(t)$  is given by Eq. (4), thus, the Fourier Transform of  $f_n(t)$  is

$$F_n(j\omega) = 2\pi \sum_{k=-n}^n a_k \delta(\omega - k\omega_0) \quad (10)$$

In general, we have

$$\begin{aligned} f_n(t) &= \frac{1}{2\pi} \int_{-\infty}^{\infty} F_n(j\omega) e^{j\omega t} d\omega \\ &= \frac{1}{2\pi} \int_{-n\omega_0}^{n\omega_0} F(j\omega) e^{j\omega t} d\omega \end{aligned} \quad (11)$$

However, from the definition of the Fourier Transform,

$$F(j\omega) = \int_{-\infty}^{\infty} f(t) e^{-j\omega t} dt \quad (12)$$

and substituting Eq. (12) into Eq. (11) using the dummy variable  $x$  for  $t$  in Eq. (12), yields

$$\begin{aligned} f_n(t) &= \frac{1}{2\pi} \int_{-n\omega_0}^{n\omega_0} \int_{-\infty}^{\infty} f(x) e^{-j\omega x} e^{j\omega t} dx d\omega \\ &= \frac{1}{2\pi} \int_{-\infty}^{\infty} f(x) \int_{-n\omega_0}^{n\omega_0} e^{j\omega(t-x)} d\omega dx \end{aligned} \quad (13)$$

Eq. (13) can be rewritten as

$$f_n(t) = \int_{-\infty}^{\infty} f(x) w_n(t-x) dx \quad (14)$$

where  $w_n(t)$  is called the aperiodic Dirichlet window,

$$w_n(t) = \frac{1}{2\pi} \int_{-n\omega_0}^{n\omega_0} e^{j\omega t} d\omega \quad (15)$$

$$= \frac{\sin(n\omega_0 t)}{\pi t} \quad (16)$$

Now, we recognize that the aperiodic Dirichlet window is an ideal low pass filter with cutoff frequency  $n\omega_0$  and unity gain. In other words, the partial sum  $f_n(t)$  can be considered as the output of the ideal low pass filter excited by  $f(t)$ . This is a more explicit interpretation of the partial sum of the Fourier series and is important for deriving the Gibbs' phenomenon and windowing effects later on.

## 2.2 GIBBS' PHENOMENON IN THE TIME DOMAIN

Since Gibbs and Böcher<sup>[15]</sup>, many investigators have worked on the property of the Fourier series of a function having points of discontinuity. Here, we adopt the derivation given by Guillemin<sup>[17]</sup>.

If the given function  $f(t)$  is discontinuous at  $t = a$ , the property of the truncated Fourier series in the vicinity of  $t = a$  is equivalent to that of replacing  $f(t)$  by the biased step function;

$$f_a(t) = Au(t-a) + f(a^-) \quad (17)$$

where

$$f(a^-) = \lim_{\epsilon \rightarrow 0} f(a-\epsilon) \quad (18)$$

and  $A$  is a real constant, such that

$$A = \lim_{\epsilon \rightarrow 0} [f(a+\epsilon) - f(a-\epsilon)] \quad (19)$$

Considering Eq. (17); the second term  $f(a^-)$  is a constant and continuous; therefore, we can drop it for the time being when studying the properties of the partial sum of the Fourier series for a function at the point of discontinuity. To drop the term  $f(a^-)$ , let

$$g(t) = f(t) - f(a^-) \quad (20)$$

For  $n$  very large, it is easily shown that

$$g_n(t) = f_n(t) - f(a^-) \quad (21)$$

Now, from Eq. (14), we have

$$g_n(t) = \int_{-\infty}^{\infty} w_n(t-x) g_a(t) dt \quad (22)$$

where

$$g_a(t) = f_a(t) - f(a^-) = Au(t-a) \quad (23)$$

Without loss of generality, let us assume  $a = 0$ . Thus we have

$$g_n(t) = \int_{-\infty}^{\infty} w_n(t-x) Au(x) dx \quad (24)$$

According to the properties of the convolution integral, we have

$$g_n(t) = A \int_{-\infty}^t w_n(x) dx \quad (25)$$

Substituting Eq. (15) into Eq. (25), yields

$$\begin{aligned}
 g_n(t) &= A \int_{-\infty}^t \frac{\sin(n\omega_0 x)}{\pi x} dx \\
 &= \frac{A}{\pi} \int_{-\infty}^{n\omega_0 t} \frac{\sin y}{y} dy \quad (26)
 \end{aligned}$$

In terms of the sine-integral function,  $Si(x)$ , defined as

$$Si(x) = \int_0^x \frac{\sin y}{y} dy \quad (27)$$

Eq. (26) can be rewritten as

$$g_n(t) = A \left[ \frac{1}{2} + \frac{1}{\pi} Si(n\omega_0 t) \right] \quad (28)$$

The above function is shown in Figure 2-1. Therefore, as  $n$  becomes very large,  $g_n(t)$  has a global maximum, occurring at  $t = \frac{\pi}{n\omega_0}$ ,

$$g_n\left(\frac{\pi}{n\omega_0}\right) = A \left[ \frac{1}{2} + \frac{1}{\pi} Si(\pi) \right] \quad (29)$$

$$= 1.0895 A \quad (30)$$

and a global minimum, occurring at  $t = -\frac{\pi}{n\omega_0}$ ,

$$\begin{aligned}
 g_n\left(-\frac{\pi}{n\omega_0}\right) &= A \left[ \frac{1}{2} + \frac{1}{\pi} Si(-\pi) \right] \\
 &= -0.0895 A \quad (31)
 \end{aligned}$$

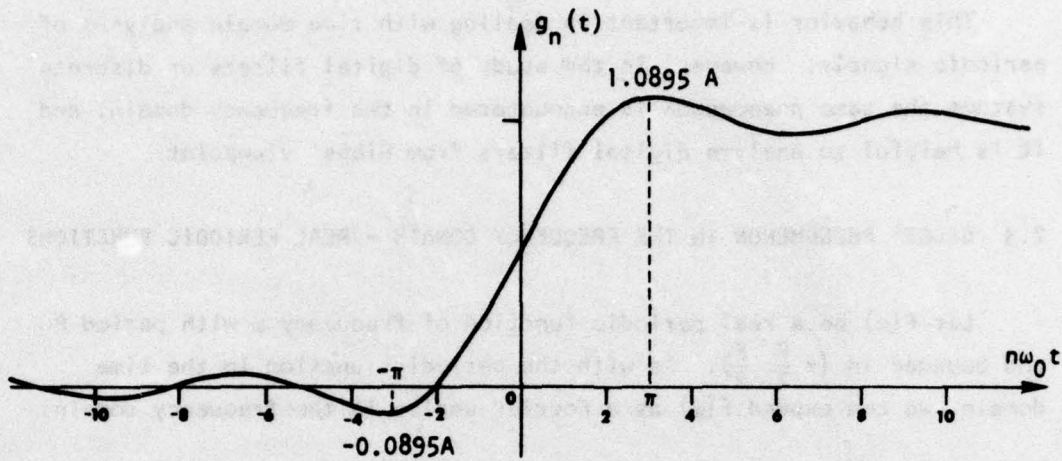


FIGURE 2-1. THE TIME FUNCTION  $g_n(t)$

As  $n \rightarrow \infty$ ,  $\frac{\pi}{n\omega_0}$  and  $-\frac{\pi}{n\omega_0}$  approach  $t = 0$  which is the point of discontinuity, and the ripples in Figure 2-1 are compressed into a single vertical line at  $t = 0$ . Eqs. (30) and (31) correspond to the top and bottom of this vertical line segment. In other words, the overshoot at the point of discontinuity is given by

$$\lim_{n \rightarrow \infty} |\text{Max } g_n(t) - A| = 0.0895 A \sim 9\% A \quad (32)$$

and the undershoot is given by

$$\lim_{n \rightarrow \infty} |\text{Min } g_n(t)| = 0.0895 A \sim 9\% A \quad (33)$$

The Fourier series of a discontinuous function results in a 9% overshoot in the vicinity of the point of discontinuity. This is known as the Gibbs' phenomenon.

This behavior is important in dealing with time domain analysis of periodic signals. However, in the study of digital filters or discrete systems the same phenomenon is encountered in the frequency domain; and it is helpful to analyze digital filters from Gibbs' viewpoint.

### 2.3 GIBBS' PHENOMENON IN THE FREQUENCY DOMAIN - REAL PERIODIC FUNCTIONS

Let  $F(\omega)$  be a real periodic function of frequency  $\omega$  with period  $P$  and bounded in  $(-\frac{P}{2}, \frac{P}{2})$ . As with the periodic function in the time domain, we can expand  $F(\omega)$  as a Fourier series in the frequency domain:

$$F(\omega) = \sum_{k=-\infty}^{\infty} A_k e^{-jkt_0\omega} \quad (34)$$

where

$$A_k = \frac{1}{P} \int_{-\frac{P}{2}}^{\frac{P}{2}} F(x) e^{jkt_0x} dx \quad (35)$$

and

$$t_0 = \frac{2\pi}{P} \quad (36)$$

The  $n$ th partial sum is defined as

$$F_n(\omega) = \sum_{k=-n}^n A_k e^{-jkt_0\omega} \quad (37)$$

Let us use the second interpretation of the partial sum of the Fourier series. If  $f(t)$  is the inverse Fourier Transform of  $F(\omega)$ , then

$$f(t) = \frac{1}{2\pi} \int_{-\infty}^{\infty} F(\omega) e^{j\omega t} d\omega \quad (38)$$

From Eq. (34), we have

$$F(t) = \sum_{k=-\infty}^{\infty} A_k \delta(t-kt_0) \quad (39)$$

From Eq. (37), the inverse Fourier Transform of the nth partial sum is

$$f_n(t) = \sum_{k=-n}^n A_k \delta(t-kt_0) \quad (40)$$

Now, according to the definition of the Fourier Transform,

$$F_n(\omega) = \int_{-\infty}^{\infty} f_n(t) e^{-j\omega t} dt \quad (41)$$

$$= \int_{-nt_0}^{nt_0} f(t) e^{-j\omega t} dt \quad (42)$$

and substituting Eq. (38) into Eq. (42), using the dummy variable  $x$  for  $\omega$  in Eq. (38), yields

$$\begin{aligned} F_n(\omega) &= \frac{1}{2\pi} \int_{-nt_0}^{nt_0} \int_{-\infty}^{\infty} F(x) e^{jxt} e^{-j\omega t} dx dt \\ &= \frac{1}{2\pi} \int_{-\infty}^{\infty} F(x) \int_{-nt_0}^{nt_0} e^{jt(x-\omega)} dt dx \end{aligned} \quad (43)$$

Eq. (43) can be rewritten in the form of a complex convolution

$$F_n(\omega) = \frac{1}{2\pi} \int_{-\infty}^{\infty} F(x) W_n(\omega-x) dx \quad (44)$$

where

$$W_n(\omega) = \int_{-nt_0}^{nt_0} e^{-j\omega t} dt \quad (45)$$

$$= \frac{2 \sin(\omega nt_0)}{\omega} \quad (46)$$

may be called the aperiodic Dirichlet kernel in the frequency domain.

Taking the inverse Fourier Transform of  $W_n(\omega)$ , yields

$$w_n(t) = \begin{cases} 1 & |t| \leq nt_0 \\ 0 & |t| > nt_0 \end{cases} \quad (47)$$

According to the complex convolution [Eq. (44)], we have

$$\begin{aligned} f_n(t) &= f(t) w_n(t) \\ &= \begin{cases} f(t) & |t| \leq nt_0 \\ 0 & |t| > nt_0 \end{cases} \end{aligned} \quad (48)$$

In other words,  $w_n(t)$  is a rectangular window in the frequency domain.

Now, assume that  $F(\omega)$  is a discontinuous function with a point of discontinuity at  $\omega = a$ . Following the derivation in Section 2.2,  $F(\omega)$  converges to the biased step function in the vicinity of  $\omega = a$ ,

$$F_a(\omega) = Au(\omega-a) + F(a^-) \quad (49)$$

where

$$F(a^-) = \lim_{\epsilon \rightarrow 0} F(a-\epsilon) \quad (50)$$

and  $A$  is the real constant,

$$A = \lim_{\epsilon \rightarrow 0} [F(a+\epsilon) - F(a-\epsilon)] \quad (51)$$

Since convergence in the vicinity of  $\omega = a$  is governed by the first term of Eq. (49), we can assume, for simplicity and without loss of generality, that  $a = 0$  and  $F(a^-) = 0$ . Under this assumption we have

$$F_a(\omega) = Au(\omega) \quad (52)$$

From Eq. (44), the partial sum is given by

$$\begin{aligned} F_n(\omega) &= \frac{1}{2\pi} \int_{-\infty}^{\infty} F_a(x) W_n(\omega-x) dx \\ &= \frac{A}{2\pi} \int_{-\infty}^{\infty} u(x) W_n(\omega-x) dx \end{aligned} \quad (53)$$

Substituting Eq. (46) into Eq. (53), yields

$$\begin{aligned} F_n(\omega) &= \frac{A}{\pi} \int_{-\infty}^{\infty} u(x) \frac{\sin [nt_0(\omega-x)]}{\omega-x} dx \\ &= \frac{A}{\pi} \int_{-\infty}^{\omega} \frac{\sin (nt_0 y)}{y} dy \end{aligned} \quad (54)$$

or

$$F_n(\omega) = \frac{A}{\pi} \int_{-\infty}^{nt_0\omega} \frac{\sin z}{z} dz \quad (55)$$

Comparing Eq. (55) with Eq. (26), we find that convergence of a real periodic function in the frequency domain in the vicinity of the point of discontinuity is similar to that of a real periodic function in the time domain. Eq. (55) can be written as

$$F_n(\omega) = A \left[ \frac{1}{2} + \frac{1}{\pi} \text{Si}(nt_0\omega) \right] \quad (56)$$

Following the reasoning in Section 2.2, the Fourier series of a real discontinuous function in frequency domain results in a 9% overshoot in the vicinity of the point of discontinuity. Therefore, we have determined the counterpart of the Gibbs' phenomenon in the time domain; that is, the Gibbs' phenomenon in the frequency domain.

We now have identical properties for the truncated Fourier series of real periodic functions in the time domain and the frequency domain:

- (1) The partial sum of a real periodic function in the time domain can be expressed as the convolution of the original function and an ideal filter with unity gain; the partial sum of a real periodic function in frequency domain can be expressed as the complex convolution of the original function and a rectangular window with unity height.
- (2) The Fourier series for both the real periodic function in the time domain and the real periodic function in the frequency domain has a 9% overshoot in the vicinity of the points of discontinuity; in other words, the Gibbs' phenomenon for a real periodic function in the frequency domain is exactly the same as that for a real periodic function in the time domain.

It is important to point out that we have limited our study to the partial sum of the truncated Fourier series for real periodic functions in the frequency domain. In reality, we often must consider complex periodic functions in the frequency domain. For this case, the first result listed above is valid; however, Gibbs' phenomenon for a complex periodic function in the frequency domain must be redefined.

#### 2.4 GIBBS' PHENOMENON IN THE FREQUENCY DOMAIN - COMPLEX PERIODIC FUNCTIONS

Since we did not place any particular restrictions on  $F(\omega)$  when we derived Eq. (44) for the partial sum of a periodic function in the frequency domain, Eqs. (44) and (46) are still valid when  $F(\omega)$  is a complex periodic function. However, if the Gibbs' phenomenon is to be considered, we need to treat the real part and imaginary parts individually. Let

$$F(\omega) = F_R(\omega) + jF_I(\omega) \quad (57)$$

The window function in Eq. (46) is real; therefore, the partial sums of  $F_R(\omega)$  and  $F_I(\omega)$  are

$$F_{Rn}(\omega) = \frac{1}{2\pi} \int_{-\infty}^{\infty} F_R(x) W_n(\omega-x) dx \quad (58)$$

and

$$F_{In}(\omega) = \frac{1}{2\pi} \int_{-\infty}^{\infty} F_I(x) W_n(\omega-x) dx \quad (59)$$

respectively. Now, if  $F(\omega)$  has a point of discontinuity at  $\omega = a$  and letting

$$C = \lim_{\epsilon \rightarrow 0} [F(a+\epsilon) - F(a-\epsilon)] \quad (60)$$

where  $C$  is, in general, complex and can be defined as

$$C = C_R + jC_I \quad (61)$$

where

$$C_R = \lim_{\epsilon \rightarrow 0} [F_R(a+\epsilon) - F_R(a-\epsilon)] \quad (62)$$

and

$$C_I = \lim_{\epsilon \rightarrow 0} [F_I(a+\epsilon) - F_I(a-\epsilon)] \quad (63)$$

Now, we can treat  $F_R(\omega)$  and  $F_I(\omega)$  as two real periodic functions in the frequency domain. From Eq. (55) we have the partial sums

$$F_{Rn}(\omega) = \frac{C_R}{\pi} \int_{-\infty}^{nt_0\omega} \frac{\sin z}{z} dz \quad (64)$$

and

$$F_{In}(\omega) = \frac{C_I}{\pi} \int_{-\infty}^{nt_0\omega} \frac{\sin z}{z} dz \quad (65)$$

In other words, in the vicinity of a point of discontinuity, the partial sum of the complex function in the frequency domain is

$$\begin{aligned} F_n(\omega) &= F_{Rn}(\omega) + jF_{In}(\omega) \\ &= \frac{C}{\pi} \int_{-\infty}^{nt_0\omega} \frac{\sin z}{z} dz \end{aligned} \quad (66)$$

Eq. (66) can be rewritten as

$$F_n(\omega) = C \left[ \frac{1}{2} + \frac{1}{\pi} \text{Si}(\pi \tau_0 \omega) \right] \quad (67)$$

Therefore, the Fourier series for the complex periodic function in the frequency domain results in an overshoot,  $C_R \left[ \frac{1}{\pi} \text{Si}(\pi) - 1 \right] = 9\% C_R$ , in the real part and an overshoot,  $C_I \left[ \frac{1}{\pi} \text{Si}(\pi) - 1 \right] = 9\% C_I$ , in the imaginary part near the point of discontinuity. Although the magnitudes of the overshoots in the real and imaginary parts are generally not equal, the percentages are still the same as the Gibbs' phenomenon in the time domain if  $C_R = C_I$ .

When dealing with the transfer function of digital filters or discrete-time control systems, we are often interested in the magnitude and phase relationships of the frequency response instead of the real part and the imaginary part. In terms of phase and magnitude, the Gibbs' phenomenon is more complicated. Figure 2-2 shows the situation for overshoots of magnitude and phase relative to those of the real part and the imaginary part. The jump-amplitude at the point of discontinuity is given by

$$\Delta M = |F(a^+)| - |F(a^-)| \quad (68)$$

The jump-phase is

$$\Delta \theta = \text{ARG}[F(a^+)] - \text{ARG}[F(a^-)] \quad (69)$$

The overshoot in amplitude is

$$\delta_1 = |F(a^+) + 9\%C| - |F(a^+)| \quad (70)$$

and the undershoot in amplitude is

$$\delta_2 = |F(a^-)| - |F(a^-) - 9\%C| \quad (71)$$

The overshoot in phase is

$$\theta_1 = \text{ARG}[F(a^+) + 9\%C] - \text{ARG}[F(a^+)] \quad (72)$$

and the undershoot in phase is

$$\theta_2 = \text{ARG}[F(a^-)] - \text{ARG}[F(a^-) - 9\%C] \quad (73)$$

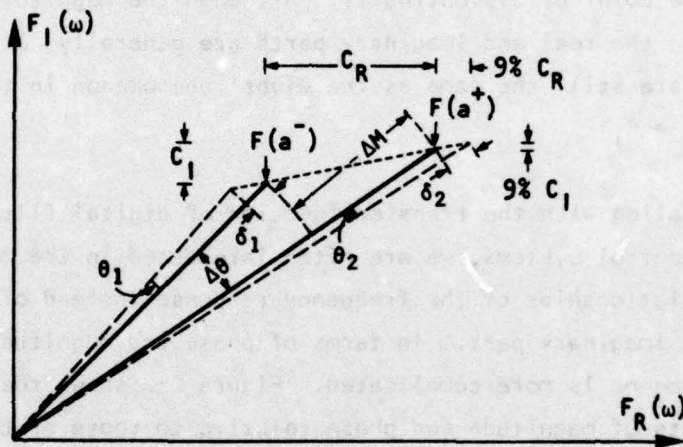


FIGURE 2-2. OVERSHOOTS OF MAGNITUDE AND PHASE RELATIVE TO THOSE OF REAL AND IMAGINARY PARTS

In general  $\delta_1 \neq \delta_2$ ,  $\theta_1 \neq \theta_2$ ; the percentages of overshoot  $(\frac{\delta_1}{\Delta M})$  and undershoot  $(\frac{\delta_2}{\Delta M})$  in amplitude are not 9% except in some special cases.

## 2.5 DEMONSTRATION OF GIBBS' PHENOMENA WITH HP FOURIER ANALYZER

In this section, Gibbs' phenomena in the time domain and the frequency domain will be demonstrated through the use of the Hewlett Packard Fourier Analyzer. The Fourier Analyzer performs the FFT algorithm<sup>[5]</sup> to compute the Discrete Fourier Transform (DFT) of discrete signals in the time domain or in the frequency domain. The DFT can be used to evaluate the coefficients of Fourier series from the periodic waveform or to synthesize the waveform from the coefficients of the Fourier series (Appendix A).

To demonstrate the Gibbs' phenomenon in the time domain, the following wave was chosen as an example:

$$f(t) = \begin{cases} 1 & -\frac{1}{2} < t < 0 \\ 0 & t = -\frac{1}{2}, 0, \frac{1}{2} \\ -1 & 0 < t < \frac{1}{2} \end{cases} \quad (74)$$

The square wave defined by Eq. (74) is characterized by an amplitude of unity and a period of 1 second. Program No. 1 (Appendix C) is a listing of the program utilized for this demonstration. The number of samples required for the FFT algorithm was 4096. Figure 2-3 shows the resulting waveforms for various partial sums of the Fourier series for Eq. (74). The maximum overshoots for different nth partial sums are shown in Figure 2-4. The maximum overshoot approaches 0.181 when n is very large. The height of the jump at the point of discontinuity is 2; thus, the ratio of overshoot to the height of the jump is 0.0905 or 9.05%. This is almost equal to the prediction of 8.95% based on Gibbs' phenomenon.

The following example is presented to demonstrate the Gibbs' phenomenon in the frequency domain. Consider the periodic function  $F(\omega) = F_R(\omega) + jF_I(\omega)$ , where

$$F_R(\omega) = \begin{cases} 1.0 & |\omega| < 0.25 \\ -1.0 & 0.25 < |\omega| \leq 0.5 \end{cases} \quad (74a)$$

$$F_I(\omega) = \begin{cases} -2.0 + 4.0\omega & -0.5 \leq \omega < -0.25 \\ 4.0\omega & |\omega| \leq 0.25 \\ 2.0 - 4.0\omega & 0.25 < \omega \leq 0.5 \end{cases} \quad (74b)$$

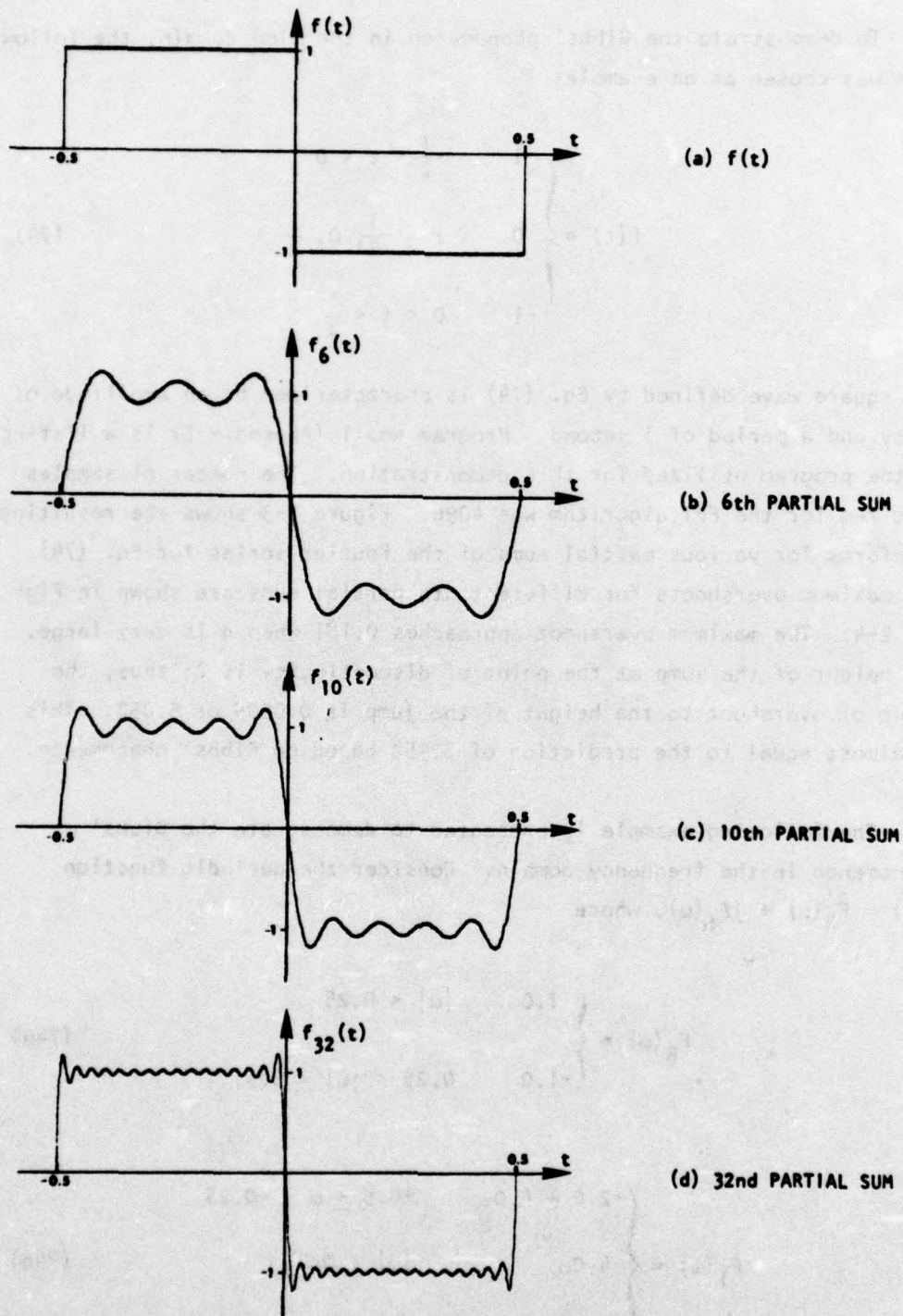


FIGURE 2-3. PARTIAL SUMS OF THE SQUARE WAVE

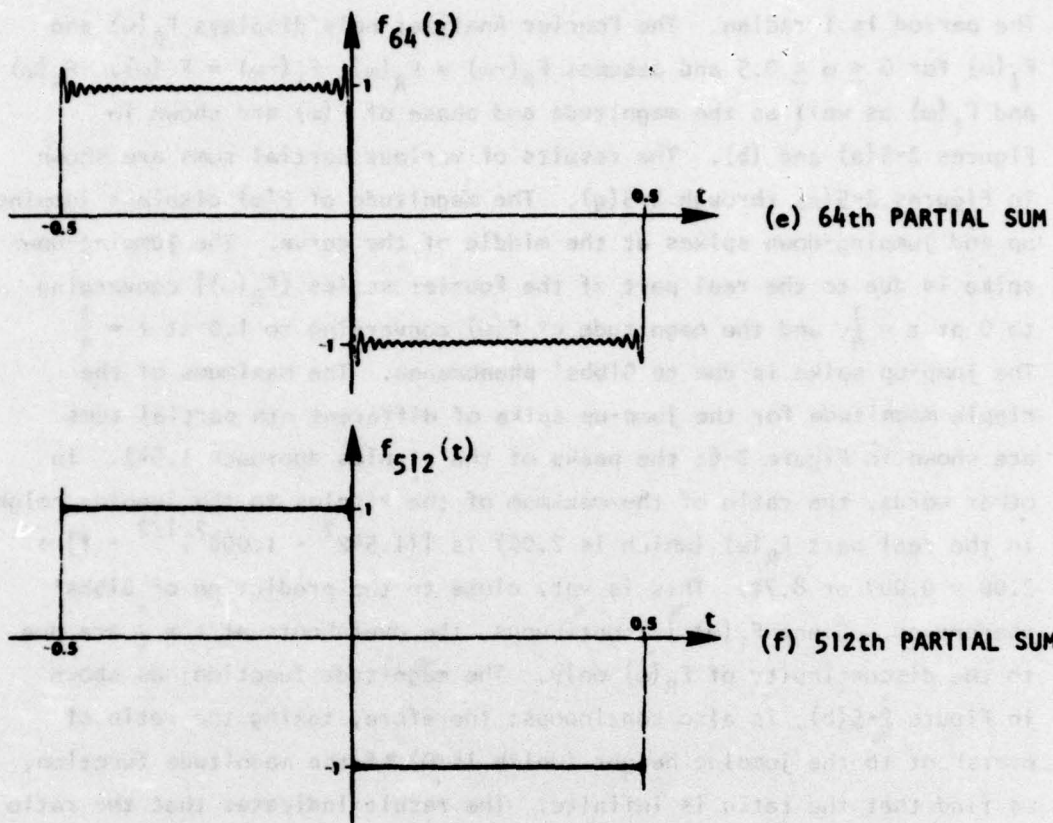


FIGURE 2-3. PARTIAL SUMS OF THE SQUARE WAVE (Concluded)

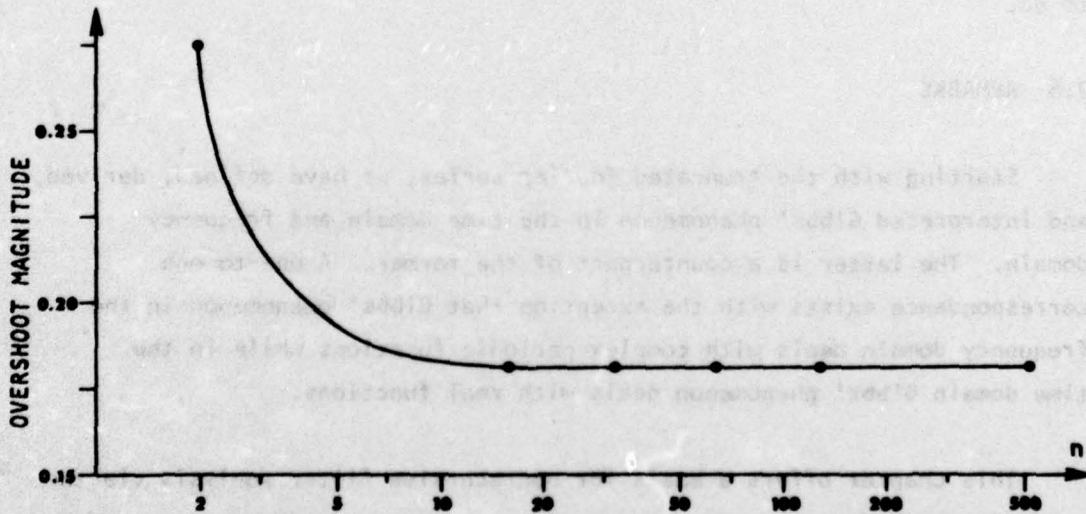


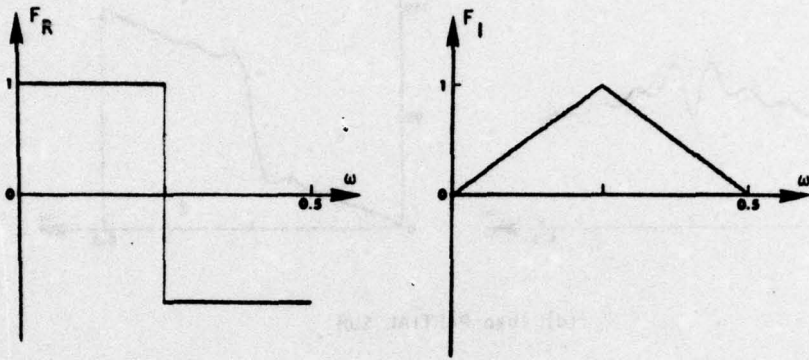
FIGURE 2-4. MAXIMUM OVERSHOOT FOR DIFFERENT PARTIAL SUMS OF EXAMPLE 1

The period is 1 radian. The Fourier Analyzer only displays  $F_R(\omega)$  and  $F_I(\omega)$  for  $0 \leq \omega \leq 0.5$  and assumes  $F_R(-\omega) = F_R(\omega)$ ,  $F_I(-\omega) = -F_I(\omega)$ .  $F_R(\omega)$  and  $F_I(\omega)$  as well as the magnitude and phase of  $F(\omega)$  are shown in Figures 2-5(a) and (b). The results of various partial sums are shown in Figures 2-5(c) through 2-5(g). The magnitude of  $F(\omega)$  displays jumping-up and jumping-down spikes at the middle of the curve. The jumping-down spike is due to the real part of the Fourier series  $[F_R(\omega)]$  converging to 0 at  $t = \frac{1}{4}$ , and the magnitude of  $F(\omega)$  converging to 1.0 at  $t = \frac{1}{4}$ . The jump-up spike is due to Gibbs' phenomenon. The maximums of the ripple magnitude for the jump-up spike of different  $n$ th partial sums are shown in Figure 2-6; the peaks of the ripples approach 1.542. In other words, the ratio of the maximum of the ripples to the jumping height in the real part  $F_R(\omega)$  (which is 2.00) is  $[(1.542^2 - 1.000^2)^{1/2} - 1] \div 2.00 = 0.087$  or 8.7%. This is very close to the prediction of Gibbs' phenomenon. Since  $F_I(\omega)$  is continuous, the overshoots at  $t = \frac{1}{4}$  are due to the discontinuity of  $F_R(\omega)$  only. The magnitude function, as shown in Figure 2-5(b), is also continuous; therefore, taking the ratio of overshoot to the jumping height (which is 0) of the magnitude function, we find that the ratio is infinite. The result indicates that the ratio of overshoot to the jumping height in the magnitude function for a complex periodic function in the frequency domain is not always equal to 9%.

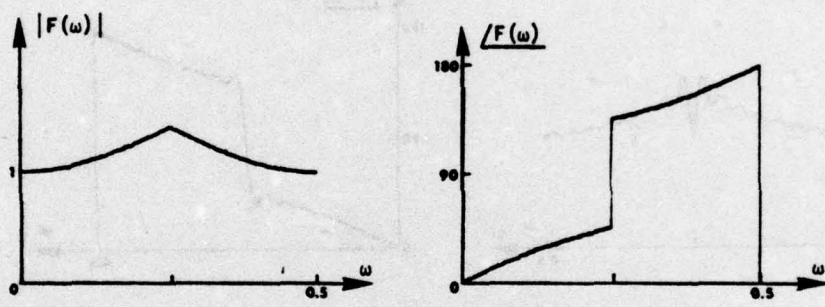
## 2.6 REMARKS

Starting with the truncated Fourier series, we have defined, derived, and interpreted Gibbs' phenomenon in the time domain and frequency domain. The latter is a counterpart of the former. A one-to-one correspondence exists with the exception that Gibbs' phenomenon in the frequency domain deals with complex periodic functions while in the time domain Gibbs' phenomenon deals with real functions.

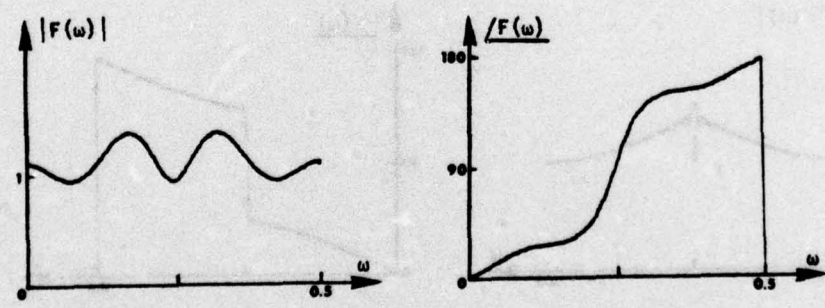
This chapter offers a basis for nonrecursive filter analysis via the windowing method.



(a) REAL AND IMAGINARY PARTS OF  $F(\omega)$

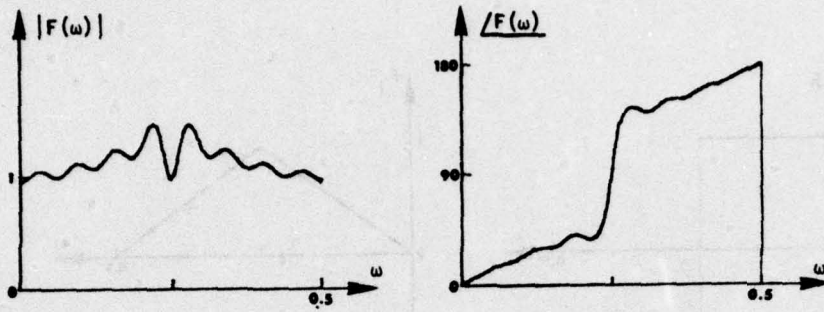


(b) MAGNITUDE AND PHASE OF  $F(\omega)$

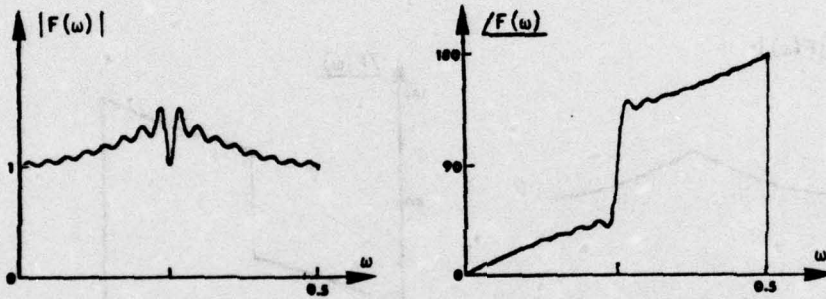


(c) 6th PARTIAL SUM

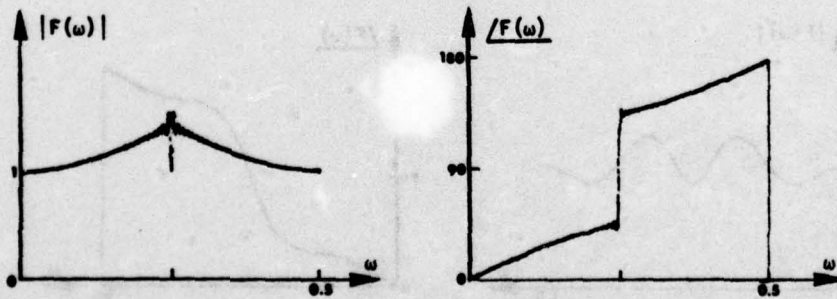
FIGURE 2-5. THE PERIODIC FUNCTION  $F(\omega)$  AND THE MAGNITUDE AND PHASE OF VARIOUS PARTIAL SUMS OF  $F(\omega)$



(d) 16th PARTIAL SUM

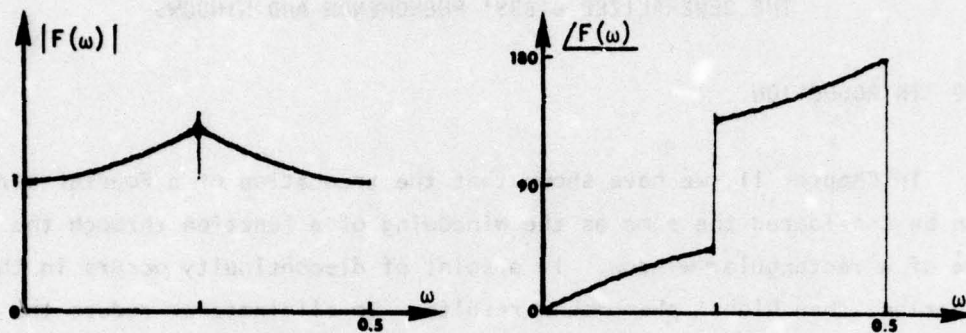


(e) 32nd PARTIAL SUM



(f) 128th PARTIAL SUM

FIGURE 2-5. THE PERIODIC FUNCTION  $F(\omega)$  AND THE MAGNITUDE AND PHASE OF VARIOUS PARTIAL SUMS OF  $F(\omega)$  (Continued)



(g) 512th PARTIAL SUM

FIGURE 2-5. THE PERIODIC FUNCTION  $F(\omega)$  AND THE MAGNITUDE AND PHASE OF VARIOUS PARTIAL SUMS OF  $F(\omega)$  (Concluded)

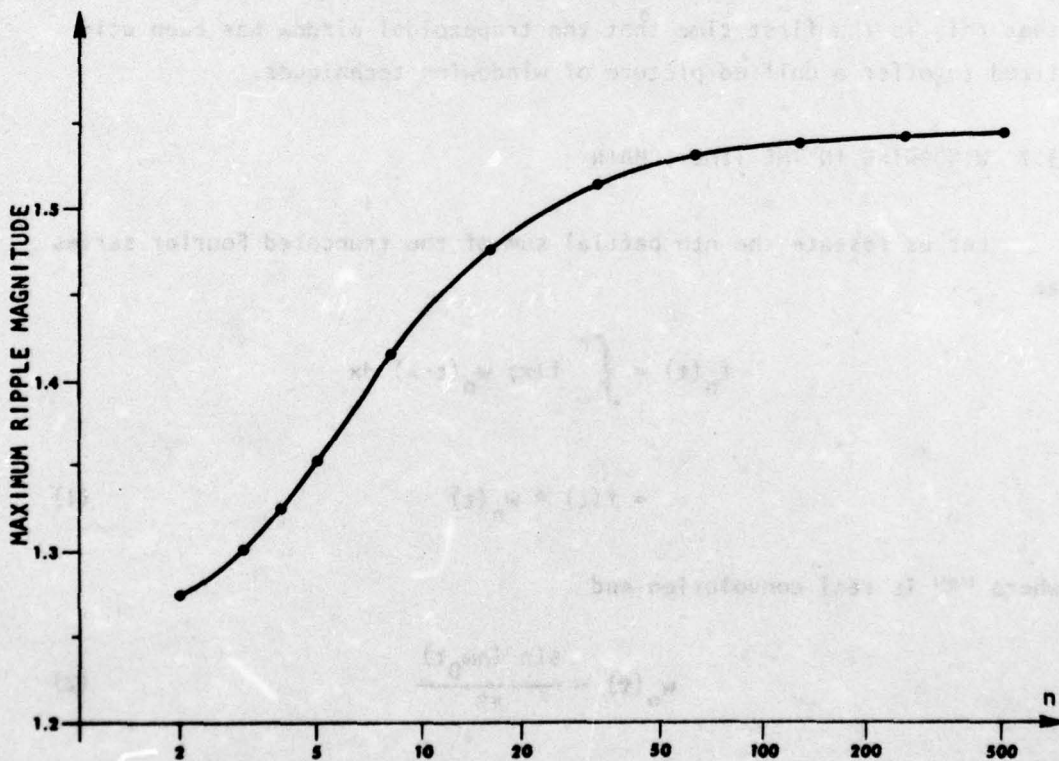


FIGURE 2-6. THE JUMP-UP SPIKE OF DIFFERENT PARTIAL SUMS OF EXAMPLE 2

CHAPTER III  
THE GENERALIZED GIBBS' PHENOMENON AND WINDOWS

3.0 INTRODUCTION

In Chapter II, we have shown that the truncation of a Fourier series can be considered the same as the windowing of a function through the use of a rectangular window. If a point of discontinuity occurs in the function, then Gibbs' phenomenon results. To eliminate or reduce the Gibbs' phenomena, rectangular windows must be modified into windows of other shapes. When modified windows are used, the corresponding effects are referred to as the generalized Gibbs' phenomena. In turn, based on the generalized Gibbs' phenomena, we will develop, classify, and investigate various windows both in the time domain and frequency domain; in particular, we will establish a trapezoidal window. It is believed that this is the first time that the trapezoidal window has been utilized to offer a unified picture of windowing techniques.

3.1 WINDOWING IN THE TIME DOMAIN

Let us restate the  $n$ th partial sum of the truncated Fourier series as

$$\begin{aligned} f_n(t) &= \int_{-\infty}^{\infty} f(x) w_n(t-x) dx \\ &= f(t) * w_n(t) \end{aligned} \tag{1}$$

where "\*" is real convolution and

$$w_n(t) = \frac{\sin(n\omega_0 t)}{\pi t} \tag{2}$$

Therefore, since it is apparent that Eq. (2) represents an ideal filter with a cutoff frequency  $n\omega_0$ , we can say that the partial sum  $f_n(t)$  is governed by the characteristics of the ideal filter  $w_n(t)$ . As shown in Figure 3-1(a),  $w_n(t)$  displays low-damped oscillations around  $t = 0$ ; resulting in (1) a slow convergence rate and (2) Gibbs' phenomenon. To improve the convergence rate and eliminate the Gibbs' phenomenon, we must use other filters or window functions instead of  $w_n(t)$  given in Eq. (2). If we filter the  $n$ th partial sum  $f_n(t)$  with a filter with impulse response  $w_{tn}(t)$ , the resulting smoothed waveform is given by

$$f_n^*(t) = f_n(t) * w_{tn}(t) \quad (3)$$

Substituting Eq. (1) into Eq. (3), yields

$$f_n^*(t) = f(t) * w_n(t) * w_{tn}(t) \quad (4)$$

Since the convolution integral is an associative operation, Eq. (4) can be rewritten as

$$f_n^*(t) = f(t) * w(t) \quad (5)$$

where

$$w(t) = w_n(t) * w_{tn}(t) \quad (6)$$

Let us assume that the Fourier Transform of  $w_{tn}(t)$  is  $W_{tn}(\omega)$  and  $W_{tn}(\omega) = 0$  for  $\omega > n\omega_0$ , where  $\omega_0 = \frac{2\pi}{T}$  and  $T$  is the period of  $f(t)$ . Taking the Fourier Transform of  $w(t)$ , we have

$$W(\omega) \triangleq F[w(t)] = W_n(\omega) W_{tn}(\omega) \quad (7)$$

Since  $W_n(\omega)$  represents an ideal filter with cutoff frequency  $n\omega_0$ ,

$$W(\omega) = W_{tn}(\omega) \quad (8)$$

and,

$$w(t) = w_{tn}(t) \quad (9)$$

Eq. (5) now becomes

$$f_n^*(t) = f(t) * w_{tn}(t) \quad (10)$$

The result,  $f_n^*(t)$ , may be called the windowed partial sum of the periodic function  $f(t)$ . From this viewpoint, truncation of the Fourier series (Chapter II) can be considered as a special case of windowing.

### 3.2 THE GENERALIZED GIBBS PHENOMENON IN THE TIME DOMAIN

As pointed out earlier, the property of the truncated Fourier series in the vicinity of a discontinuous point is equivalent to that of replacing  $f(t)$  by a biased step function. If only the oscillations in the vicinity of the point of discontinuity are considered, we can replace  $f(t)$  by

$$f_a(t) = Au(t) \quad (11)$$

where  $A$  is the jump height of  $f(t)$  at the discontinuous point  $t = 0$ . When the periodic function  $f(t)$  is windowed by  $w_{tn}(t)$ , we can apply this idea and evaluate the overshoot in the vicinity of the discontinuous point. Let us define

$$g_n(t) = f_a(t) * w_{tn}(t) \quad (12)$$

Then

$$g_n(t) = A \int_{-\infty}^{\infty} u(x) w_{tn}(t-x) dx \quad (13)$$

$$= A \int_{-\infty}^t w_{tn}(x) dx \quad (14)$$

To facilitate our discussion, let us define the unit window  $w_t(t)$  for the class of windows  $w_{tn}(t)$ , for  $n = 1, 2, \dots$ , such that

$$W_t(\omega) \triangleq F[w_t(t)] = 0 \quad \text{for } \omega = 1 \quad (15)$$

and

$$W_{tn}(\omega) \triangleq F[w_{tn}(t)] = W_t\left(\frac{\omega}{n\omega_0}\right) \quad (16)$$

Thus, we have

$$w_{tn}(t) = n\omega_0 w_t(n\omega_0 t) \quad (17)$$

Substituting Eq. (17) into Eq. (14) yields

$$\begin{aligned} g_n(t) &= A \int_{-\infty}^t n\omega_0 w_t(n\omega_0 x) dx \\ &= A \int_{-\infty}^{n\omega_0 t} w_t(y) dy \end{aligned} \quad (18)$$

Letting

$$g(t) = A \int_{-\infty}^t w_t(y) dy \quad (19)$$

Then

$$g_n(t) = g(n\omega_0 t) \quad (20)$$

Assume that  $g(t)$  has several ripples with the local maxima occurring at  $t = t_1, t_2, \dots$ , then  $g_n(t)$  has local maxima occurring at

$t = \frac{t_1}{n\omega_0}, \frac{t_2}{n\omega_0}, \dots$ . Therefore, when  $n \rightarrow \infty$ , all the ripples of  $g_n(t)$  are compressed into a single vertical line at  $t = 0$ . This may cause the same effect as Gibbs' phenomenon.

In order to obtain the same jump height (A) after windowing for  $n \rightarrow \infty$ , we need to have

$$\lim_{\epsilon \rightarrow 0^+} [\lim_{n \rightarrow \infty} g_n(\epsilon)] = A \int_{-\infty}^{\infty} w_t(y) dy = A \quad (21)$$

or

$$W_t(0) = \int_{-\infty}^{\infty} w_t(y) dy = 1 \quad (22)$$

In other words, the necessary conditions for an acceptable time domain window are the following:

- (1) Its Fourier Transform  $W_{tn}(\omega)$  vanishes for  $|\omega| > n\omega_0$ .
- (2)  $W_{tn}(\omega) = 1$  for  $\omega = 0$ .
- (3)  $W_{tn}(-\omega) = W_{tn}(\omega)$

Let us define

$$g^*(\tau) = \int_{-\infty}^{\tau} w_t(y) dy \quad (23)$$

and

$$g_c = \text{l.u.b. } \{g^*(t)\} - 1 \quad t \in (0, \infty) \quad (24)$$

Then

$$g_c = \frac{1}{A} \text{l.u.b. } \{g_n(t)\} - 1 \quad t \in (0, \infty) \quad (25)$$

From Eqs. (19), (23) and (24), and following the same arguments used in Section 2.1 of Chapter II, we can define the generalized Gibbs' phenomenon in the time domain as:

- (1) If a periodic function has a discontinuous point with jump height (A) and is windowed by a time domain window  $w_{tn}(t)$ , then the overshoot in the vicinity of the point of discontinuity is given by

$$\Delta = g_c A \quad (26)$$

- (2) The ratio of the overshoot to the jump height is a constant,  $g_c$ , which is dependent on the unit window  $w_t(t)$  for the specific class of windows generated by  $w_{tn}(t) = w_t(nw_0 t)$ .

The unit window for the rectangular window or the ideal filter is

$$w_t(\omega) = \begin{cases} 1 & |\omega| \leq 1 \\ 0 & |\omega| > 1 \end{cases} \quad (27)$$

and

$$w_t(t) = \frac{\sin t}{\pi t} \quad (28)$$

Thus from Eq. (23), we have

$$g^*(t) = \int_{-\infty}^t \frac{\sin \zeta}{\pi \zeta} d\zeta \quad (29)$$

and

$$\begin{aligned} g_c &= \text{l.u.b. } \{g^*(t)\} - 1 \quad t \in (0, \infty) \\ &= \int_{-\infty}^{\pi} \frac{\sin \zeta}{\pi \zeta} d\zeta - 1 \\ &= \frac{1}{\pi} \text{Si}(\pi) - \frac{1}{2} \end{aligned} \quad (30)$$

Eq. (30) is approximately equal to 0.0895 or 8.95%. This is the overshoot ratio for the well-known Gibbs' phenomenon caused by the truncation of the Fourier series.

In order to reduce the overshoot ratio, we have to choose the window with  $g_c$  as small as possible. If  $g_c = 0$ , no overshoot occurs. From Eq. (24), we note that the Gibbs' phenomenon was eliminated, if and only if,

$$\text{l.u.b. } \{g^*(t)\} = 1 \quad \text{for } t \in (0, \infty) \quad (31)$$

Consider the special kind of windows with unit window

$$w_t(t) \geq 0 \quad \text{for } t \in (0, \infty) \quad (32)$$

If  $g^*(t)$  is monotonic increasing; then

$$\begin{aligned}
 \text{l.u.b. } \{g^*(t)\} &= \lim_{t \rightarrow \infty} g^*(t) \\
 &= \int_{-\infty}^{\infty} w_f(t) dt \\
 &= 1
 \end{aligned} \tag{33}$$

In other words if  $w_t(t)$  or  $w_{tn}(t)$  is non-negative,  $g_c = 0$ .

Consider the triangular window which has the unit window

$$w_t(\omega) = \begin{cases} 1 - \omega & 0 \leq \omega \leq 1 \\ 1 + \omega & -1 \leq \omega < 0 \end{cases} \tag{34}$$

The corresponding time function is given by

$$w_t(t) = \frac{1}{2\pi} \left[ \frac{\sin\left(\frac{t}{2}\right)}{\frac{t}{2}} \right]^2 \tag{35}$$

It is evident that  $w_t(t) \geq 0$  for  $t \in (0, \infty)$ . Therefore  $g_c = 0$  and we may conclude that the triangular window can be used to eliminate the Gibbs' phenomenon completely.

### 3.3 THE TRAPEZOIDAL WINDOW IN THE TIME DOMAIN

Consider the class of trapezoidal windows with unit window

$$w_t(\omega) = \begin{cases} \frac{1 - \omega}{2b} & 1 - 2b < \omega \leq 1 \\ 1 & |\omega| \leq 1 - 2b \\ \frac{1 + \omega}{2b} & -1 \leq \omega < -(1 - 2b) \end{cases} \tag{36}$$

where  $0 \leq b \leq 0.5$

The corresponding time function is given by

$$w_t(t) = \left[ \frac{1-b}{\pi} \right] \left[ \frac{\sin(bt)}{bt} \right] \left[ \frac{\sin[(1-b)t]}{(1-b)t} \right] \quad (37)$$

From Eqs. (36) and (37) we recognize that the trapezoidal windows become rectangular windows if  $b = 0$  and triangular windows if  $b = 0.5$ . Therefore, the trapezoidal window is a generalization for straight segment windows. The overshoot ratio is  $g_c = 8.95\%$  when  $b = 0$  and  $g_c = 0$  when  $b = 0.5$ . Figures 3-1 through 3-6 show the trapezoidal window  $w_t(t)$  and  $\int_{-\infty}^t w_t(\tau) d\tau$  for various  $b$ 's. Program No. 3 (Appendix C) was used for this purpose. The overshoot ratios  $g_c$  for different  $b$ 's are shown in Table 3-1 and Figure 3-7.

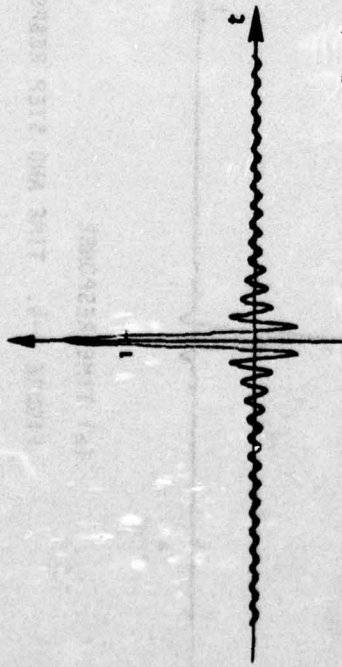
The width of the main lobe is defined as twice the interval from  $t = 0$  to the first zero-crossing of  $w_t(t)$ . From Eq. (37) we find that the width of the main lobe is given by

$$T_w^* = \frac{2\pi}{1-b} \quad (38)$$

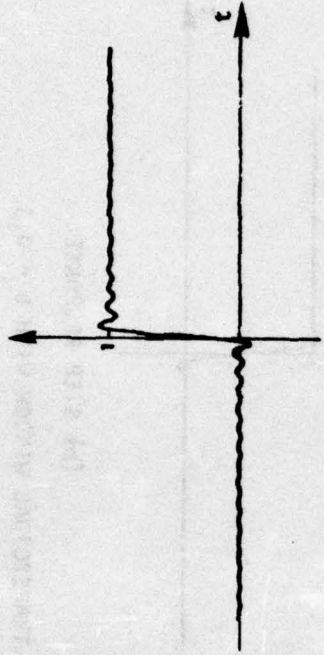
for the unit window. Figure 3-8 shows  $T_w^*$  as the function of  $b$ . If the trapezoidal window has a cutoff frequency  $n\omega_0$ , the width of the main lobe is given by

$$T_w = \frac{T_w^*}{n\omega_0} \quad (39)$$

From Figure 3-1 through 3-6 we see that as  $b$  increases, not only does the overshoot ratio  $g_c$  become smaller and smaller, but also the side lobe becomes smaller and damps out more quickly. From this viewpoint, the triangular window is the best window for the overshoot ratio  $g_c = 0$  since the side lobe damps out quickly. However, if we examine Figure 3-8, we find that the width of main lobe increases with  $b$ ; therefore, the width of the main lobe is largest for the triangular window.

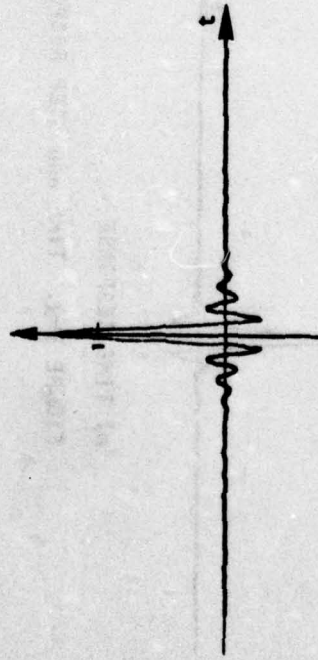


(a) TIME RESPONSE

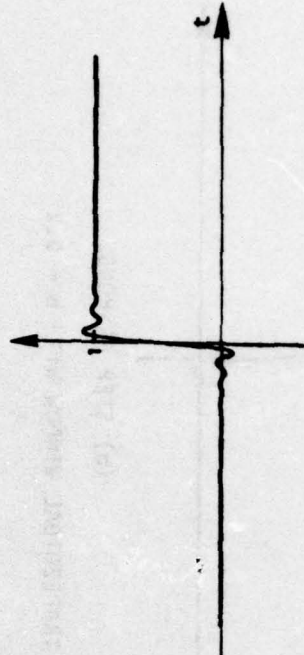


(b) STEP RESPONSE

FIGURE 3-1. TIME AND STEP RESPONSES OF TRAPEZOIDAL WINDOW WITH  $b = 0$

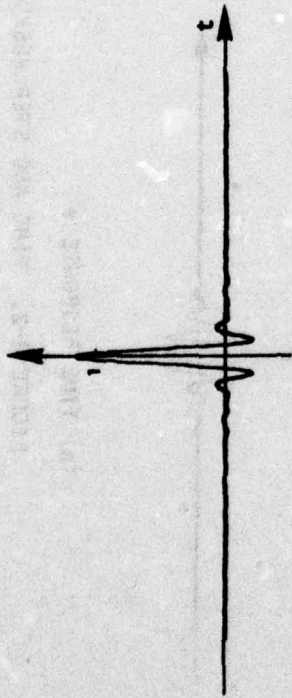


(a) TIME RESPONSE

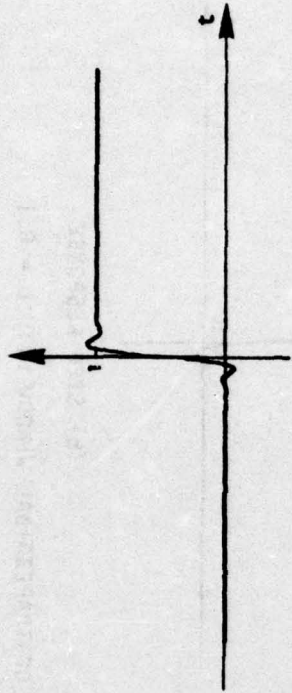


(b) STEP RESPONSE

FIGURE 3-2. TIME AND STEP RESPONSES OF TRAPEZOIDAL WINDOW WITH  $b = 0.1$

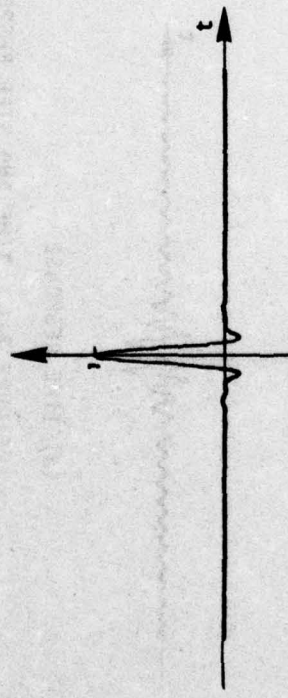


(a) TIME RESPONSE

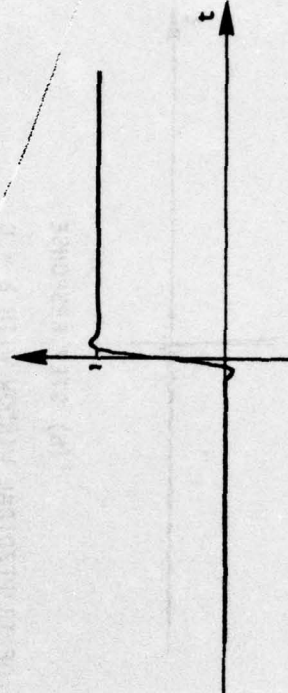


(b) STEP RESPONSE

FIGURE 3-3. TIME AND STEP RESPONSES OF TRAPEZOIDAL WINDOW WITH  $b = 0.2$

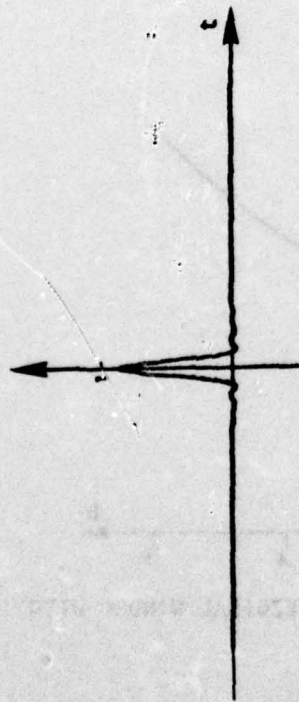


(a) TIME RESPONSE

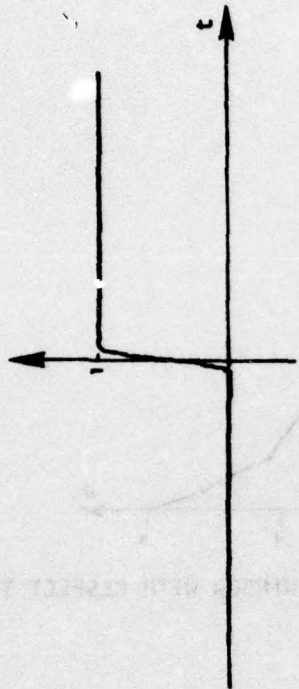


(b) STEP RESPONSE

FIGURE 3-4. TIME AND STEP RESPONSES OF TRAPEZOIDAL WINDOW WITH  $b = 0.3$

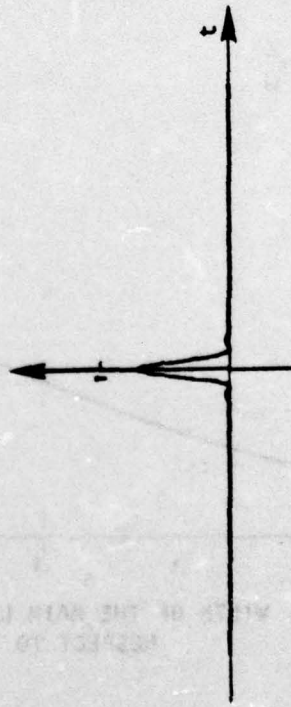


(a) TIME RESPONSE

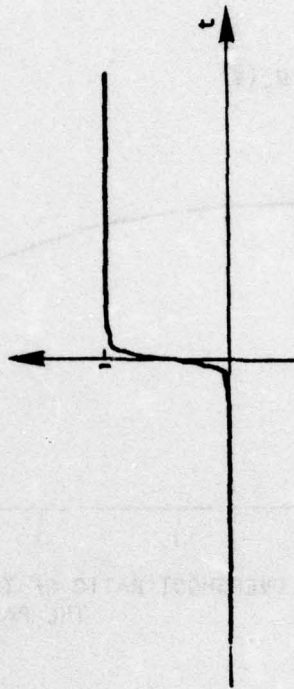


(b) STEP RESPONSE

FIGURE 3-5. TIME AND STEP RESPONSES OF TRAPEZOIDAL WINDOW WITH  $b = 0.4$



(a) TIME RESPONSE



(b) STEP RESPONSE

FIGURE 3-6. TIME AND STEP RESPONSES OF TRAPEZOIDAL WINDOW WITH  $b = 0.5$

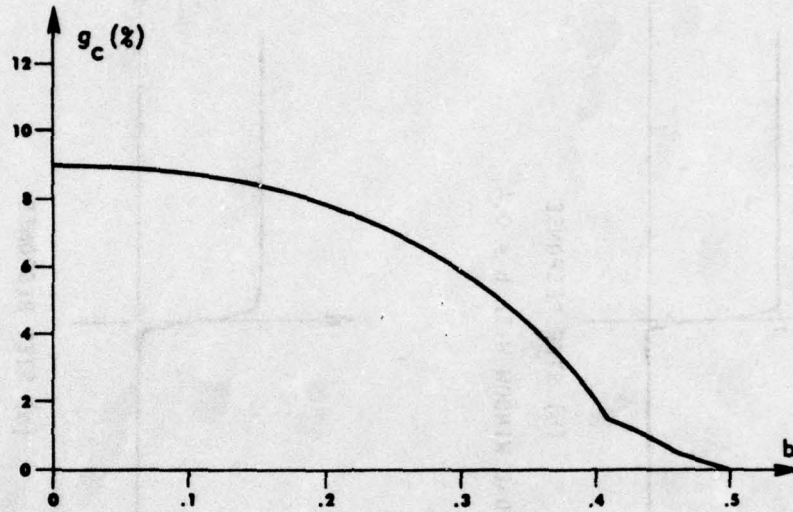


FIGURE 3-7. OVERSHOOT RATIO OF THE TRAPEZOIDAL WINDOW WITH RESPECT TO THE PARAMETER  $b$

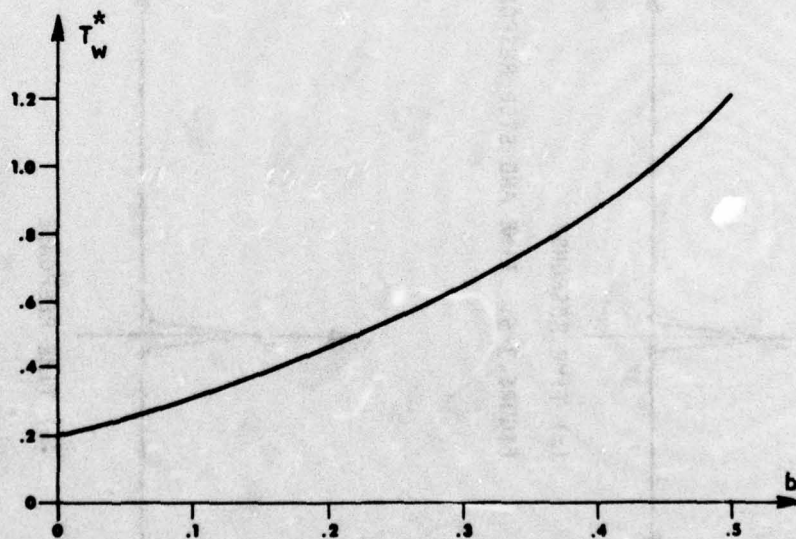


FIGURE 3-8. WIDTH OF THE MAIN LOBE OF THE TRAPEZOIDAL WINDOW WITH RESPECT TO THE PARAMETER  $b$

From the properties of the convolution integral, an increase in the width of the main lobe means a decrease in the resolution of the windowed waveform. A good window is characterized by the following: (1) the width of the main lobe is small, (2) the side lobes damp out quickly and (3) the overshoot ratio is small or zero.

TABLE 3-1  
OVERSHOOT RATIO  $g_c$  AND THE WIDTH OF  
MAIN LOBE  $T_w^*$

b	$g_c$ (%)	$\frac{T_w^*}{2\pi}$
0	9.0	1.00
0.05	8.8	1.05
0.10	8.7	1.11
0.15	8.4	1.18
0.20	7.9	1.25
0.25	7.0	1.33
0.30	5.9	1.43
0.35	4.3	1.54
0.40	2.1	1.67
0.45	0.7	1.82
0.50	0.0	2.00

Consider the square wave discussed in Chapter 11. The partial sum converges slowly and the Gibbs' phenomenon with an overshoot ratio of approximately 9% occurs. Figure 3-9(a) shows the 15th partial sum of its truncated Fourier series. Figures 3-9(b), (c) and (d) show the 15th partial sums of the windowed Fourier series utilizing trapezoidal windows with  $b = 0.33$ ,  $0.4$  and  $0.5$  respectively. From Figure 3-9 we see that the underdamped oscillation is eliminated and the overshoot spike is reduced after windowing by trapezoidal window with  $b = 0.33$ . Figures 3-10(a) through 3-10(d) show the 255th partial sums of the

windowed Fourier series utilizing trapezoidal windows with  $b = 0, 0.33, 0.4$  and  $0.5$  respectively. From Figures 3-9 and 3-10, the effect of windowing is evident.

### 3.4 WINDOWING AND THE GENERALIZED GIBBS' PHENOMENON IN THE FREQUENCY DOMAIN

In the frequency domain we have a complex periodic function to deal with and we can develop windowing techniques accordingly. Consider Eq. (44) in Chapter II, rewritten as

$$F_n(\omega) = F(\omega) \otimes W_n(\omega)$$

where " $\otimes$ " implies complex convolution and

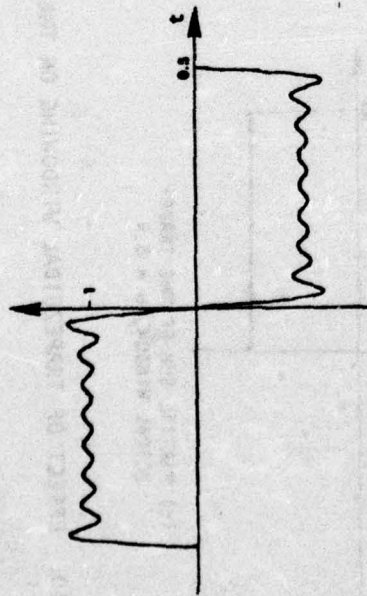
$$W_n(\omega) = \frac{2 \sin(n\omega t_0)}{\omega} \quad (41)$$

is the Dirichlet kernel or rectangular window in the frequency domain. Following the same reasoning given in Section 3-1, if the  $n$ th partial sum  $F_n(\omega)$  is windowed by a frequency domain window  $W_{fn}(\omega)$  with  $w_{fn}(t)$  having the nonzero interval  $|t| \leq nt_0$ , it yields

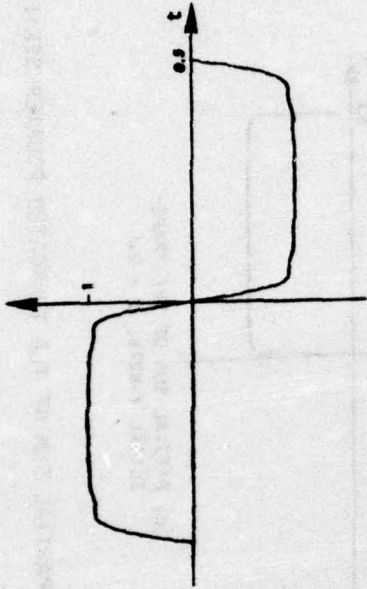
$$\begin{aligned} F_n^*(\omega) &= F_n(\omega) \otimes W_{fn}(\omega) \\ &= F(\omega) \otimes W_{fn}(\omega) \end{aligned} \quad (42)$$

In order to study the oscillation in the vicinity of the point of discontinuity after windowing by  $W_{fn}(\omega)$ , we replace  $F(\omega)$  by

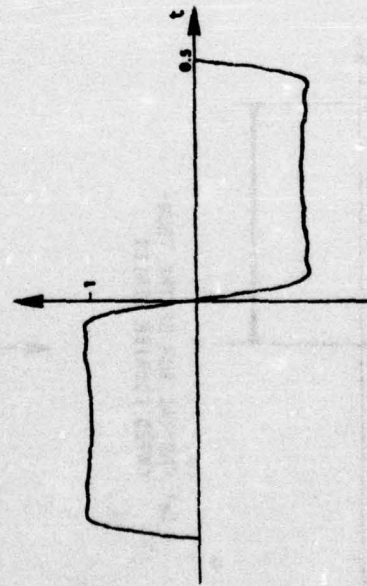
$$F_c(\omega) = Cu(\omega) \quad (43)$$



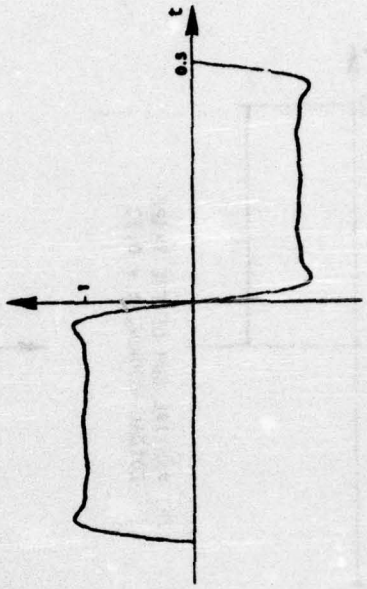
(a) PARTIAL SUM OF THE TRUNCATED FOURIER SERIES



(b) PARTIAL SUM OF THE TRAPEZOIDAL WINDOW,  $b = 0.33$

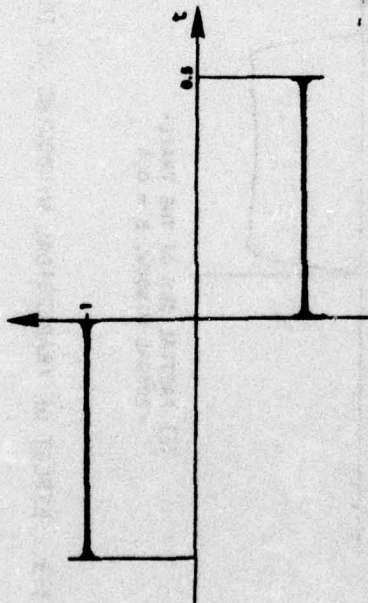


(c) PARTIAL SUM OF THE TRAPEZOIDAL WINDOW,  $b = 0.4$

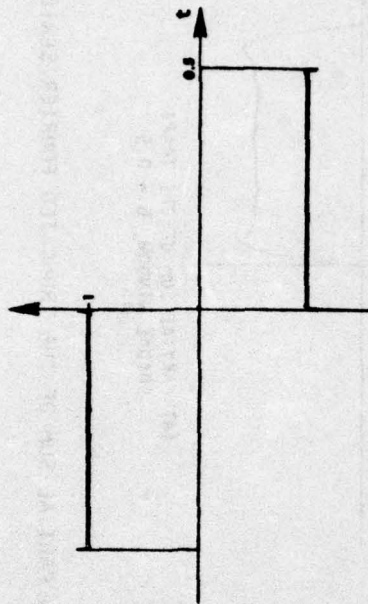


(d) PARTIAL SUM OF THE TRAPEZOIDAL WINDOW,  $b = 0.5$

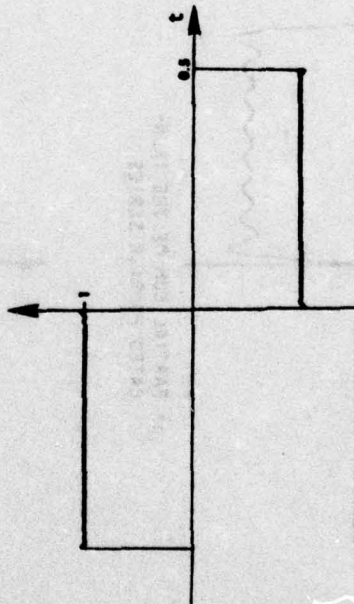
FIGURE 3-9. EFFECT OF TRAPEZOIDAL WINDOWING ON THE 15th PARTIAL SUM OF THE TRUNCATED FOURIER SERIES



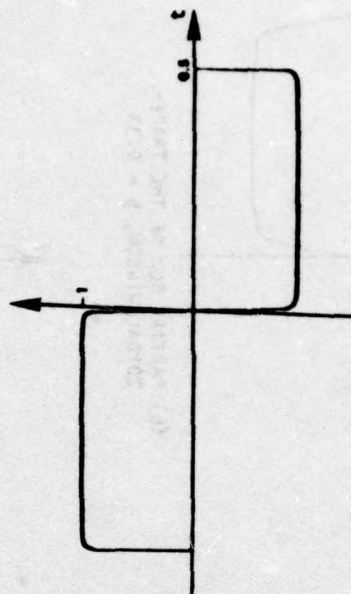
(a) PARTIAL SUM OF THE TRUNCATED FOURIER SERIES



(b) PARTIAL SUM OF THE TRAPEZOIDAL WINDOW,  $b = 0.33$



(c) PARTIAL SUM OF THE TRAPEZOIDAL WINDOW,  $b = 0.4$



(d) PARTIAL SUM OF THE TRAPEZOIDAL WINDOW,  $b = 0.5$

FIGURE 3-10. EFFECT OF TRAPEZOIDAL WINDOWING ON THE 255th PARTIAL SUM OF THE TRUNCATED FOURIER SERIES

where  $C = C_R + C_I j$ , and  $C_R, C_I$  are the jump heights of  $F_R(\omega)$  and  $F_I(\omega)$  at the discontinuous point, respectively; and  $u(\omega)$  is the unit step function of  $\omega$ . Let us define

$$\begin{aligned} G_n(\omega) &\triangleq F_c(\omega) \otimes W_{fn}(\omega) \\ &= \frac{C}{2\pi} \int_{-\infty}^{\infty} u(x) W_{fn}(\omega-x) dx \\ &= \frac{C}{2\pi} \int_{-\infty}^{\omega} W_{fn}(x) dx \end{aligned} \quad (44)$$

Similar to the time domain window, we can define the unit window  $W_f(\omega)$  for the class of windows  $W_{fn}(\omega)$ ,  $n = 1, 2, \dots$ , such that

$$w_f(t) \triangleq F^{-1}[W_f(\omega)] = 0 \quad \text{for } t > 1 \quad (45)$$

and

$$w_{fn}(t) \triangleq F^{-1}[W_{fn}(\omega)] = w_f\left(\frac{t}{nt_0}\right) \quad (46)$$

From Eq. (46) we have

$$W_{fn}(\omega) = nt_0 W_f(nt_0\omega) \quad (47)$$

Substituting Eq. (47) into Eq. (44) we have

$$\begin{aligned} G_n(\omega) &= \frac{C}{2\pi} \int_{-\infty}^{\omega} nt_0 W_f(nt_0x) dx \\ &= \frac{C}{2\pi} \int_{-\infty}^{nt_0\omega} W_f(y) dy \end{aligned} \quad (48)$$

If we let

$$G_n(\omega) = \frac{C}{2\pi} \int_{-\infty}^{\omega} W_f(y) dy \quad (49)$$

Then we have

$$G_n(\omega) = G(nt_0\omega) \quad (50)$$

If  $G(\omega)$  has ripples with local maxima occurring at  $\omega = \omega_1, \omega_2, \dots$ , then  $G_n(\omega)$  has local maxima occurring at  $\omega = \frac{\omega_1}{nt_0}, \frac{\omega_2}{nt_0}, \dots$ . Therefore, as  $n \rightarrow \infty$ , all the ripples of  $G_n(\omega)$  are compressed into a single vertical line at  $\omega = 0$ . In order to obtain the same jump height ( $C$ ) after windowing for  $n \rightarrow \infty$ , we need to have

$$\begin{aligned} \lim_{\epsilon \rightarrow 0^+} \lim_{n \rightarrow \infty} G_n(\zeta) &= \frac{C}{2\pi} \int_{-\infty}^{\infty} W_f(y) dy \\ &= C \end{aligned} \quad (51)$$

or

$$w_f(0) = \frac{1}{2\pi} \int_{-\infty}^{\infty} W_f(y) dy = 1 \quad (52)$$

Therefore, the necessary conditions for an acceptable window in the frequency domain are the following:

- (1) Its inverse Fourier Transform  $w_{fn}(t)$  vanishes for  $|t| > nt_0$
- (2)  $w_{fn}(t) = 1$  for  $t = 0$ .
- (3)  $w_{fn}(-t) = -w_{fn}(t)$

Let us define

$$G^*(\omega) = \frac{1}{2} \int_{-\infty}^{\omega} W_f(y) dy = \frac{G(\omega)}{C} \quad (53)$$

and

$$G_c = \text{l.u.b. } \{G^*(\omega)\} - 1 \quad \omega \in (0, \infty) \quad (54)$$

Then, from Eq. (50), we have

$$G_c = \frac{1}{C} \text{l.u.b. } \{G_n(\omega)\} - 1 \quad \omega \in (0, \infty) \quad (55)$$

We can now define the generalized Gibbs' phenomenon in the frequency domain;

- (1) If a complex periodic function in the frequency domain has a point of discontinuity with jump heights  $C_R$  in the real part and  $C_I$  in the imaginary part, and is windowed by a frequency domain window  $W_{fn}(\omega)$ , the overshoot in the vicinity of the point of discontinuity is given by

$$\Delta_R = G_c C_R \quad \text{in the real part.} \quad (56)$$

and

$$\Delta_I = G_c C_I \quad \text{in the imaginary part.} \quad (57)$$

- (2) The ratio of overshoot to the jump height, defined as  $\frac{\Delta_R}{C_R}$  and  $\frac{\Delta_I}{C_I}$ , is a constant  $G_c$  which is real and dependent on the unit window  $W_f(\omega)$  for the class of windows generated by  $W_{fn}(\omega) = W_f(nt_0\omega)$ .

The unit window for the rectangular window is

$$w_f(t) = \begin{cases} 1 & |t| \leq 1 \\ 0 & |t| > 1 \end{cases} \quad (58)$$

and

$$W_f(\omega) = \frac{2 \sin \omega}{\omega} \quad (59)$$

From Eq. (53) we have

$$G^*(\omega) = \frac{1}{2\pi} \int_{-\infty}^{\omega} \frac{2 \sin y}{y} dy \quad (60)$$

and

$$\begin{aligned} G_c &= \text{l.u.b. } \{G^*(\omega)\} - 1 \quad \text{for } \omega \in (0, \infty) \\ &= \int_{-\infty}^{\pi} \frac{\sin y}{\pi y} dy - 1 \\ &= \frac{1}{\pi} \text{Si}(\pi) - \frac{1}{2} \end{aligned} \quad (61)$$

$G_c$  in Eq. (61) is about 8.95%. This is the overshoot ratio for the Gibbs' phenomenon in the frequency domain caused by truncating the Fourier series.

In order to eliminate the generalized Gibbs' phenomenon, we must choose a window such that

$$G_c = \text{l.u.b. } \{G^*(\omega)\} - 1 = 0$$

or

$$\text{l.u.b. } \{G^*(\omega)\} = 1 \quad (62)$$

For a class of windows with unit window

$$W_f(\omega) > 0 \quad \text{for } \omega \in (0, \infty) \quad (63)$$

then  $G^*(\omega)$  is monotonic increasing, and  $G_c = 0$ . Therefore, Eq. (63) gives the sufficient condition for eliminating the generalized Gibbs' phenomenon. The triangular window with the unit window defined as

$$w_f(t) = \begin{cases} 1 - t & 0 \leq t \leq 1 \\ 1 + t & -1 \leq t < 0 \end{cases} \quad (64)$$

has a corresponding frequency function given by

$$W_f(\omega) = \left[ \frac{\sin\left(\frac{\omega}{2}\right)}{\frac{\omega}{2}} \right]^2 \quad (65)$$

Since  $W_f(\omega) \geq 0$  for  $\omega \in (0, \infty)$ , the triangular window can be used to eliminate the Gibbs' phenomenon.

When overshoots of magnitude and phase instead of the real and imaginary parts of the windowed complex period functions are concerned, Eqs. (70) through (73) of Chapter II are valid except that the overshoot ratio (9%) in those equations must be replaced by  $G_c$  of the window which is used.

### 3.5 THE TRAPEZOIDAL WINDOW IN THE FREQUENCY DOMAIN

Consider the trapezoidal window in the frequency domain with the

unit window defined as

$$w_f(t) = \begin{cases} \frac{1-t}{2b} & 1-2b < t \leq 1 \\ 1 & |t| \leq 1-2b \\ \frac{1+t}{2b} & -1 \leq t < -(1-2b) \end{cases} \quad (66)$$

where  $0 < b < 0.5$ . The Fourier Transform of Eq. (66) is given by

$$W_f(\omega) = 2(1-b) \left[ \frac{\sin(b\omega)}{b\omega} \right] \frac{\sin[(1-b)\omega]}{(1-b)\omega} \quad (67)$$

Figures 3-11 through 3-16 show the amplitude response of  $\frac{W_f(\omega)}{W_f(0)}$  for  $\omega \geq 0$  and for  $b = 0, 0.1, 0.2, 0.3, 0.4$  and  $0.5$ , respectively, in both the linear and the logarithmic scale. For  $b = 0$ , as shown in Figure 3-11, the side lobes are underdamped; as a matter of fact, it is a rectangular window. The peak of the highest side lobe, denoted by  $S_m$ , is  $-13.3$  dB. As  $b$  increases,  $S_m$  decreases. When  $b$  is  $0.418$ , as shown in Figure 3-17,  $S_m$  approaches a minimum of  $-32$  dB. When  $b$  is greater than  $0.418$ ,  $S_m$  increases. When  $b = 0.5$ , a triangular window results with  $S_m = -26.5$  dB. Table 3-2 and Figure 3-18 show the peak of the highest side lobe as the function of parameter  $b$ .

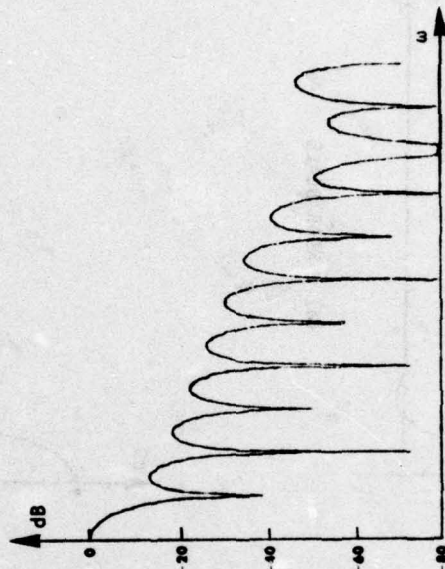
The bandwidth of the main lobe, from Eq. (67), is given by

$$B_w^* = \frac{2\pi}{1-b} \quad (68)$$

and is the same as  $T_w^*$  shown in Figure 3-8. The overshoot ratio  $G_c$  for the generalized Gibbs' phenomenon is the same as  $g_c$  which is the overshoot ratio for the generalized Gibbs' phenomenon in the time domain as shown in Figure 3-7. From Figures 3-7 and 3-18 we see that for  $0.38 < b < 0.5$ , the overshoot ratio  $G_c$  is less than 3% and  $S_m$  is less than  $-26$  dB; therefore, the trapezoidal windows with  $0.38 < b < 0.5$  give good windowing resulting in a small overshoot ratio and overdamped side lobes.

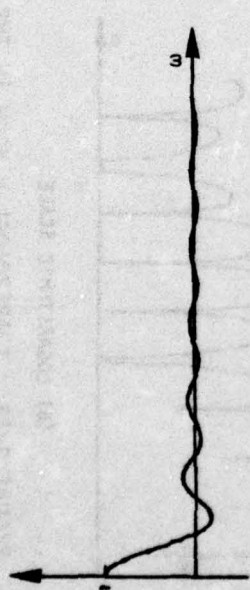


(a) LINEAR SCALE

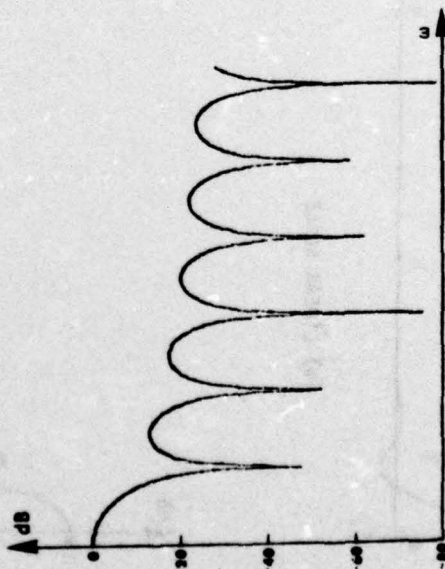


(b) LOGARITHMIC SCALE

FIGURE 3-12. TRAPEZOIDAL WINDOW IN THE FREQUENCY DOMAIN,  $b = 0.1$



(a) LINEAR SCALE

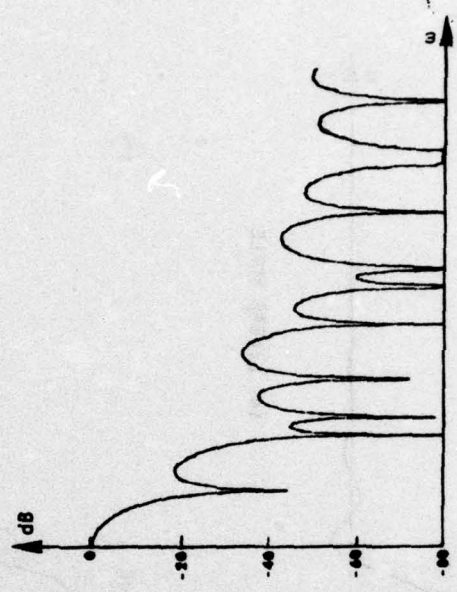


(b) LOGARITHMIC SCALE

FIGURE 3-11. TRAPEZOIDAL WINDOW IN THE FREQUENCY DOMAIN,  $b = 0$

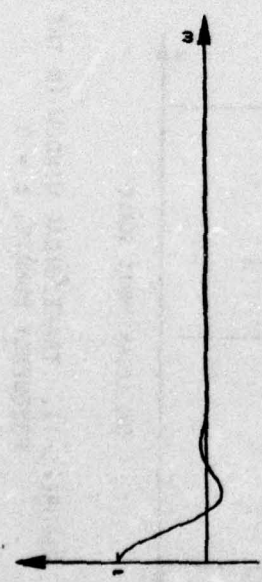


(a) LINEAR SCALE

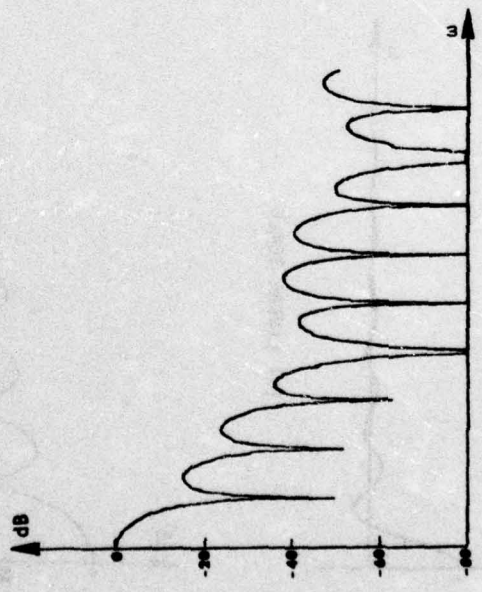


(b) LOGARITHMIC SCALE

FIGURE 3-14. TRAPEZOIDAL WINDOW IN THE FREQUENCY DOMAIN,  $b = 0.3$



(a) LINEAR SCALE



(b) LOGARITHMIC SCALE

FIGURE 3-13. TRAPEZOIDAL WINDOW IN THE FREQUENCY DOMAIN,  $b = 0.2$

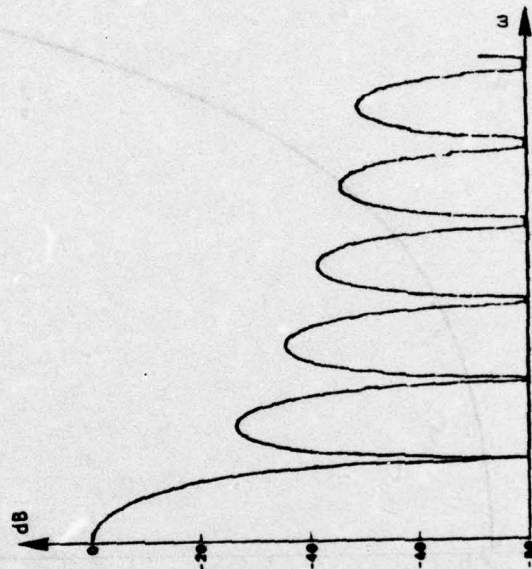
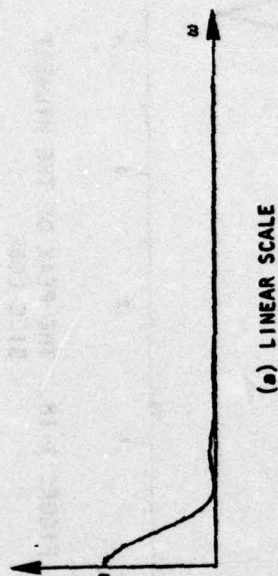


FIGURE 3-15. TRAPEZOIDAL WINDOW IN THE FREQUENCY DOMAIN,  $b = 0.4$

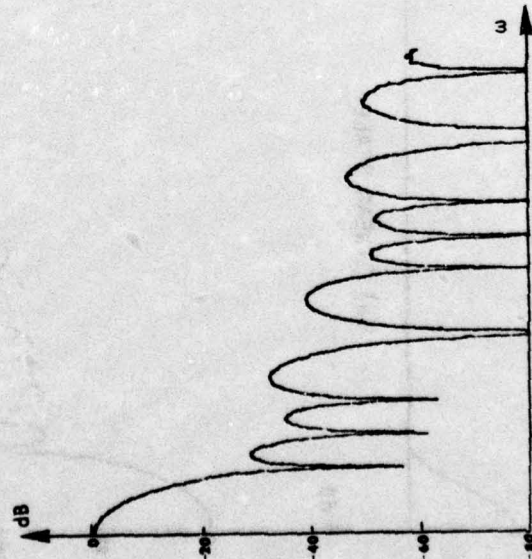
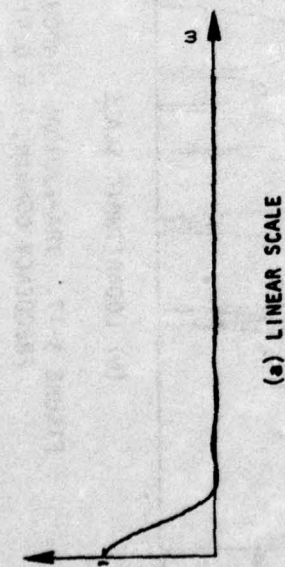


FIGURE 3-16. TRAPEZOIDAL WINDOW IN THE FREQUENCY DOMAIN,  $b = 0.5$

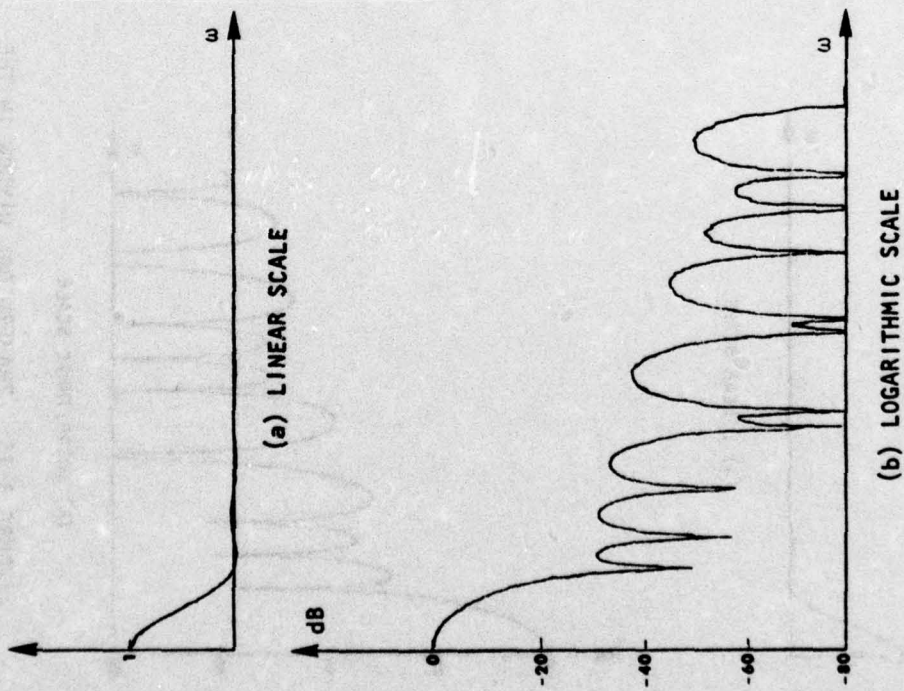


FIGURE 3-17. TRAPEZOIDAL WINDOW IN THE FREQUENCY DOMAIN,  $b = 0.418$

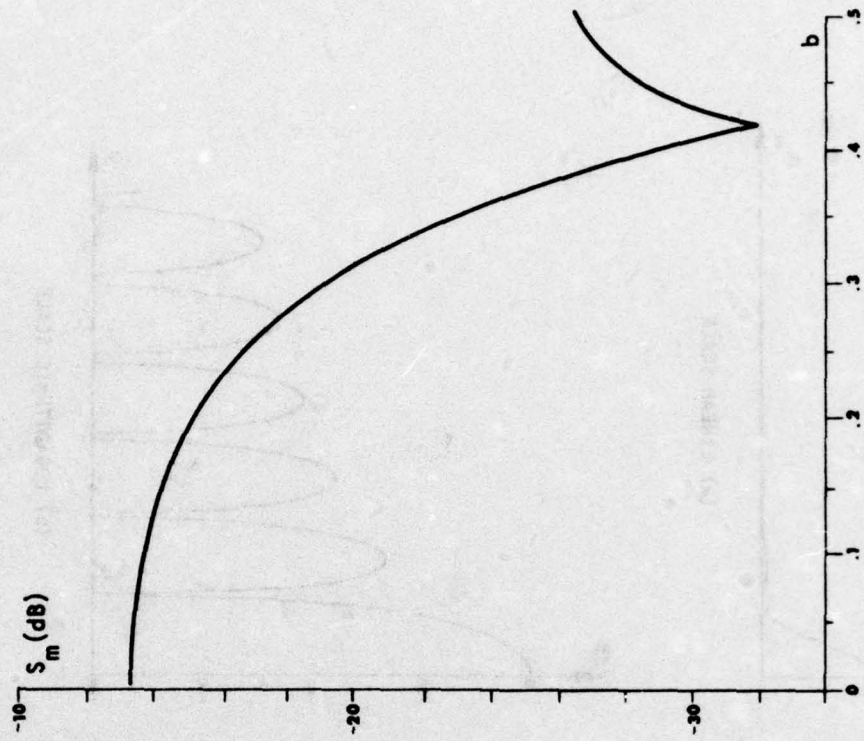


FIGURE 3-18. THE PEAK OF THE HIGHEST SIDE LOBE

TABLE 3-2  
PEAK OF THE HIGHEST SIDE LOBE

b	$S_m$ (dB)
0	-13.3
0.1	-13.6
0.2	-15.1
0.3	-19.0
0.35	-22.7
0.4	-28.8
0.418	-32.0
0.42	-31.6
0.45	-28.4
0.50	-26.5

From Figure 3-17 for  $b = 0.418$ , the peak of the highest side lobe is -32 dB which is the lowest  $S_m$  as shown in Figure 3-18. This is the optimal trapezoidal window and shall be used in the design of nonrecursive filters and compensators.

Program No. 4 (Appendix C) was used to determine the amplitude response of the trapezoidal windowed Fourier Transform of Eq. (1).

The well known Hanning and Hamming windows are defined as:

(1) Unit window for Hanning window

$$\begin{aligned}
 w(\tau) &= 0.5 + 0.5 \cos(\pi\tau) & |t| < 1 \\
 &= 0 & |t| > 1
 \end{aligned} \tag{69}$$

and

$$W(\omega) = \frac{\sin \omega}{\omega} + \frac{1}{2} \frac{\sin(\pi+\omega)}{\pi+\omega} + \frac{1}{2} \frac{\sin(\pi-\omega)}{\pi-\omega} \tag{70}$$

(2) Unit window for Hamming window

$$w(t) = \begin{cases} 0.54 + 0.46 \cos(\pi t) & |t| < 1 \\ 0 & |t| > 1 \end{cases} \quad (71)$$

and

$$W(\omega) = 1.08 \frac{\sin \omega}{\omega} + 0.46 \frac{\sin(\pi + \omega)}{\pi + \omega} + 0.46 \frac{\sin(\pi - \omega)}{\pi - \omega} \quad (72)$$

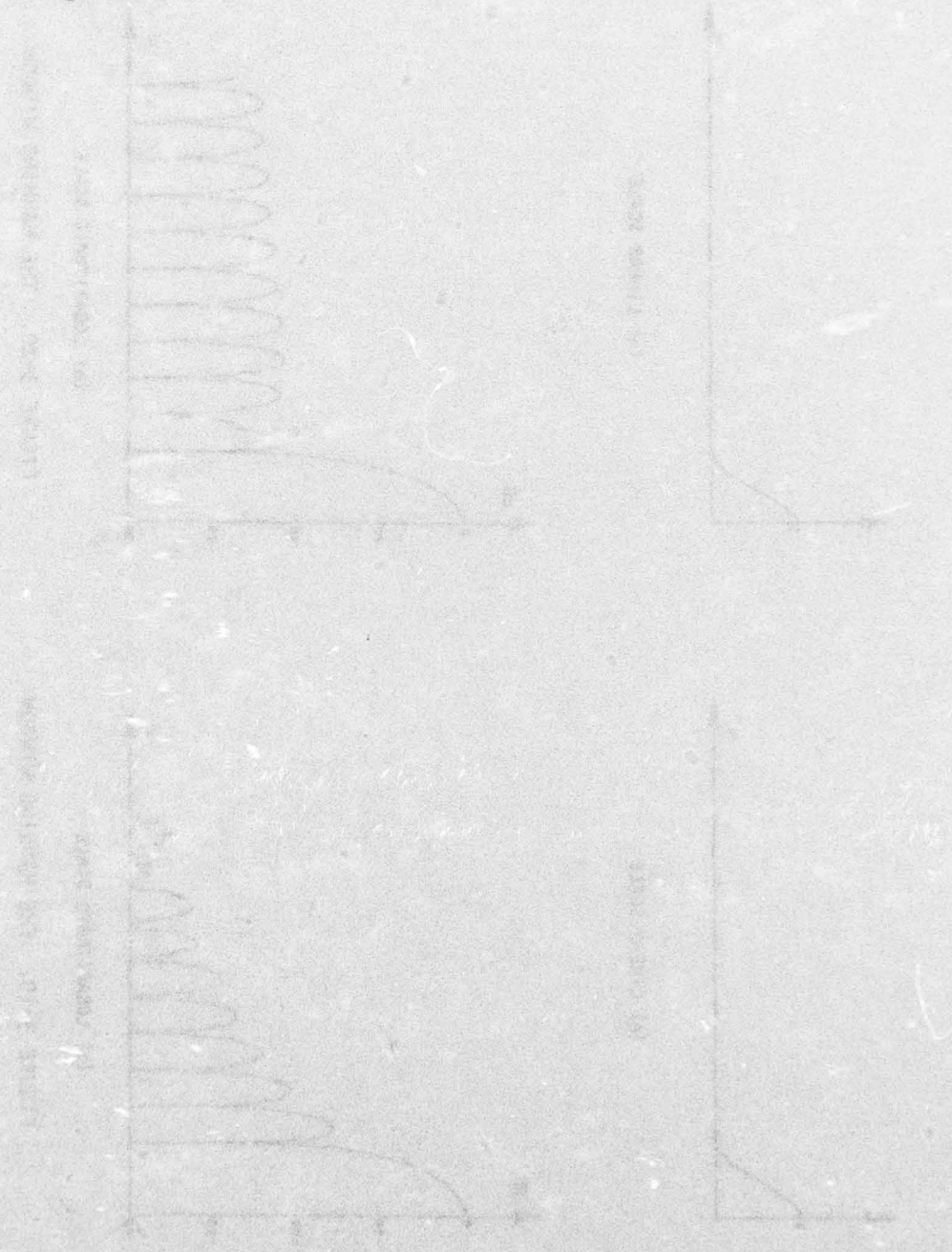
Figures 3-19 and 3-20 show the amplitude response of the Hanning and the Hamming window respectively. The peak of highest side lobes of the Hanning window is -31.5 dB which is somewhat greater than the peak of the optimal trapezoidal window. For the Hamming window,  $S_m$  is equal to -43.2 dB and is much lower than the Hanning window. However, the bandwidth of the main lobe is  $3.44 \pi$  for the optimal trapezoidal window, and  $4\pi$  for both the Hanning and the Hamming windows.

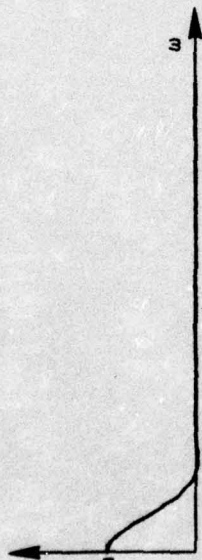
Considering the second example at the end of Chapter II as an illustration of the effect of windowing in the frequency domain, Figures 3-21 and 3-25 show the magnitudes and phases of the truncated Fourier series windowed by a rectangular window for  $n = 16$  and  $256$ , respectively. The results of windowing by trapezoidal windows with  $b = \frac{11}{32}$ ,  $\frac{13}{32}$  and  $\frac{1}{2}$  for  $n = 16$  are shown in Figures 3-22, 3-24 and 3-25 respectively. Figures 3-26, 3-27 and 3-28 show the results of windowing by trapezoidal windows with  $b = \frac{171}{512}$ ,  $\frac{212}{512}$  and  $\frac{1}{2}$ , respectively, for  $n = 256$ . Examination of these waveforms indicates that trapezoidal windows with  $b > 0.3$  are acceptable for windowing in the frequency domain.

### 3.6 REMARKS

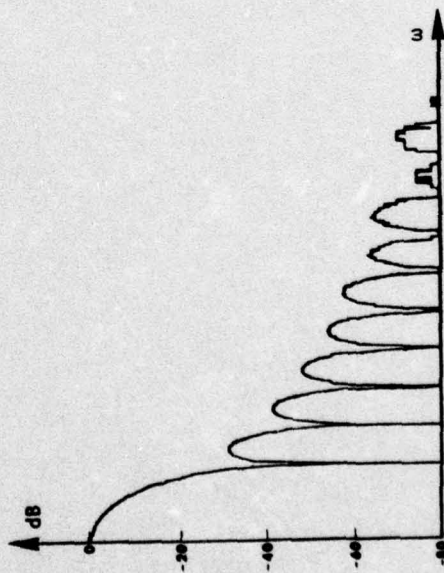
Based on the analysis of the generalized Gibbs' phenomenon, we have explained important functions of various windows both in the time domain and in the frequency domain. For simplicity in exploring the idea, the

trapezoidal window was used to offer a unified picture. In the following chapters, we shall show that this approach is powerful and helpful in design work.



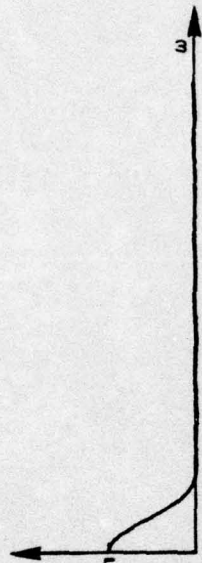


(a) LINEAR SCALE

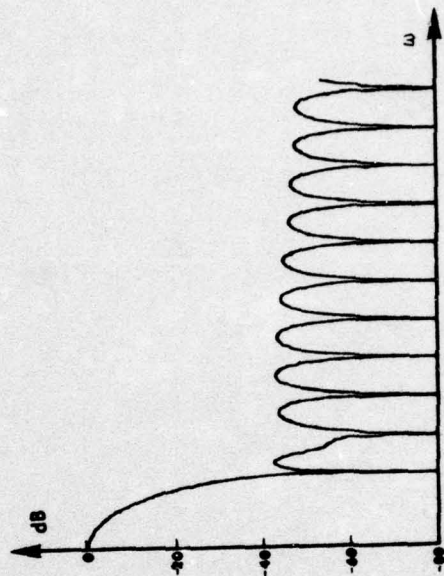


(b) LOGARITHMIC SCALE

FIGURE 3-19. THE HANNING WINDOW



(a) LINEAR SCALE



(b) LOGARITHMIC SCALE

FIGURE 3-20. THE HAMMING WINDOW

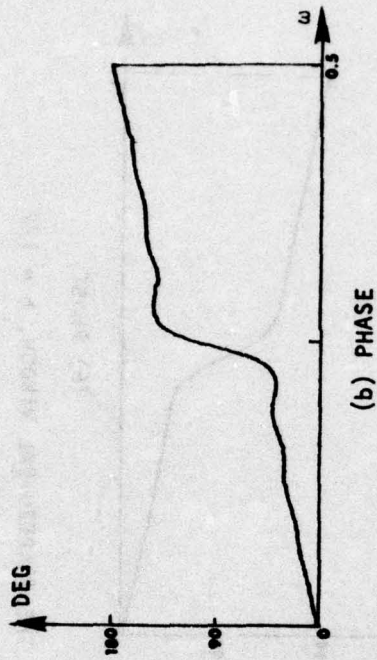
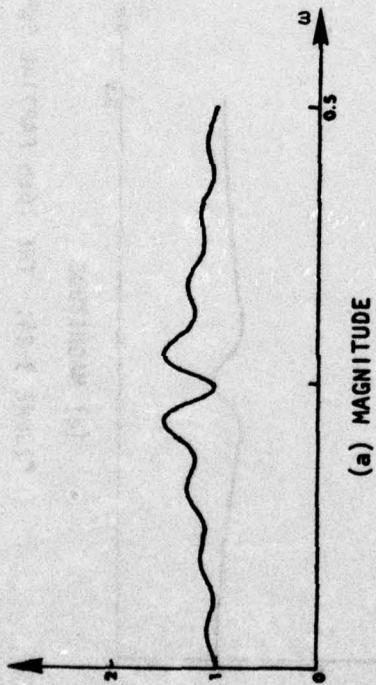


FIGURE 3-21. THE 16th PARTIAL SUM OF THE TRUNCATED FOURIER SERIES

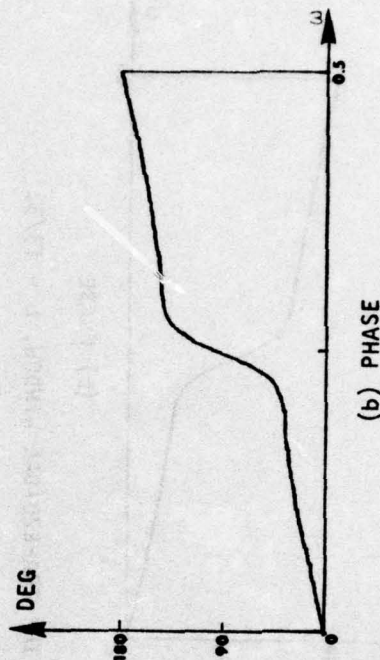
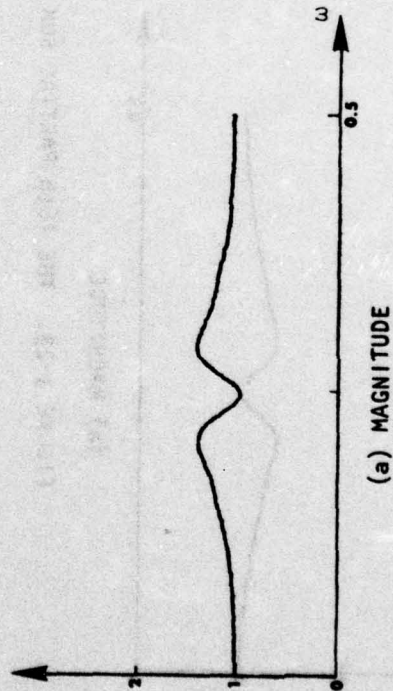
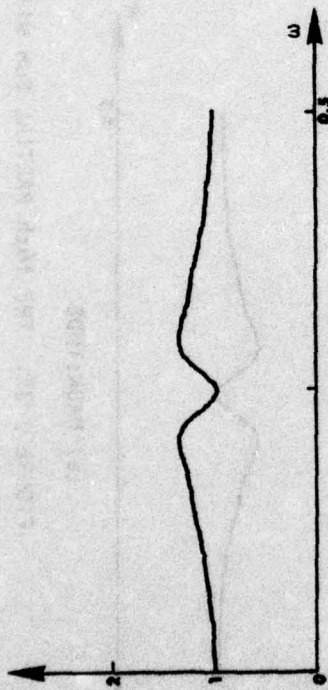
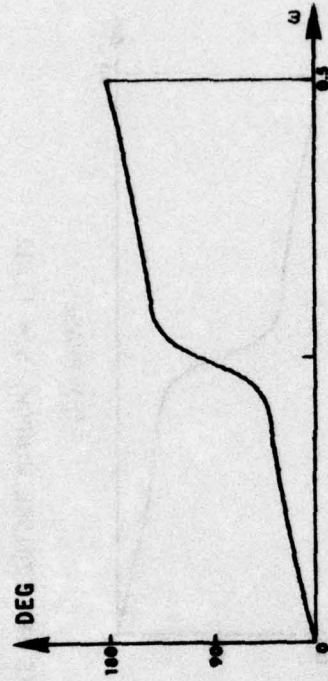


FIGURE 3-22. THE 16th PARTIAL SUM WITH THE TRAPEZOIDAL WINDOW,  $b = 11/32$

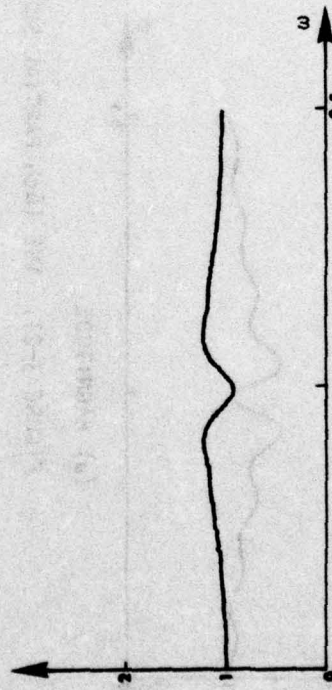


(a) MAGNITUDE



(b) PHASE

FIGURE 3-23. THE 16th PARTIAL SUM WITH THE TRAPEZOIDAL WINDOW,  $b = 13/32$

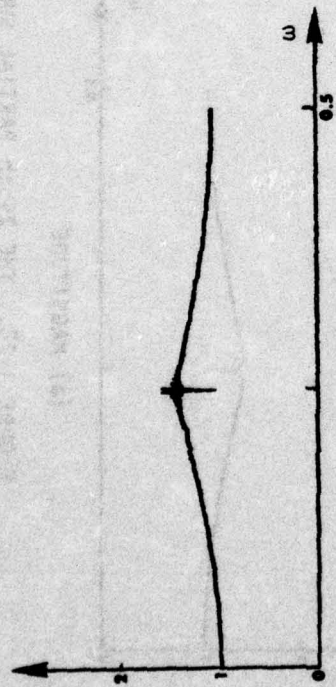


(a) MAGNITUDE

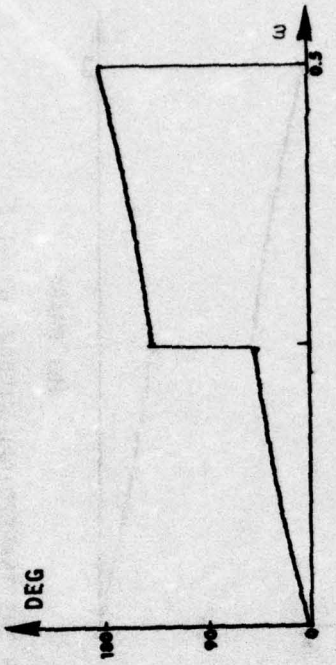


(b) PHASE

FIGURE 3-24. THE 16th PARTIAL SUM WITH THE TRAPEZOIDAL WINDOW,  $b = 1/2$

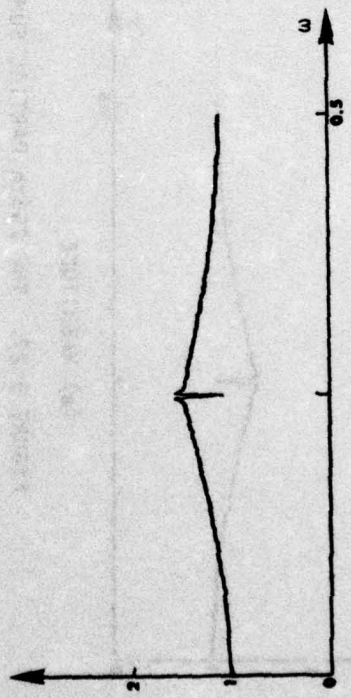


(a) MAGNITUDE

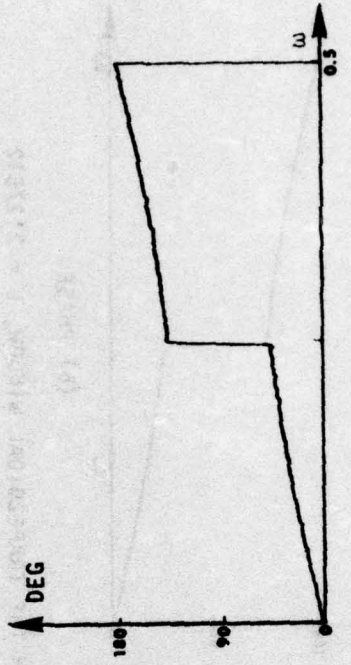


(b) PHASE

FIGURE 3-25. THE 256th PARTIAL SUM OF THE TRUNCATED FOURIER SERIES

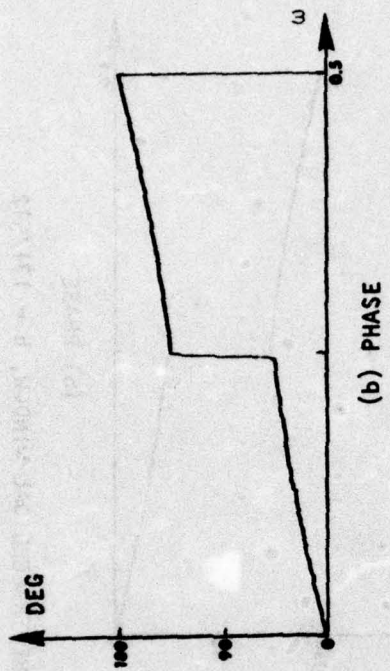


(a) MAGNITUDE



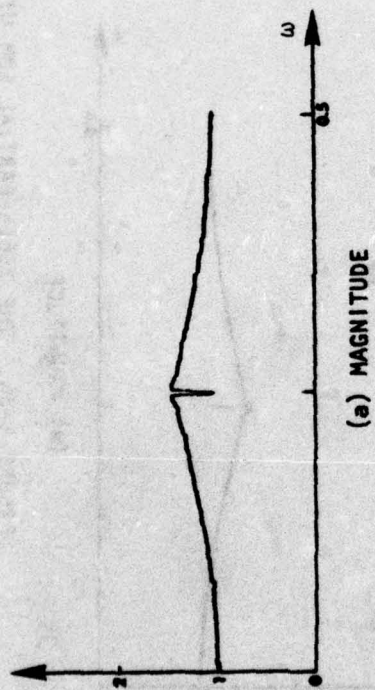
(b) PHASE

FIGURE 3-26. THE 256th PARTIAL SUM WITH THE TRAPEZOIDAL WINDOW,  $b = 171/512$

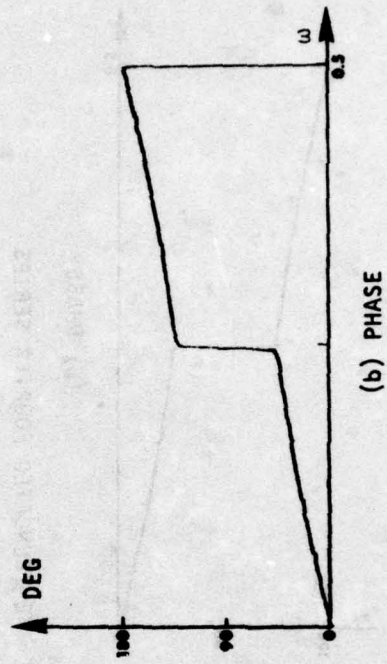


(b) PHASE

FIGURE 3-27. THE 256th PARTIAL SUM WITH THE TRAPEZOIDAL WINDOW,  $b = 212/512$

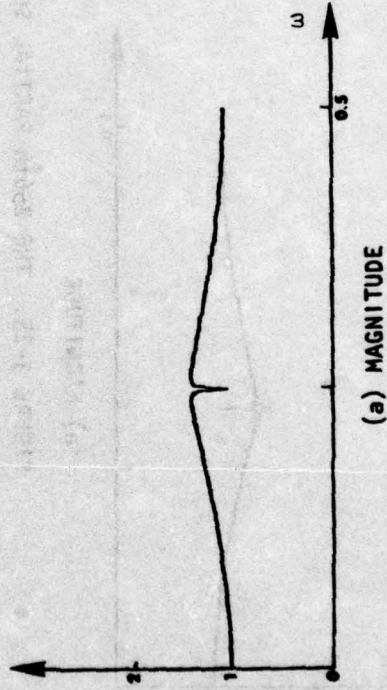


(a) MAGNITUDE



(b) PHASE

FIGURE 3-28. THE 256th PARTIAL SUM WITH THE TRAPEZOIDAL WINDOW,  $b = 1/2$



(a) MAGNITUDE

CHAPTER IV  
DESIGN OF NONRECURSIVE FILTERS USING THE WINDOW METHOD

4.0 INTRODUCTION

Digital filters can be divided into two general classes: recursive and nonrecursive filters. In control systems applications, the nonrecursive filter has two important advantages;

1. A nonrecursive filter has a linear phase function with poles located at  $z = 0$ , therefore, a higher degree of stability is inherent in the system.
2. Since the impulse response of a nonrecursive filter is finite in length, the filter has only a finite memory, so when a short duration disturbance occurs in the input signal, the effect on the output signal will die out after a finite number of sampling periods.

The frequency response of a digital filter is periodic and can be expanded as a Fourier series in the frequency domain. If only a finite number of terms of the Fourier series is taken for practical purposes, we must truncate the Fourier series. Since the frequency response of an ideal filter is always specified as a discontinuous function with a point of discontinuity occurring at the cutoff frequency, the truncation of Fourier series involves the Gibbs' phenomenon and the underdamped side lobe problems. The most straightforward way to solve these problems is through the use of windows.

In this chapter, we will develop a concrete procedure to design nonrecursive filters via the window method<sup>[6-9]</sup>. Starting with low-pass filters and extending the discussion to high-pass, band-pass and band-rejection filters, a new technique of frequency transformation will be established such that the high-pass, band-pass or band-rejection filters designed using this technique will remain nonrecursive.

#### 4.1 LOW-PASS FILTER DESIGN

The transfer function of an  $n$ th order nonrecursive filter can be expressed as

$$F(Z) = \sum_{k=0}^n a_k Z^{-k} \quad (1)$$

Its frequency response is

$$F(e^{j\omega T}) = \sum_{k=0}^n a_k e^{-jk\omega T} \quad (2)$$

where  $T$  is the sample period. Assuming  $n = 2m$ , we have

$$F(e^{j\omega T}) = e^{-jm\omega T} \sum_{k=-m}^m b_k e^{-jk\omega T} \quad (3)$$

where

$$b_k = a_{k-m} \quad (4)$$

Defining

$$F_m(e^{j\omega T}) \triangleq \sum_{k=-m}^m b_k e^{-jk\omega T} \quad (5)$$

Then, we obtain

$$F(e^{j\omega T}) = e^{-jm\omega T} F_m(e^{j\omega T}) \quad (6)$$

In fact, Eq. (5) can be treated as the Fourier series in the frequency domain with period  $\omega_s = \frac{2\pi}{T}$  which is the sampling frequency. In other words, we have

$$b_k = \frac{1}{\omega_s} \int_{-\frac{\omega_s}{2}}^{\frac{\omega_s}{2}} F_m(e^{j\omega T}) e^{jk\omega T} d\omega \quad (7)$$

From Eq. (6), we have

$$|F(Z)| = |F_m(Z)| \quad (8)$$

and

$$\angle F(Z) = \angle F_m(Z) - m\omega T \quad (9)$$

Letting  $\angle F_m(Z) = 0$ , yields

$$\phi(Z) = \angle F(Z) = -m\omega T \quad (10)$$

which means that  $F(Z)$  is a nonrecursive filter with linear phase. From Eq. (5), in order to have  $\angle F_m(Z) = 0$ , we must let

$$b_k = b_{-k} \quad (11)$$

Now, the procedure for designing the nonrecursive filter utilizing the FFT and window techniques can be outlined as follows:

- (1) Specify the magnitude response,  $|F(Z)|$ , and the slope of the linear phase function, defined by  $k_\phi = \frac{d\phi}{d\omega} = -mT$ .
- (2) If the maximum frequency of the signal to be filtered is  $\omega_{\max}$ , then, according to the well known Shannon sampling theorem, the sampling frequency must be equal to or greater than  $2\omega_{\max}$ , or the sampling period  $T$  must be less than or equal to  $\frac{\pi}{\omega_{\max}}$ .

- (3) The order of the nonrecursive filter is  $2m$ , where  $m$  is  $\frac{-k\phi}{T}$ .
- (4) Find the inverse Fourier Transform of the magnitude response,  $|F(Z)| = |F_m(Z)|$ , by using the FFT algorithm.
- (5) The first  $m + 1$  components of the inverse Fourier Transform of  $|F(Z)|$  are  $b_k$ , for  $k = 0, 1, \dots, m$ .
- (6) In order to have a smooth frequency response, windows must be used to modify the coefficients  $b_k$ , obtaining  $b'_k$ , for  $k = 0, 1, \dots, m$ .
- (7) The transfer function of the nonrecursive filter is given by

$$F(Z) = \sum_{k=0}^n a_k Z^{-k} \quad (12)$$

where  $a_k = b'_{k-m}$  and  $b'_{-k} = b'_k$ .

It is often necessary to find the transient and frequency responses of the nonrecursive filter. From Eq. (12), the impulse response is

$$f(t) = \sum_{k=0}^n a_k \delta(t-kt) \quad (12a)$$

Therefore, the impulse response is very easily found once the coefficients of nonrecursive filters are given. The frequency response of the nonrecursive filter is as shown in Eq. (2). Of course, we can find the frequency response directly from Eq. (2) if the coefficients ( $a_k$ 's) are given. However, the frequency response is the Fourier Transform of the impulse response as shown in Eq. (12a). Thus, the "fast" way to find the frequency response is to take the Fourier Transform of the

impulse response using the FFT algorithm (Appendix A). Program No. 5 (Appendix C) is the keyboard program for nonrecursive filter design and for finding the frequency response.

Example 1. A low-pass filter with the amplitude response

$$|F(Z)| = \begin{cases} 1 & |f| < 100 \text{ Hz} \\ 0 & |f| > 100 \text{ Hz} \end{cases}$$

and

$$k_{\phi} = \frac{d\phi}{d\omega} = -0.005 \text{ sec}$$

is required. The sampling frequency is 1600 Hz. Find the nonrecursive filter using the window method.

Solution. Since  $k_{\phi} = \frac{d\phi}{d\omega} = -0.005 = -mT$ , we have

$$m = \frac{k_{\phi}}{T} = 8 \quad (13)$$

Using four different windows, the coefficients of four different nonrecursive filters were determined and listed in Table 4-1. The frequency response of each of the resulting filters is shown in Figures 4-1 through 4-4.

Figure 4-3 depicts the frequency response of the nonrecursive filter designed with the trapezoidal window ( $b = 0.438$ ); note that the peak of the highest side lobe is -39 dB. In Figure 4-4 the frequency response of the nonrecursive filter designed with the Hanning window is shown; note that for this filter the peak of the highest side lobe is -44 dB. From Figures 4-3 and 4-4 we see that the trapezoidal window and the Hanning window are comparable; however, an important advantage

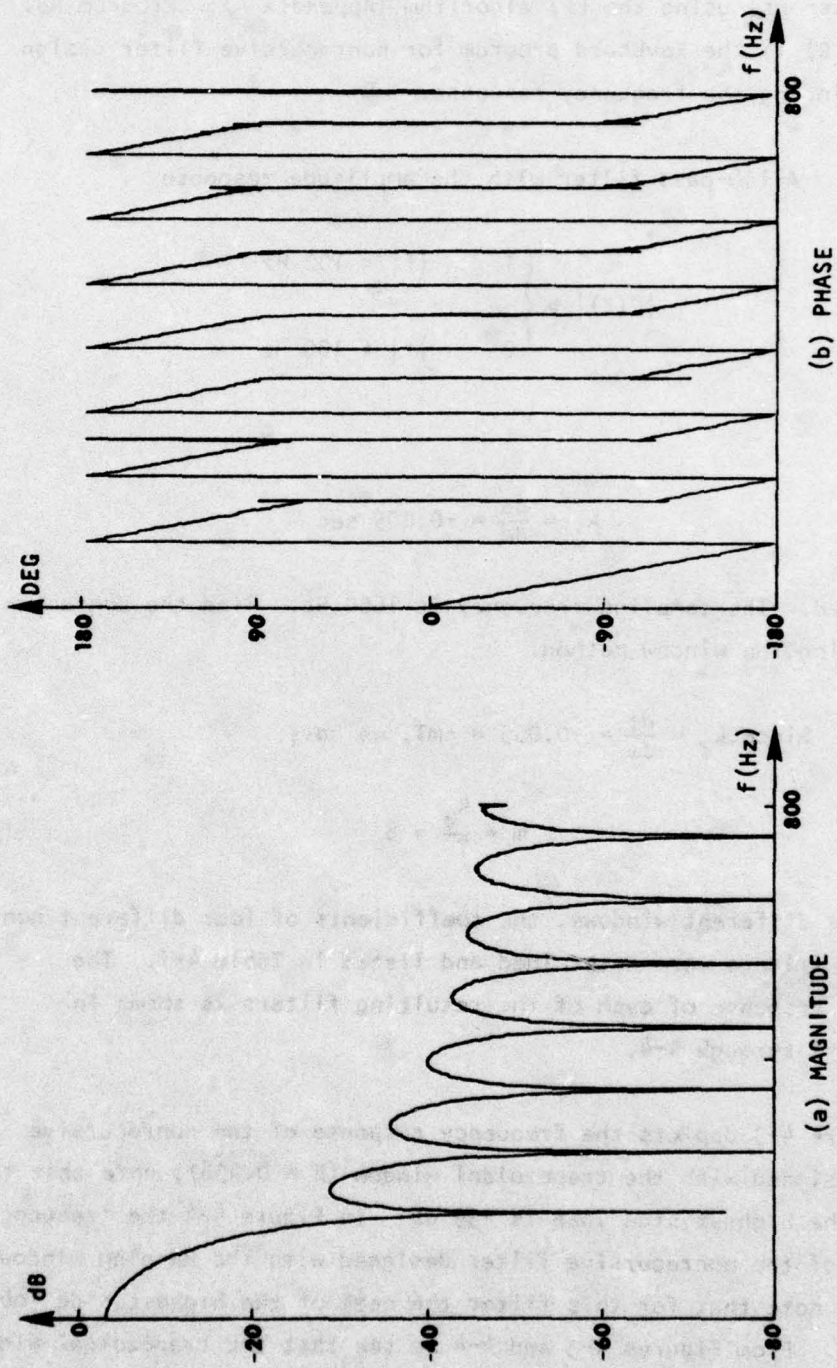


FIGURE 4-1. FREQUENCY RESPONSE OF LOW-PASS FILTER WITH THE RECTANGULAR WINDOW

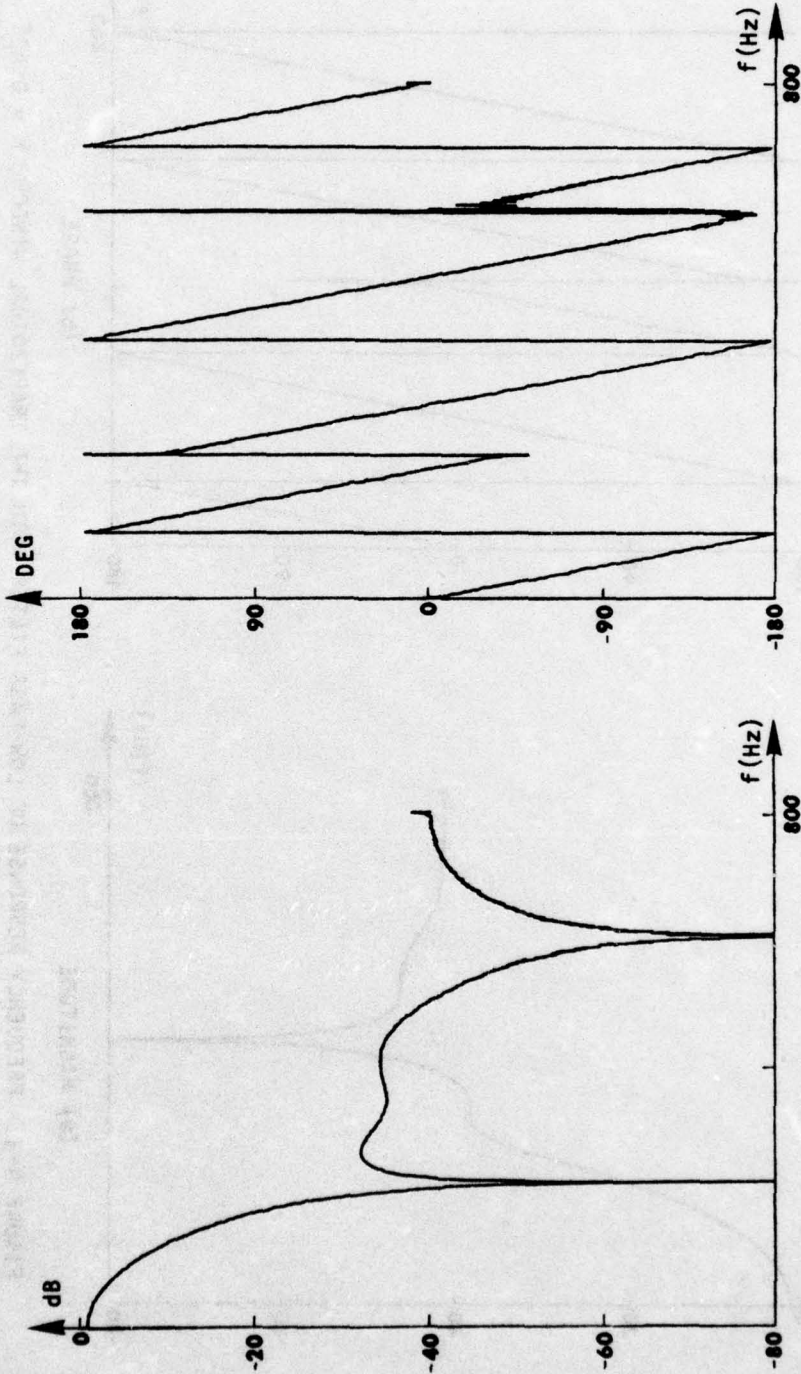


FIGURE 4-2. FREQUENCY RESPONSE OF LOW-PASS FILTER WITH THE TRAPEZOIDAL WINDOW,  $b = 0.375$

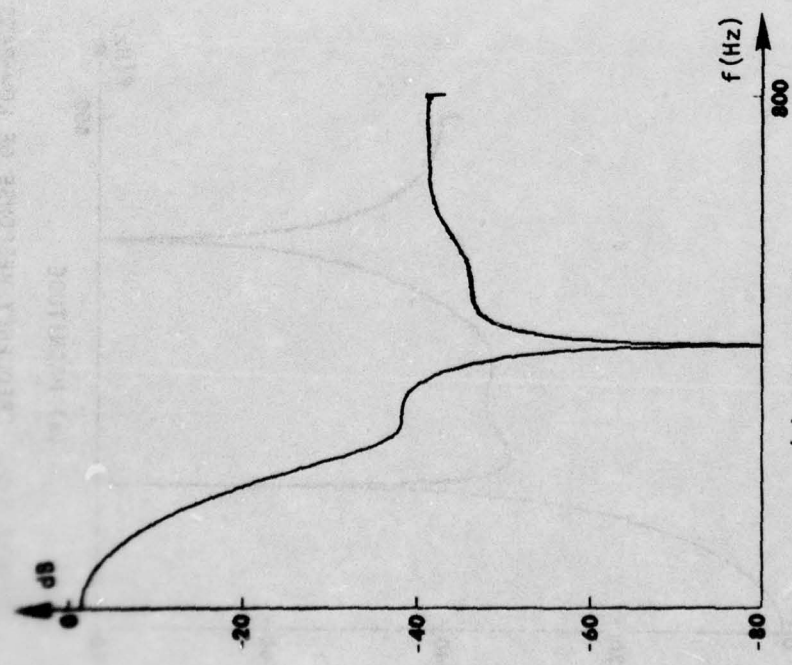
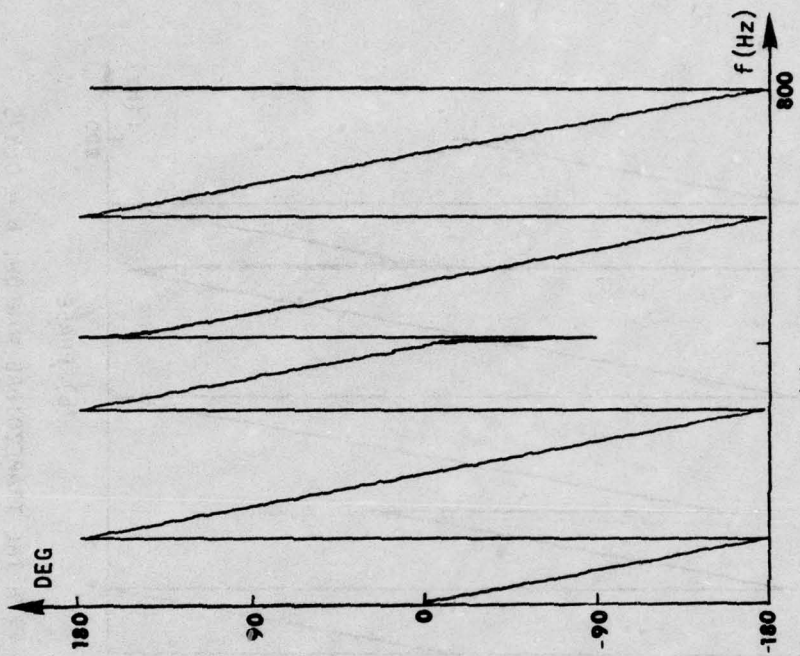


FIGURE 4-3. FREQUENCY RESPONSE OF LOW-PASS FILTER WITH THE TRAPEZOIDAL WINDOW,  $b = 0.438$

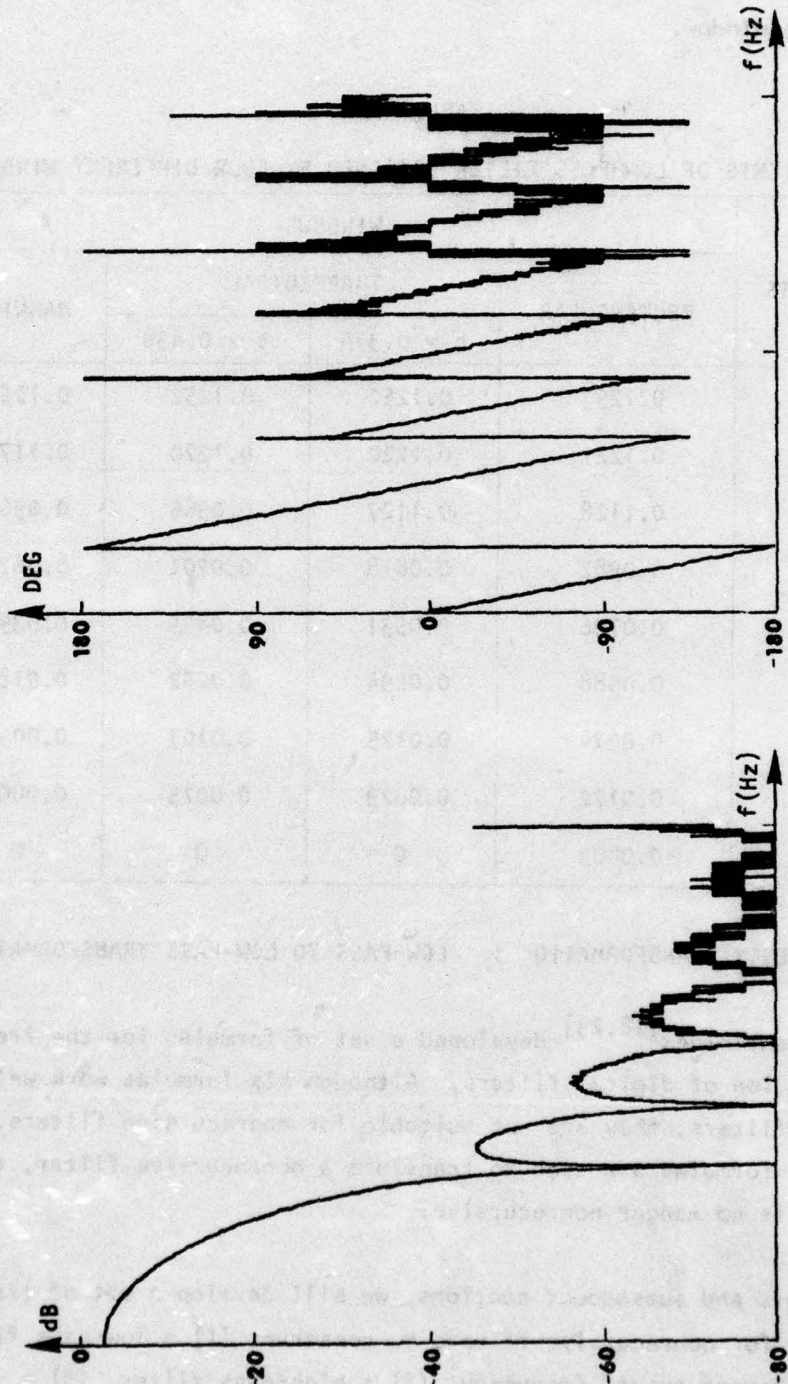


FIGURE 4-4. FREQUENCY RESPONSE OF LOW-PASS FILTER WITH THE HANNING WINDOW

of the trapezoidal window is that it is much easier to construct than the Hanning window.

TABLE 4-1

COEFFICIENTS OF LOW-PASS FILTER DESIGNED BY FOUR DIFFERENT WINDOWS

COEFFICIENTS	WINDOWS			
	RECTANGULAR	TRAPEZOIDAL		HANNING
		b = 0.375	b = 0.438	
$a_8$	0.1253	0.1252	0.1252	0.1252
$a_7 = a_9$	0.1221	0.1220	0.1220	0.1174
$a_6 = a_{10}$	0.1128	0.1127	0.0966	0.0962
$a_5 = a_{11}$	0.0982	0.0818	0.0701	0.0678
$a_4 = a_{12}$	0.0796	0.0531	0.0455	0.0398
$a_3 = a_{13}$	0.0588	0.0294	0.0252	0.0182
$a_2 = a_{14}$	0.0374	0.0125	0.0107	0.0055
$a_1 = a_{15}$	0.0172	0.0029	0.0025	0.0007
$a_0 = a_{16}$	-0.0003	0	0	0

#### 4.2 FREQUENCY TRANSFORMATION 1: LOW-PASS TO LOW-PASS TRANSFORMATION

Constantinides<sup>[18,23]</sup> developed a set of formulas for the frequency transformation of digital filters. Although his formulas work well for recursive filters, they are not suitable for nonrecursive filters. When any of his formulas are used to transform a nonrecursive filter, the resultant is no longer nonrecursive.

In this and subsequent sections, we will develop a set of transformations for nonrecursive filters to construct (1) a low-pass filter with a different cutoff frequency, (2) a high-pass filter, (3) a band-pass filter, and (4) a band-rejection filter, from a low-pass filter

prototype. Let us start with the low-pass filter.

Figure 4-5(a) shows the amplitude response for the ideal low-pass filter with cutoff frequency  $f_c$  and sampling frequency  $f_s$ . A new non-recursive filter with cutoff frequency  $f_d$  as shown in Figure 4-5(b) is required. The coefficients of the low-pass filter with a rectangular window are given by

$$b_k = \frac{1}{\omega_s} \int_{-\frac{\omega_s}{2}}^{\frac{\omega_s}{2}} F_m(e^{j\omega T}) e^{-jk\omega T} d\omega \quad (14)$$

$$= \frac{1}{f_s} \int_{-\frac{f_s}{2}}^{\frac{f_s}{2}} F_m(j2\pi f T) e^{-j2\pi k f T} df \quad (15)$$

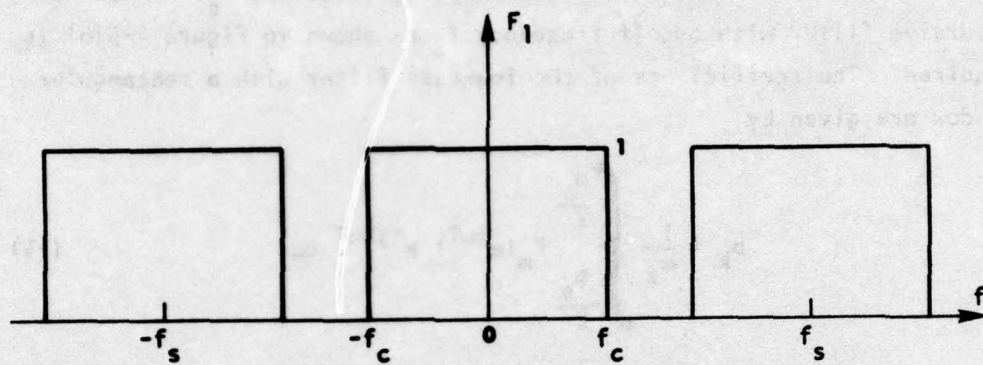
where

$$f_s = \frac{\omega_s}{2\pi} \quad (16)$$

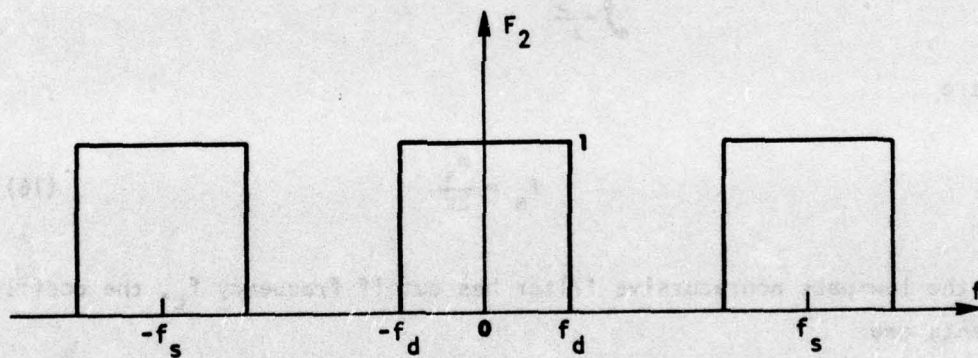
If the low-pass nonrecursive filter has cutoff frequency  $f_c$ , the coefficients are

$$\begin{aligned} b_{kc}^* &= \frac{1}{f_s} \int_{-f_c}^{f_c} e^{-j2\pi k f T} df \\ &= \frac{\sin(2kf_c T)}{\pi k f_s T} \end{aligned} \quad (17)$$

When the window,  $w(t)$ , is used for smoothing the amplitude response, the modified coefficients become



(a) LOW-PASS FILTER WITH CUTOFF FREQUENCY  $f_c$



(b) LOW-PASS FILTER WITH CUTOFF FREQUENCY  $f_d$

FIGURE 4-5. FREQUENCY RESPONSES OF TWO LOW-PASS FILTERS

$$b_{kc} = b_{kc} * w_k \quad (18)$$

where  $w_k$  is the window function sampled at  $t = kT$ , or  $w_k = w(kT)$ . If the cutoff frequency is  $f_d$ , we have the coefficients of the nonrecursive filter with a rectangular window:

$$b_{kd}^* = \frac{\sin(2\pi k f_d T)}{\pi k f_s T} \quad (19)$$

If the window,  $w(t)$ , is used for smoothing the amplitude response, the modified coefficients of the nonrecursive filter are

$$b_{kd} = b_{kd} * w_k \quad (20)$$

From Eqs. (18) and (20) we have

$$b_{kd} = \frac{b_{kd}^*}{b_{kc}^*} b_{kc} \quad (21)$$

Substituting Eqs. (17) and (19) into Eq. (21), yields

$$b_{kd} = \frac{\sin(2\pi k f_d T)}{\sin(2\pi k f_c T)} b_{kc} \quad (22)$$

if  $\sin(2\pi k f_c T) \neq 0$ .

Let us now state the following rule for the low-pass to low-pass transformation:

If the low-pass nonrecursive digital filter is given by

$$F(z) = z^{-m} \sum_{k=-m}^m b_{kc} z^{-k} \quad (23)$$

with cutoff frequency  $f_c$ , the new filter

$$F(Z) = Z^{-m} \sum_{k=-m}^m b_{kd} Z^{-k} \quad (24)$$

where

$$b_{kd} = \frac{\sin(2\pi k f_d T)}{\sin(2\pi k f_c T)} b_{kc} \quad (25)$$

will have the cutoff frequency  $f_f$ , if  $\sin(2\pi k f_c T) \neq 0$ .

**Example 2.** Using the results of Example 1, design a low-pass nonrecursive filter with a cutoff frequency of 200 Hz and the same sampling frequency (1600 Hz).

**Solution.** From Eq. (25), we have

$$b_{kd} = \frac{\sin\left[\frac{\pi}{4} k\right]}{\sin\left[\frac{\pi}{8} k\right]} b_k \quad (26)$$

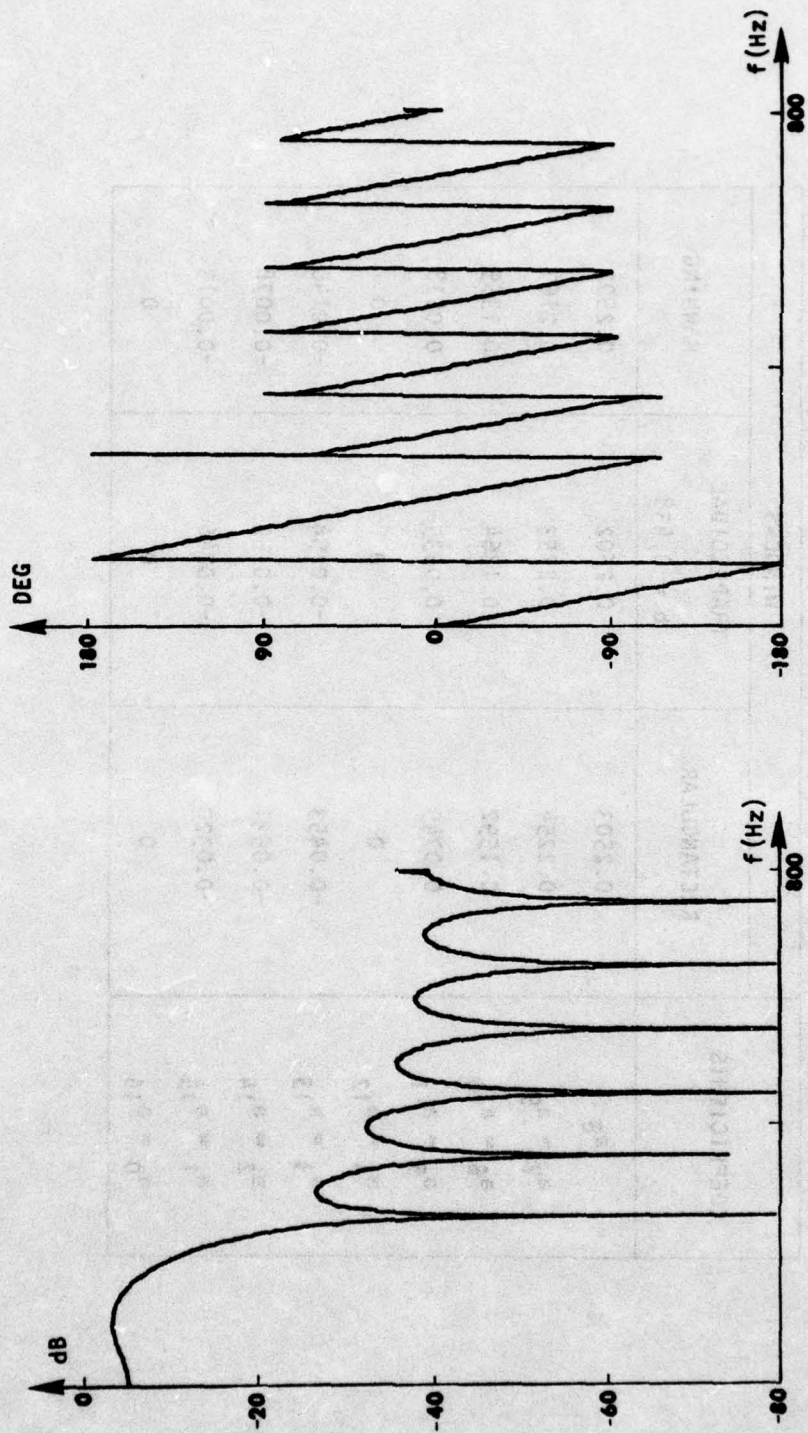
The coefficients of the required nonrecursive filter are listed in Table 4-2. The frequency responses of these three nonrecursive filters are shown in Figures 4-6, 4-7 and 4-8, respectively.

#### 4.3 FREQUENCY TRANSFORMATION II: LOW-PASS TO HIGH-PASS TRANSFORMATION

Figure 4-9 shows the amplitude response of an ideal high-pass filter. If the vertical axis is shifted to  $\frac{f_s}{2}$ , we find that the amplitude response of the high-pass filter with cutoff frequency  $f_h$  and sampling frequency  $f_s$  becomes the amplitude response of the low-pass filter with cutoff frequency  $f_c = \frac{f_s}{2} - f_h$ .

TABLE 4-2  
 COEFFICIENTS OF LOW-PASS FILTERS WITH A CUTOFF FREQUENCY OF 200 HZ

COEFFICIENTS	WINDOWS		
	RECTANGULAR	TRAPEZOIDAL b = 0.438	MANNING
$a_8$	0.2503	0.2502	0.2502
$a_7 = a_9$	0.2254	0.2253	0.2167
$a_6 = a_{10}$	0.1592	0.1364	0.1359
$a_5 = a_{11}$	0.0749	0.0535	0.0518
$a_4 = a_{12}$	0	0	0
$a_3 = a_{13}$	-0.0453	-0.0194	-0.0140
$a_2 = a_{14}$	-0.0531	-0.0152	-0.0078
$a_1 = a_{15}$	-0.0320	-0.0046	-0.0013
$a_0 = a_{16}$	0	0	0



(a) MAGNITUDE  
 (b) PHASE  
 FIGURE 4-6. FREQUENCY RESPONSE OF LOW-PASS FILTER WITH RECTANGULAR WINDOW

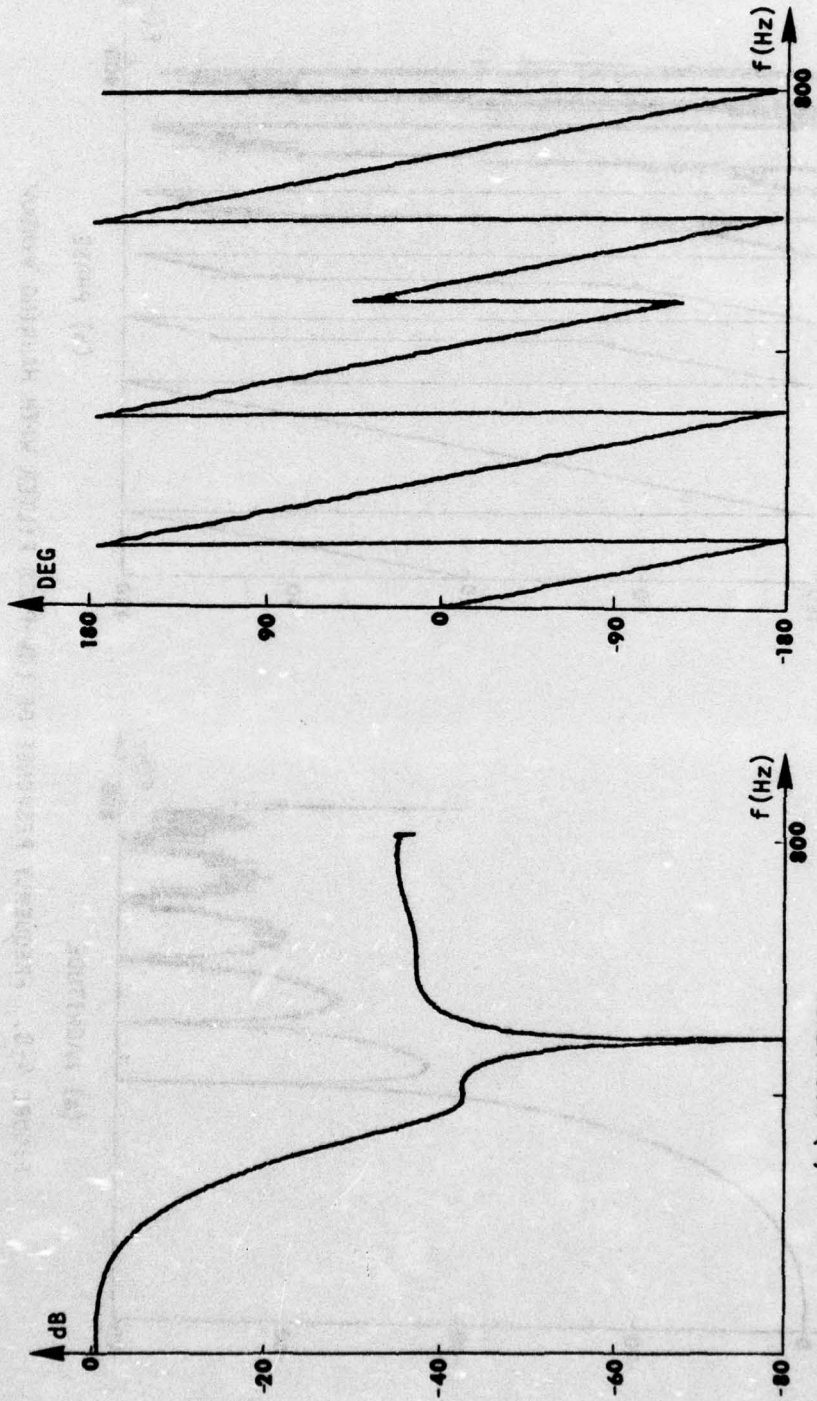


FIGURE 4-7. FREQUENCY RESPONSE OF LOW-PASS FILTER WITH TRAPEZOIDAL WINDOW,  $b = 0.438$

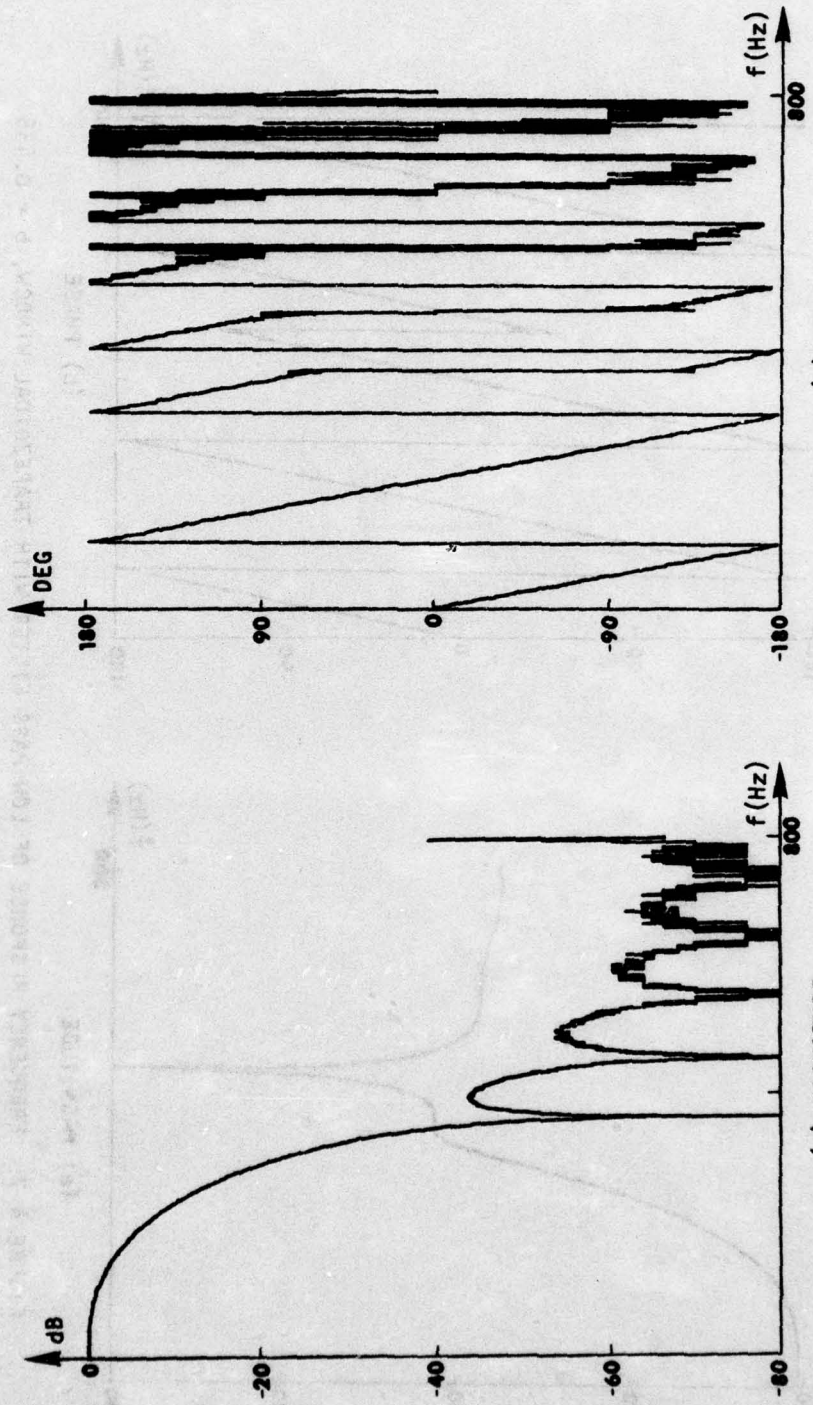


FIGURE 4-8. FREQUENCY RESPONSE OF LOW-PASS FILTER WITH HANNING WINDOW

Mathematically we have

$$\begin{aligned}
 F_h(e^{j2\pi fT}) &= F_h(Z) \Big|_{Z = e^{j2\pi fT}} \\
 &= F_\ell \left[ e^{j2\pi T \left( f - \frac{f_s}{2} \right)} \right]
 \end{aligned} \tag{27}$$

where  $F_h(Z)$  is the transfer function of the high-pass filter and  $F_\ell(Z)$  is the transfer function of the low-pass filter. Assume that the transfer function of the low-pass filter with cutoff frequency  $f_c$  is

$$F_\ell(Z) = Z^{-m} \sum_{k=-m}^m a_k Z^{-k} \tag{28}$$

From Eq. (27) we have

$$F_h(Z) = F_\ell(e^{-j\pi f_s T} Z) \tag{29}$$

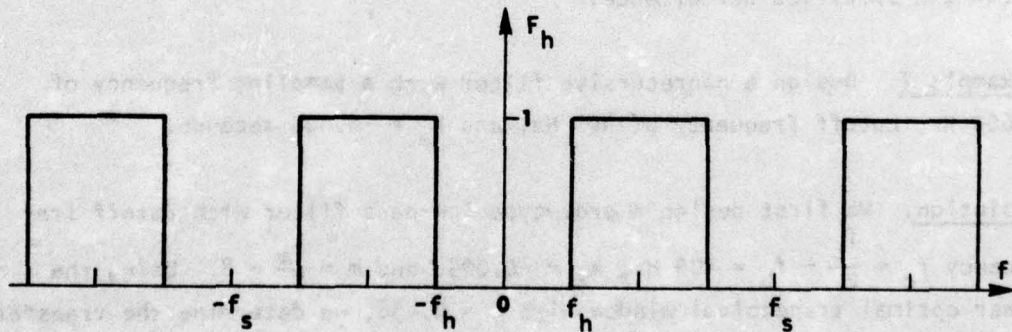


FIGURE 4-9. THE AMPLITUDE RESPONSE OF AN IDEAL HIGH-PASS FILTER

Since  $f_s = \frac{1}{T}$ , Eq. (29) becomes

$$\begin{aligned} F_h(Z) &= F_1(e^{-j\pi}Z) \\ &= F_1(-Z) \end{aligned} \quad (30)$$

Combining Eqs. (28) and (30), yields

$$\begin{aligned} F_h(Z) &= (-Z)^{-m} \sum_{k=-m}^m a_k (-Z)^{-k} \\ &= Z^{-m} \sum_{k=-m}^m (-1)^{m-k} a_k Z^{-k} \end{aligned} \quad (31)$$

In brief, we have the following rule for the low-pass to high-pass transformation:

If a high-pass nonrecursive filter with  $\frac{d\phi}{d\omega} = k_\phi$ , cutoff frequency  $f_h$ , and sampling frequency  $f_s$  is required, we first design a low-pass nonrecursive filter with cutoff frequency  $f_c = \frac{f_s}{2} - f_h$  and  $\frac{d\phi}{d\omega} = k_\phi$ ; then substituting  $Z$  by  $-Z$ , we arrive at the high-pass nonrecursive filter with the specified performance.

**Example 3.** Design a nonrecursive filter with a sampling frequency of 1600 Hz, cutoff frequency of 400 Hz, and  $k_\phi = -0.005$  seconds.

**Solution.** We first design a prototype low-pass filter with cutoff frequency  $f_c = \frac{f_s}{2} - f_h = 400$  Hz,  $k_\phi = -0.005$ , and  $m = \frac{k_\phi}{T} = 8$ . Using the near optimal trapezoidal window with  $b = 0.438$ , we determine the transfer function of the prototype low-pass filter

$$F_1(Z) = Z^{-8} \sum_{k=-8}^8 a_k Z^{-k} \quad (32)$$

where

$$a_8 = a_{-8} = 0$$

$$a_7 = a_{-7} = -0.0065$$

$$a_6 = a_{-6} = -0.0001$$

$$a_5 = a_{-5} = 0.0273$$

$$a_4 = a_{-4} = 0.0002$$

$$a_3 = a_{-3} = -0.0759$$

$$a_2 = a_{-2} = -0.0003$$

$$a_1 = a_{-1} = 0.3183$$

$$a_0 = 0.5001 \quad (33)$$

Now, replacing  $Z$  by  $-Z$ , we have the nonrecursive high-pass filter

$$F_h(z) = z^{-8} \sum_{k=-8}^8 b_k z^{-k} \quad (34)$$

AD-A034 027

ARMY MISSILE RESEARCH DEVELOPMENT AND ENGINEERING LAB--ETC F/8 9/4  
ANALYSIS AND DESIGN OF DIGITAL CONTROL SYSTEMS. PART II. PRINCI--ETC(U)  
OCT 76 R E YATES, Y T TSAY, C F CHEN

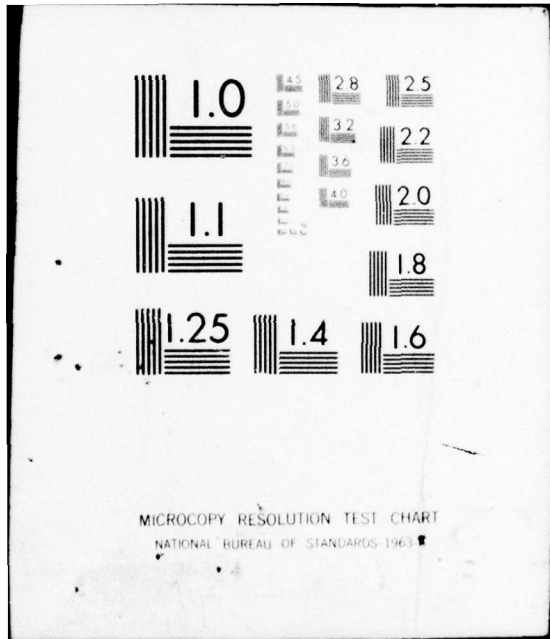
UNCLASSIFIED

R6-77-3

NL

2 of 3  
AD  
A034027





MICROCOPY RESOLUTION TEST CHART  
NATIONAL BUREAU OF STANDARDS-1963-A

where

$$b_8 = b_{-8} = 0$$

$$b_7 = b_{-7} = 0.0065$$

$$b_6 = b_{-6} = -0.0001$$

$$b_5 = b_{-5} = -0.0273$$

$$b_4 = b_{-4} = 0.0002$$

$$b_3 = b_{-3} = 0.0759$$

$$b_2 = b_{-2} = -0.0003$$

$$b_1 = b_{-1} = -0.3183$$

$$b_0 = 0.5001 \quad (35)$$

The amplitude response and phase characteristics of the filter defined by Eq. (34) are shown in Figure 4-10.

#### 4.4 DESIGN OF A NONRECURSIVE BAND-PASS FILTER

Let

$$F_h(z) = z^{-m} \sum_{k=-m}^m a_k z^{-k} \quad (36)$$

and

$$F_l(z) = z^{-m} \sum_{k=-m}^m b_k z^{-k} \quad (37)$$

be the transfer functions of a high-pass filter with cutoff frequency  $f_h$  and a low-pass filter with cutoff frequency  $f_c$ , respectively.

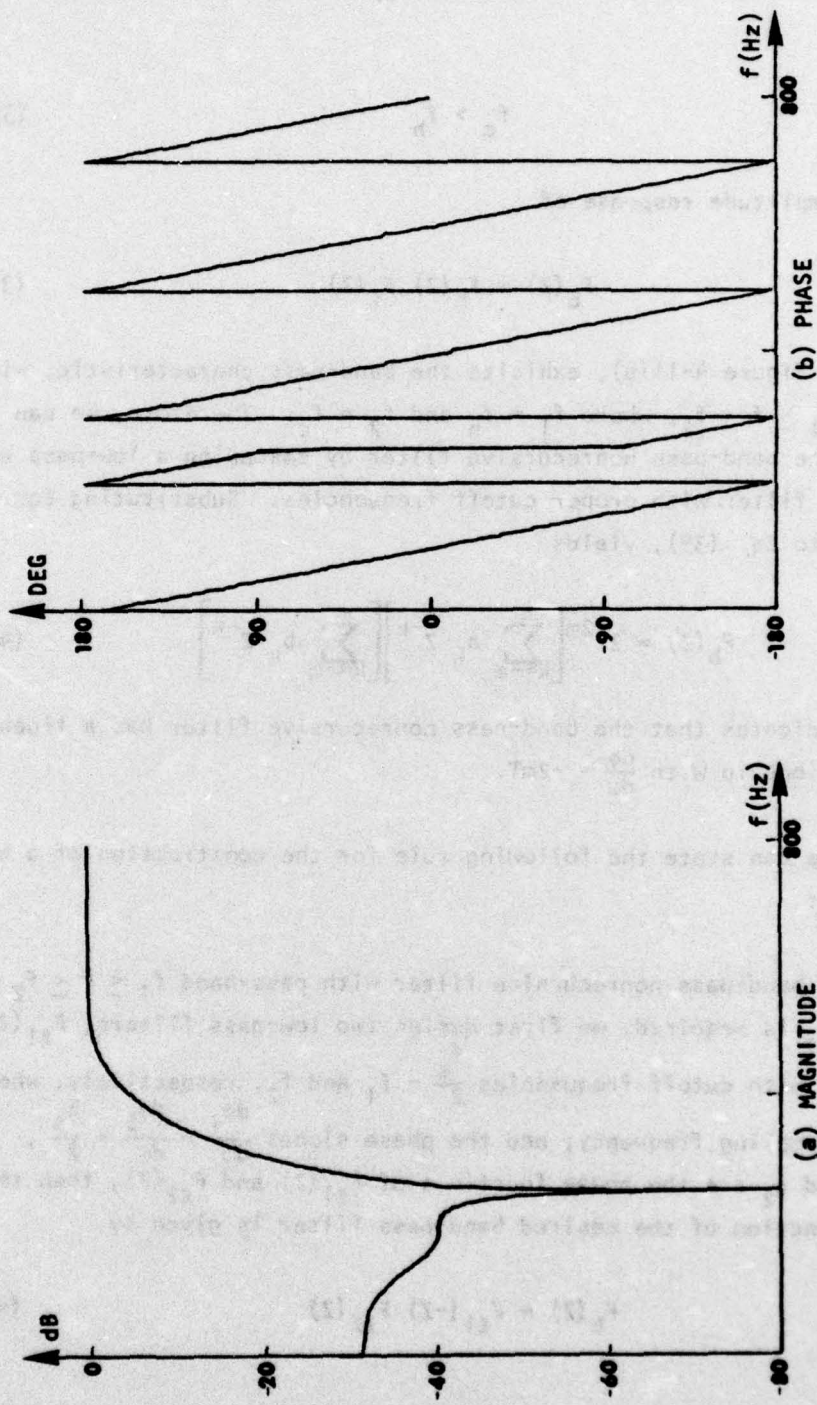


FIGURE 4-10. FREQUENCY RESPONSE OF HIGH-PASS FILTER WITH TRAPEZOIDAL WINDOW,  $b = 0.438$

Figure 4-11(a) shows the amplitude responses of Eqs. (36) and (37). Assume that

$$f_c > f_h \quad (38)$$

Then, the amplitude response of

$$F_b(z) = F_h(z) F_l(z) \quad (39)$$

as shown in Figure 4-11(b), exhibits the band-pass characteristic, with pass band  $f_1 \leq f \leq f_2$ , where  $f_1 = f_h$  and  $f_2 = f_c$ . Therefore, we can construct the band-pass nonrecursive filter by cascading a low-pass and a high-pass filter with proper cutoff frequencies. Substituting Eqs. (36) and (37) into Eq. (39), yields

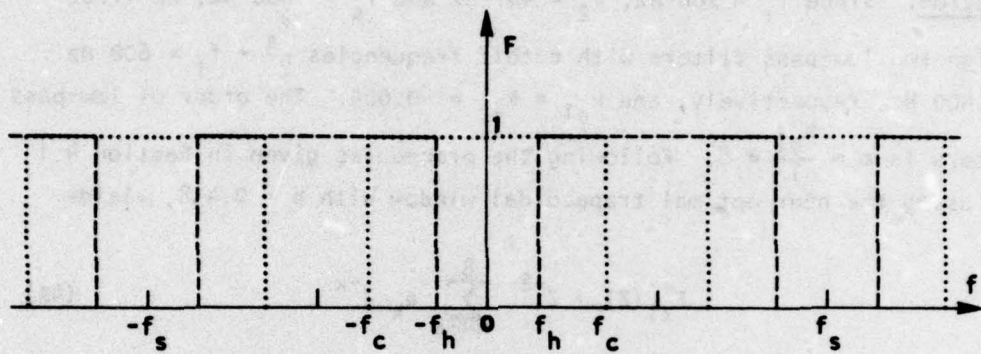
$$F_b(z) = z^{-2m} \left[ \sum_{k=-m}^m a_k z^{-k} \right] \left[ \sum_{k=-m}^m b_k z^{-k} \right] \quad (40)$$

Eq. (40) indicates that the band-pass nonrecursive filter has a linear phase relationship with  $\frac{d\phi}{d\omega} = -2mT$ .

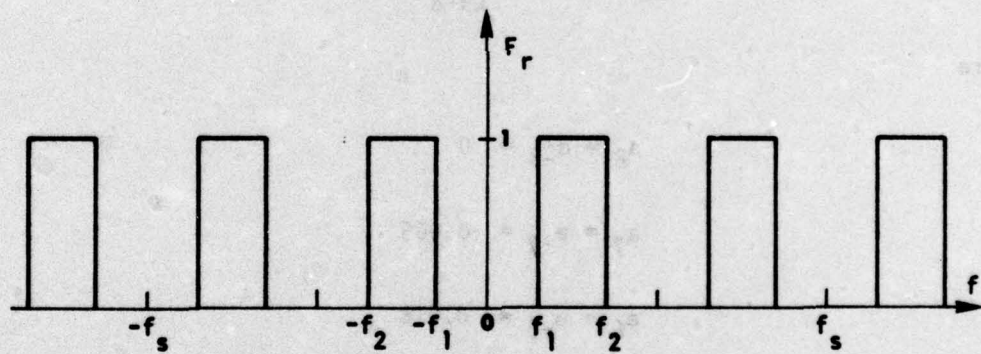
Now, we can state the following rule for the construction of a band-pass filter:

If the band-pass nonrecursive filter with pass-band  $f_1 \leq f \leq f_2$  and  $\frac{d\phi}{d\omega} = k_\phi$  is required, we first design two low-pass filters,  $F_{l1}(z)$  and  $F_{l2}(z)$ , with cutoff frequencies  $\frac{f_s}{2} - f_1$  and  $f_2$ , respectively, where  $f_s$  is the sampling frequency; and the phase slopes  $\frac{d\phi_1}{d\omega} = \frac{d\phi_2}{d\omega} = \frac{k_\phi}{2}$ , where  $\phi_1$  and  $\phi_2$  are the phase functions of  $F_{l1}(z)$  and  $F_{l2}(z)$ , then the transfer function of the desired band-pass filter is given by

$$F_b(z) = F_{l1}(-z) F_{l2}(z) \quad (41)$$



(a) LOW-PASS AND HIGH-PASS FILTER



(b) BAND-PASS FILTER

FIGURE 4-11. CONSTRUCTION OF THE BAND-PASS FILTER FROM A LOW-PASS AND A HIGH-PASS FILTER

**Example 4.** Design a band-pass filter with pass band  $200 \text{ Hz} \leq f \leq 400 \text{ Hz}$  and  $\frac{d\phi}{d\omega} = -0.01 \text{ sec}$ . The sampling frequency is 1600 Hz.

**Solution.** Since  $f_1 = 200 \text{ Hz}$ ,  $f_2 = 400 \text{ Hz}$  and  $f_s = 1600 \text{ Hz}$ , we first design two low-pass filters with cutoff frequencies  $\frac{f_s}{2} - f_1 = 600 \text{ Hz}$  and  $400 \text{ Hz}$ , respectively, and  $k_{\phi 1} = k_{\phi 2} = -0.005$ . The order of low-pass filters is  $m = \frac{k_{\phi 1}}{T} = 8$ . Following the procedures given in Section 4.1 and using the near optimal trapezoidal window with  $b = 0.438$ , yields

$$F_{L1}(z) = z^{-8} \sum_{k=-8}^8 a_k z^{-k} \quad (42)$$

and

$$F_{L2}(z) = z^{-8} \sum_{k=-8}^8 b_k z^{-k} \quad (43)$$

where

$$a_8 = a_{-8} = 0$$

$$a_7 = a_{-7} = -0.005$$

$$a_6 = a_{-6} = 0.016$$

$$a_5 = a_{-5} = -0.020$$

$$a_4 = a_{-4} = -0.001$$

$$a_3 = a_{-3} = 0.054$$

$$a_2 = a_{-2} = -0.137$$

$$a_1 = a_{-1} = 0.225$$

$$a_0 = 0.750 \quad (44)$$

and

$$b_8 = b_{-8} = 0$$

$$b_7 = b_{-7} = -0.0065$$

$$b_6 = b_{-6} = -0.0001$$

$$b_5 = b_{-5} = 0.0273$$

$$b_4 = b_{-4} = 0.0002$$

$$b_3 = b_{-3} = -0.0759$$

$$b_2 = b_{-2} = -0.0003$$

$$b_1 = b_{-1} = 0.3183$$

$$b_0 = 0.5001 \quad (45)$$

Now, using Eq. (41) the transfer function of the band-pass filter becomes

$$\begin{aligned} F_b(z) &= F_{l1}(-z) F_{l2}(z) \\ &= z^{-16} \sum_{k=-16}^{16} c_k z^{-k} \end{aligned} \quad (46)$$

where

$$c_{16} = c_{-16} = 0$$

$$c_{15} = c_{-15} = 0$$

$$c_{14} = c_{-14} = -0.0001$$

$$c_{13} = c_{-13} = -0.0002$$

$$c_{12} = c_{-12} = -0.0001$$

$$c_{11} = c_{-11} = 0.0004$$

$$c_{10} = c_{-10} = 0.0005$$

$$c_9 = c_{-9} = -0.0004$$

$$c_8 = c_{-8} = -0.0001$$

$$c_7 = c_{-7} = -0.0015$$

$$c_6 = c_{-6} = 0.0145$$

$$c_5 = c_{-5} = 0.0460$$

$$c_4 = c_{-4} = -0.0001$$

$$c_3 = c_{-3} = -0.1320$$

$$c_2 = c_{-2} = -0.1429$$

$$c_1 = c_{-1} = 0.0935$$

$$c_0 = 0.2410$$

(47)

The frequency response of the band-pass filter as expressed in Eq. (46) is shown in Figure 4-12.

#### 4.5 DESIGN OF A NONRECURSIVE BAND-REJECTION FILTER

Let

$$F_h(z) = z^{-m} \sum_{k=-m}^m a_k z^{-k} \quad (48)$$

and

$$F_l(z) = z^{-m} \sum_{k=-m}^m b_k z^{-k} \quad (49)$$

be the transfer functions of a high-pass filter with cutoff frequency  $f_h$  and a low-pass filter with cutoff frequency  $f_c$ , respectively. Figure 4-13(a) shows the amplitude responses of Eqs. (48) and (49). Assume that

$$f_h > f_c \quad (50)$$

Then the amplitude response of

$$F_r(z) = F_h(z) + F_l(z) \quad (51)$$

as shown in Figure 4-13(b), exhibits the band-rejection characteristics, with rejection band  $f_1 \leq f \leq f_2$  where  $f_1 = f_c$  and  $f_2 = f_h$ . Therefore, we can construct the band-rejection nonrecursive filter by the parallel connection of a high-pass and a low-pass filter with proper cutoff frequencies. Substituting Eqs. (48) and (49) into Eq. (51), yields

$$F_r(z) = z^{-m} \sum_{k=-m}^m (a_k + b_k) z^{-k} \quad (52)$$

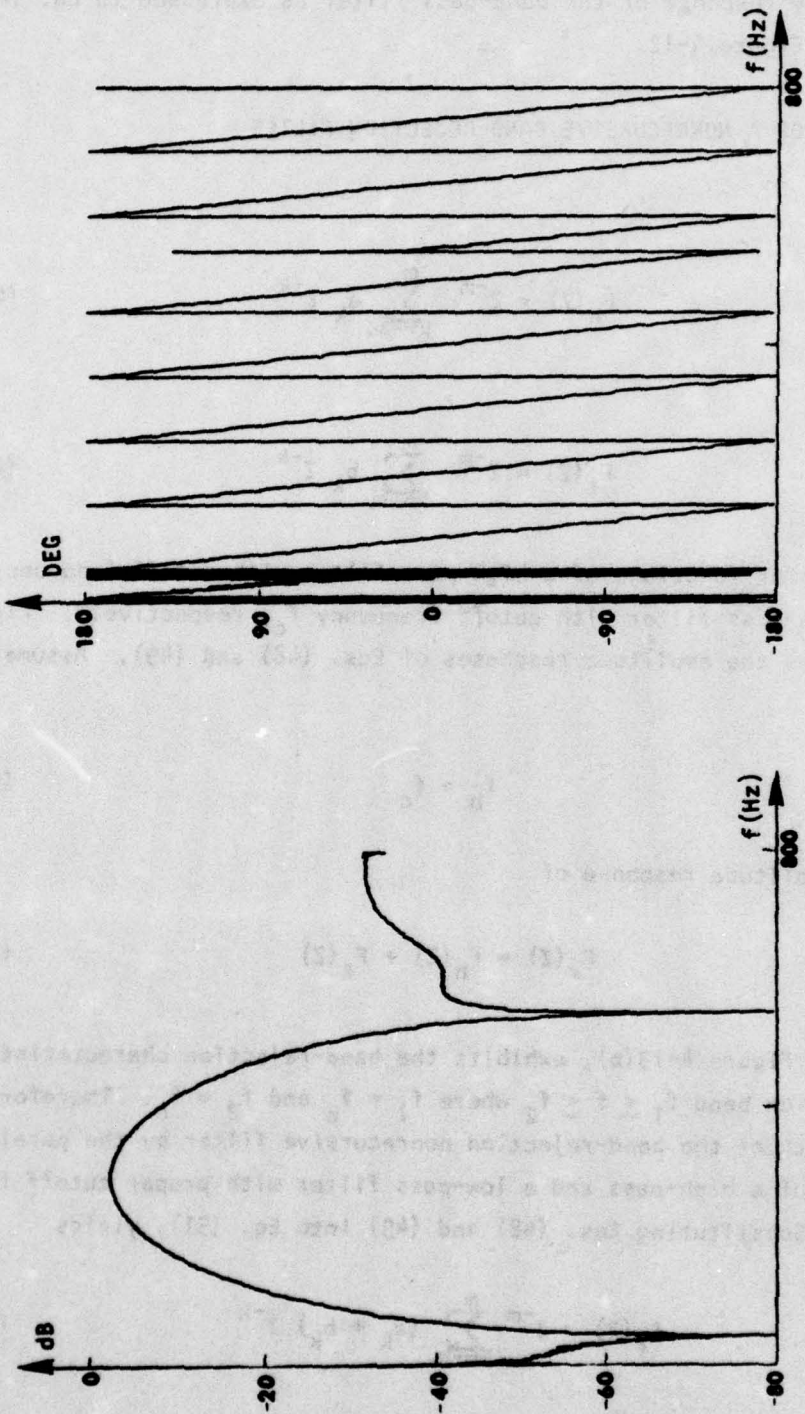
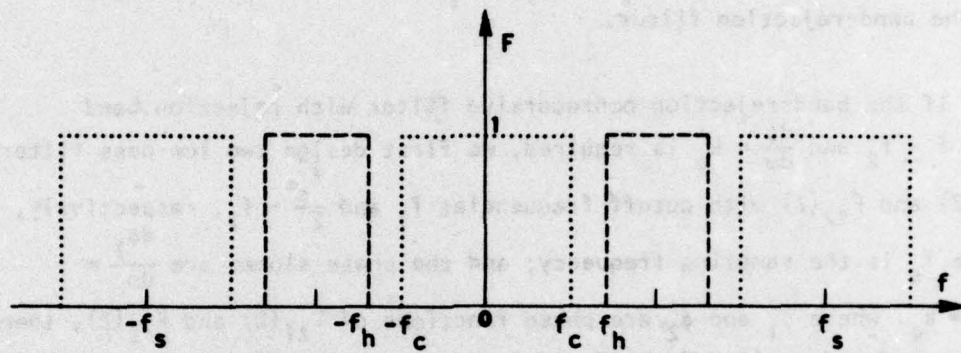
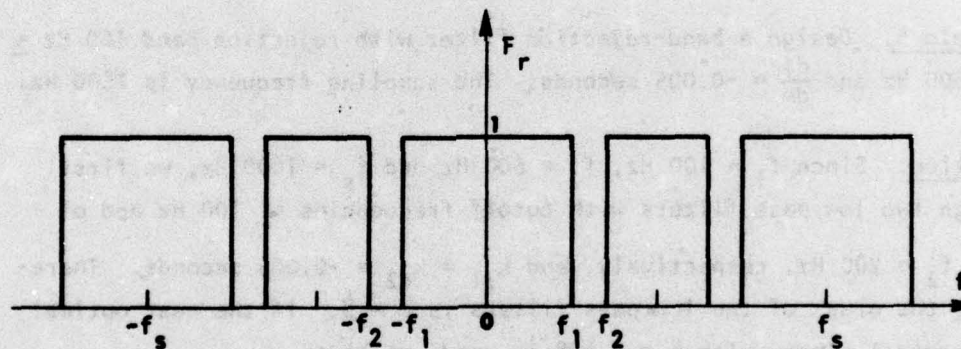


FIGURE 4-12. FREQUENCY RESPONSE OF BAND-PASS FILTER WITH TRAPEZOIDAL WINDOW,  $b = 0.438$



(a) LOW-PASS AND HIGH-PASS FILTER



(b) BAND-REJECTION FILTER

FIGURE 4-13. CONSTRUCTION OF THE BAND-REJECTION FILTER FROM A LOW-PASS AND A HIGH-PASS FILTER

It is evident that the band-rejection filter as represented by Eq. (52) has a linear phase relationship with  $\frac{d\phi}{d\omega} = -mT$ .

Accordingly, we can now state the following rule for the construction of the band-rejection filter.

If the band-rejection nonrecursive filter with rejection band  $f_1 \leq f \leq f_2$  and  $\frac{d\phi}{d\omega} = k_\phi$  is required, we first design two low-pass filters  $F_{\ell 1}(Z)$  and  $F_{\ell 2}(Z)$  with cutoff frequencies  $f_1$  and  $\frac{f_s}{2} - f_2$ , respectively, where  $f_s$  is the sampling frequency; and the phase slopes are  $\frac{d\phi_1}{d\omega} = \frac{d\phi_2}{d\omega} = k_\phi$ , where  $\phi_1$  and  $\phi_2$  are phase functions of  $F_{\ell 1}(Z)$  and  $F_{\ell 2}(Z)$ , then the transfer function of the desired band-rejection filter is given by

$$F_r(Z) = F_{\ell 1}(Z) + F_{\ell 2}(-Z) \quad (53)$$

**Example 5.** Design a band-rejection filter with rejection band  $100 \text{ Hz} \leq f \leq 600 \text{ Hz}$  and  $\frac{d\phi}{d\omega} = -0.005$  seconds. The sampling frequency is  $1600 \text{ Hz}$ .

**Solution.** Since  $f_1 = 100 \text{ Hz}$ ,  $f_2 = 600 \text{ Hz}$  and  $f_s = 1600 \text{ Hz}$ , we first design two low pass filters with cutoff frequencies of  $100 \text{ Hz}$  and of  $\frac{f_s}{2} - f_2 = 200 \text{ Hz}$ , respectively, and  $k_{\phi 1} = k_{\phi 2} = -0.005$  seconds. Therefore, the order of the low-pass filters is  $m = 8$ . If the near optimal trapezoidal window with  $b = 0.438$  is used, we have

$$F_{\ell 1}(Z) = Z^{-8} \sum_{k=-8}^8 a_k Z^{-k} \quad (54)$$

and

$$F_{\ell 2}(Z) = Z^{-8} \sum_{k=-8}^8 b_k Z^{-k} \quad (55)$$

where

$$a_8 = a_{-8} = 0$$

$$a_7 = a_{-7} = 0.0025$$

$$a_6 = a_{-6} = 0.0107$$

$$a_5 = a_{-5} = 0.0252$$

$$a_4 = a_{-4} = 0.0455$$

$$a_3 = a_{-3} = 0.0701$$

$$a_2 = a_{-2} = 0.0966$$

$$a_1 = a_{-1} = 0.1220$$

$$a_0 = 0.1252$$

(56)

and

$$b_8 = b_{-8} = 0$$

$$b_7 = b_{-7} = 0.0046$$

$$b_6 = b_{-6} = -0.0152$$

$$b_5 = b_{-5} = 0.0194$$

$$b_4 = b_{-4} = 0$$

$$b_3 = b_{-3} = -0.0535$$

$$b_2 = b_{-2} = 0.1364$$

$$b_1 = b_{-1} = -0.2253$$

$$b_0 = 0.2502$$

(57)

Therefore, the required band-rejection nonrecursive filter is given by

$$F_r(z^{-1}) = z^{-8} \sum_{k=-8}^8 c_k z^{-k} \quad (58)$$

where

$$c_8 = c_{-8} = 0$$

$$c_7 = c_{-7} = 0.0070$$

$$c_6 = c_{-6} = -0.0045$$

$$c_5 = c_{-5} = 0.0446$$

$$c_4 = c_{-4} = 0.0454$$

$$c_3 = c_{-3} = 0.0167$$

$$c_2 = c_{-2} = 0.2329$$

$$c_1 = c_{-1} = -0.1032$$

$$c_0 = 0.3754$$

The frequency response of this band-rejection nonrecursive filter is shown in Figure 4-14.

#### 4.6 REMARKS

The design of various kinds of nonrecursive digital filters using the FFT algorithm and windows has been presented. It is evident that an arbitrary frequency response can be realized through a nonrecursive digital filter of the proper order. This technique will be employed to design nonrecursive digital compensators for control systems.

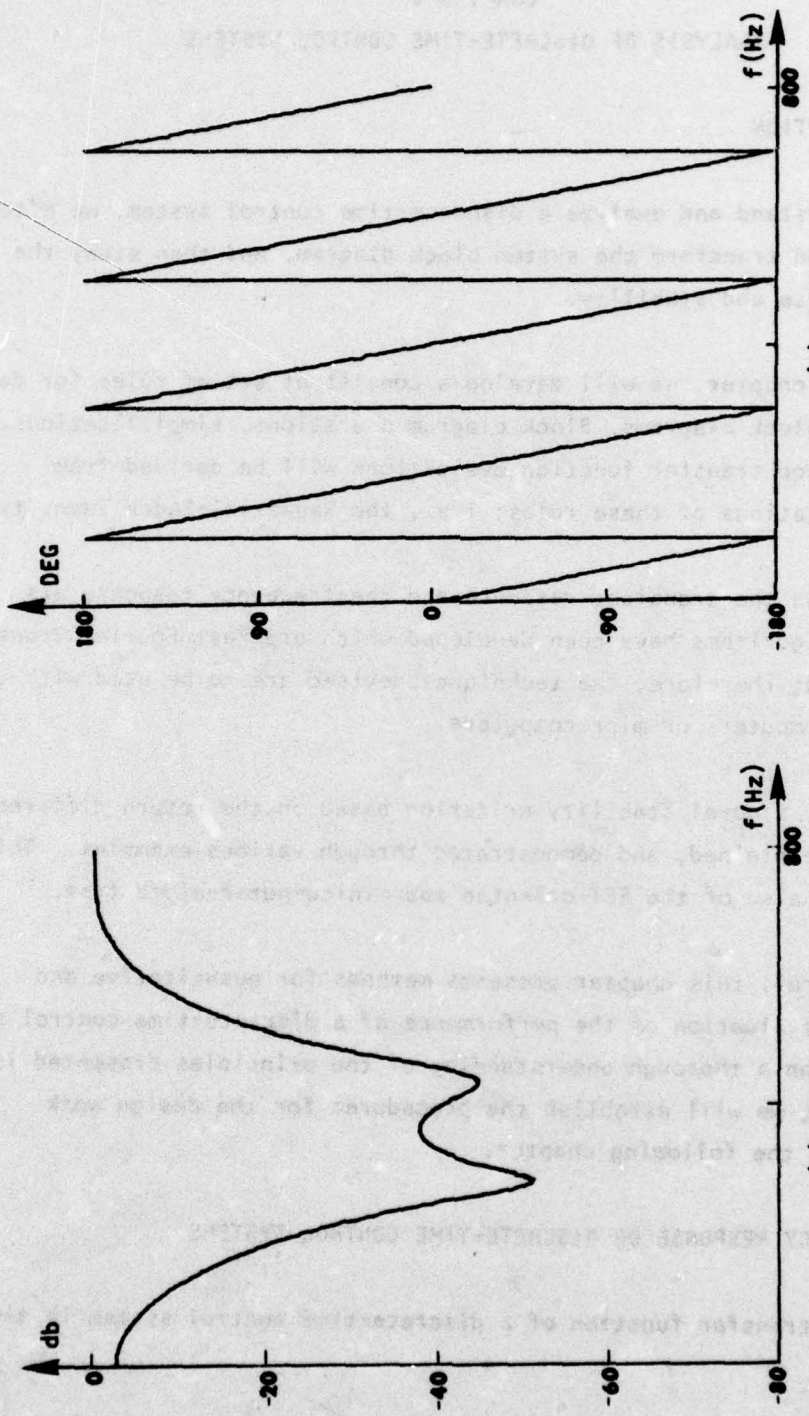


FIGURE 4-14. FREQUENCY RESPONSE OF BAND-REJECTION FILTER WITH TRAPEZOIDAL WINDOW,  $b = 0.438$

CHAPTER V  
ANALYSIS OF DISCRETE-TIME CONTROL SYSTEMS\*

5.0 INTRODUCTION

To understand and analyze a discrete-time control system, we often manipulate and transform the system block diagram, and then study the system response and stability.

In this chapter, we will develop a consistent set of rules for dealing with system block diagrams. Block diagram operations, simplifications, and closed-loop transfer function evaluations will be derived from direct applications of these rules; i.e., the Ragazzini-Zadeh identity.

As far as the transient response and the frequency response are concerned, algorithms have been developed which are Fast Fourier Transform oriented; therefore, the techniques devised are to be used with the aid of minicomputers or microcomputers.

Finally, a novel stability criterion based on the return difference is derived, explained, and demonstrated through various examples. This criterion is also of the FFT-oriented and minicomputer-aided type.

In general, this chapter presents methods for quantitative and qualitative evaluation of the performance of a discrete-time control system. Based on a thorough understanding of the principles presented in this chapter, we will establish the procedures for the design work presented in the following chapter.

5.1 FREQUENCY RESPONSE OF DISCRETE-TIME CONTROL SYSTEMS

If the transfer function of a discrete-time control system is given by

$$G(z) = \frac{a_0 + a_1 z + a_2 z^2 + \dots + a_m z^m}{b_0 + b_1 z + b_2 z^2 + \dots + b_n z^n} \quad (1)$$

then the frequency response of the system is given by

$$G(j\omega) \triangleq G(z) \Big|_{z = e^{j\omega T}}$$

$$= \frac{a_0 + a_1 e^{j\omega T} + a_2 e^{j2\omega T} + \dots + a_m e^{jm\omega T}}{b_0 + b_1 e^{j\omega T} + b_2 e^{j2\omega T} + \dots + b_n e^{jn\omega T}} \quad (2)$$

where  $T$  is the sampling period and  $\omega_s = \frac{2\pi}{T}$  is the sampling frequency. Since  $e^{j(\omega+\omega_s)T} = e^{j\omega T}$ , we see that  $G(j\omega)$  is a complex periodic function in the frequency domain with period  $\omega_s$ . Therefore, Eq. (2) can be expressed as a Fourier series;

$$G(j\omega) = \sum_{n=-\infty}^{\infty} a_n e^{-jn\omega T} \quad (3)$$

The inverse Fourier Transform of  $G(j\omega)$ , which is the impulse response of the discrete-time control system, is given by

$$g(t) = F^{-1}[G(j\omega)]$$

$$= \sum_{n=-\infty}^{\infty} a_n \delta(t-nT) \quad (4)$$

For a causal system, the impulse response must be

$$g(t) = 0 \quad \text{for } t < 0 \quad (5)$$

In other words, in Eq. (4)

$$a_n = 0 \quad \text{for } n < 0 \quad (6)$$

For simplicity, Eqs. (3) and (4) can be rewritten as

$$G(j\omega) = \sum_{n=0}^{\infty} a_n e^{-jn\omega T} \quad (7)$$

and

$$g(t) = \sum_{n=0}^{\infty} a_n \delta(t-nT) \quad (8)$$

The conventional methods to obtain the  $a_n$  coefficients of Eq. (8) are the partial fraction expansion, long division algorithm, etc. A new method of using the DFT to find the frequency response  $G(j\omega)$  and then taking the inverse Fourier Transformation of  $G(j\omega)$  to get  $g(t)$  has been developed and can be adopted.

In the preceding chapter, the frequency response of the nonrecursive filter was determined using the FFT algorithm. Eq. (1) can be rewritten as

$$G(z) = \frac{N(z)}{D(z)} \quad (9)$$

where

$$N(z) = a_m z^{m-n} + a_{m-1} z^{m-n-1} + \dots + a_1 z^{1-n} + a_0 z^{-n} \quad (10)$$

and

$$D(z) = b_n + b_{n-1} z^{-1} + \dots + b_1 z^{1-n} + b_0 z^{-n} \quad (11)$$

and  $m < n$ . Of course,  $N(z)$  and  $D(z)$  can be treated as transfer functions of two nonrecursive filters. Therefore, utilizing the technique developed in Chapter IV, the frequency response of  $N(z)$  and  $D(z)$  can be determined using the FFT algorithm. Next, dividing  $N(e^{j\omega T})$  by  $D(e^{j\omega T})$ , the frequency response of the system transfer function  $G(z)$  is obtained. The procedure suggested here is actually a fast method to calculate the frequency response of discrete-time control systems. Program No. 6 (Appendix C) was developed according to this procedure.

**Example 1.** Find the frequency response of the system with the transfer function

$$G(z) = \frac{1.264z}{z^2 - 0.104z + 0.368} \quad (12)$$

and sampling period  $T = 0.1$  seconds.

**Solution.** Rewrite Eq. (12) as

$$G(z) = \frac{1.264z^{-1}}{1 - 0.104z^{-1} + 0.368z^{-2}} \quad (13)$$

Case (1). Choose  $N = 64$  for performing the FFT.

The frequency resolution of the frequency response is given by

$$\Delta\omega = \frac{\omega_s}{N} = \frac{2\pi}{NT} \quad (14)$$

In this case,  $T = 0.1$  seconds and  $\Delta\omega = \frac{5\pi}{16} = 0.9818$ . The resulting frequency response is shown in Figure 5-1 for  $0 \leq \omega \leq \frac{\omega_s}{2}$ .

Case (2). Choose  $N = 1024$  for performing the FFT.

In this case,  $\Delta\omega = \frac{5\pi}{256} = 0.06136$  is much smaller than that in Case (1). The frequency response for  $0 \leq \omega \leq \frac{\omega_s}{2}$  is shown in Figure 5-2. Increasing the value of  $N$  results in a much smoother curve compared to that of Case (1).

## 5.2 TRANSIENT RESPONSE OF DISCRETE-TIME CONTROL SYSTEMS

If the discrete-time control system has the transfer function  $G(z)$  and input  $R(z)$ , then the output is given by

$$C(z) = G(z) R(z) \quad (15)$$

and the transient response is

$$c(t) = Z^{-1}[G(z) R(z)] \quad (16)$$

Many methods exist for finding the transient response  $c(t)$ , such as the long division method, and partial fraction expansion, etc. However, if we take advantage of the FFT algorithm for finding the inverse Z-transform as in Eq. (16) and using Eq. (15), we have the Fourier Transform of  $C(z)$  which can be expressed as

$$C(e^{j\omega T}) = G(e^{j\omega T}) R(e^{j\omega T}) \quad (17)$$

Then, the transient response is

$$\begin{aligned} c(t) &= F^{-1}[C(e^{j\omega T})] \\ &= F^{-1}[G(e^{j\omega T}) R(e^{j\omega T})] \end{aligned} \quad (18)$$

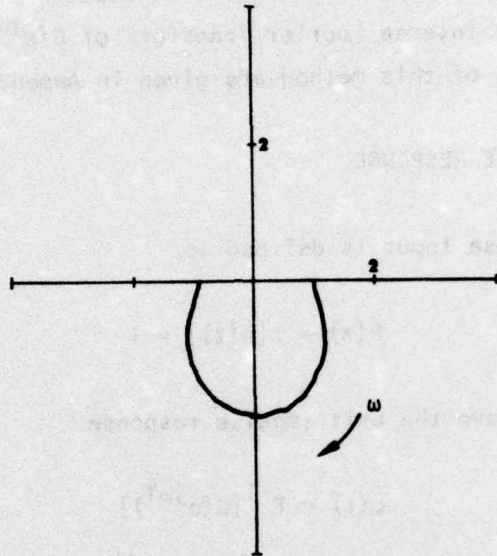


FIGURE 5-1. FREQUENCY RESPONSE OF  $G(z)$ ,  $N = 64$

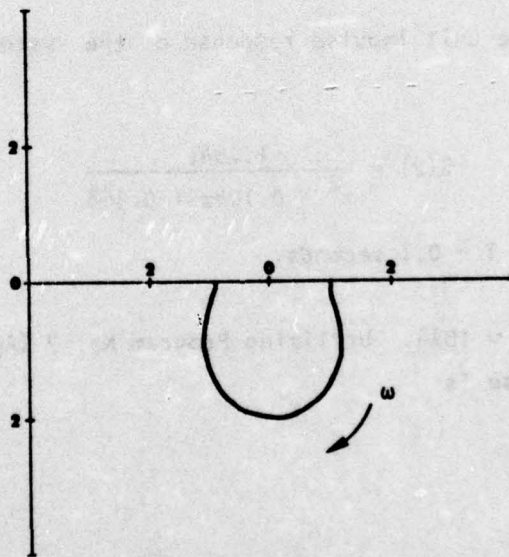


FIGURE 5-2. FREQUENCY RESPONSE OF  $G(z)$ ,  $N = 1024$

Thus, we first find the frequency response  $G(e^{j\omega T})$  and the Fourier Transform  $R(e^{j\omega T})$  using the FFT, as discussed in Section 5.1, then we use the FFT to evaluate the inverse Fourier Transform of  $G(e^{j\omega T}) R(e^{j\omega T})$  to determine  $c(t)$ . Details of this method are given in Appendix B.

### 5.2.1 UNIT IMPULSE RESPONSE

The unit impulse input is defined as

$$R(z) = Z[\delta(t)] = 1 \quad (19)$$

From Eq. (18), we have the unit impulse response

$$c(t) = F^{-1}[G(e^{j\omega T})] \quad (20)$$

Program No. 7 (Appendix C) was written to evaluate the unit impulse response from the transfer function  $G(z)$ .

**Example 2.** Find the unit impulse response of the system with the transfer function

$$G(z) = \frac{1.264z}{z^2 - 0.104z + 0.368} \quad (21)$$

and sampling period  $T = 0.1$  seconds.

**Solution.** Choose  $N = 1024$ . Utilizing Program No. 7 (Appendix C) the unit impulse response is

$$\begin{aligned}
c(t) = & 1.264 \delta(t-0.1) + 0.132 \delta(t-0.2) \\
& - 0.0452 \delta(t-0.3) - 0.096 \delta(t-0.4) \\
& + 0.157 \delta(t-0.5) + 0.052 \delta(t-0.6) \\
& - 0.053 \delta(t-0.7) - 0.025 \delta(t-0.8) \\
& + 0.017 \delta(t-0.9) - 0.011 \delta(t-1.0) \\
& - 0.005 \delta(t-1.1)
\end{aligned} \tag{22}$$

The resulting transient response is shown in Figure 5-3.

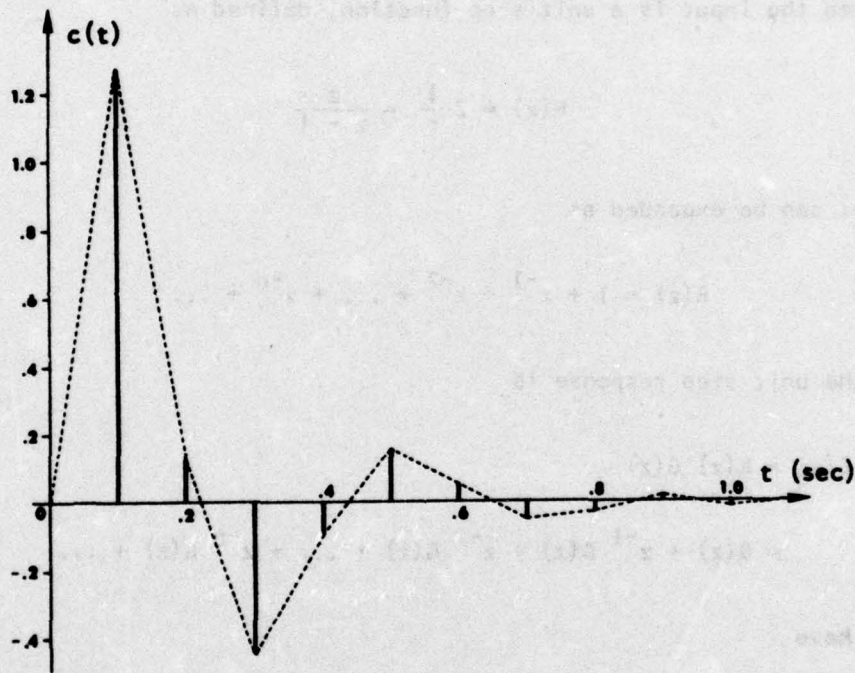


FIGURE 5-3. THE UNIT IMPULSE RESPONSE OF EXAMPLE 2

If the system has poles at  $z = 1$ , the frequency response is undefined in the neighborhood of  $\omega = 0$ ; therefore, the impulse response cannot be evaluated directly by FFT algorithm. To overcome this difficulty, we

can factor out  $\left(\frac{z}{z-1}\right)^k$ , and define

$$G_1(z) = \left(\frac{z-1}{z}\right)^k G(z) \quad (23)$$

such that no pole exists at  $z = 1$  in  $G_1(z)$ . The impulse response of  $G_1(z)$  is determined; and the method for evaluating the step response, which is discussed in the following section, is used to find the impulse response of  $G(z)$ .

### 5.2.2 UNIT STEP RESPONSE

When the input is a unit step function, defined as

$$R(z) = Z \frac{1}{s} = \frac{z}{z-1} \quad (24)$$

Eq. (24) can be expanded as

$$R(z) = 1 + z^{-1} + z^{-2} + \dots + z^{-n} + \dots \quad (25)$$

Thus, the unit step response is

$$\begin{aligned} C(z) &= R(z) G(z) \\ &= G(z) + z^{-1} G(z) + z^{-2} G(z) + \dots + z^{-n} G(z) + \dots \end{aligned} \quad (26)$$

and we have

$$c(t) = \sum_{I=0}^{\infty} g(t-IT) \quad (27)$$

where

$$g(t) = Z^{-1}[G(z)] \quad (28)$$

is the unit impulse response of the system. Since the physical system is causal,

$$g(t) = 0 \quad \text{for } t < 0 \quad (29)$$

From Eq. (27), we find

$$c(nT) = \sum_{i=0}^n g(nT) \quad \text{for } n = 0, 1, \dots \quad (30)$$

The Fourier Analyzer has an integration algorithm which actually performs the summation exactly as shown in Eq. (30); therefore, the integration operation can be used to evaluate the unit step response. Program No. 8 (Appendix C) was written to determine the unit step response from the transfer function of the system.

**Example 3.** Find the unit step response of the system with transfer function

$$G(z) = \frac{1.264z}{z^2 - 0.104z + 0.368} \quad (31)$$

and sampling period  $T = 0.1$  seconds.

**Solution.** Using Program No. 8 (Appendix C), the unit step response is

$$\begin{aligned} c(t) = & 1.264 \delta(t-0.1) + 1.395 \delta(t-0.2) \\ & + 0.944 \delta(t-0.3) + 0.849 \delta(t-0.4) \\ & + 1.005 \delta(t-0.5) + 1.056 \delta(t-0.6) \\ & + 1.004 \delta(t-0.7) + 0.980 \delta(t-0.8) \\ & + 1.007 \delta(t-0.9) + 1.002 \delta(t-1.0) \\ & + 0.998 \delta(t-1.1) + \dots \end{aligned} \quad (32)$$

The resulting step response is shown in Figure 5-4.

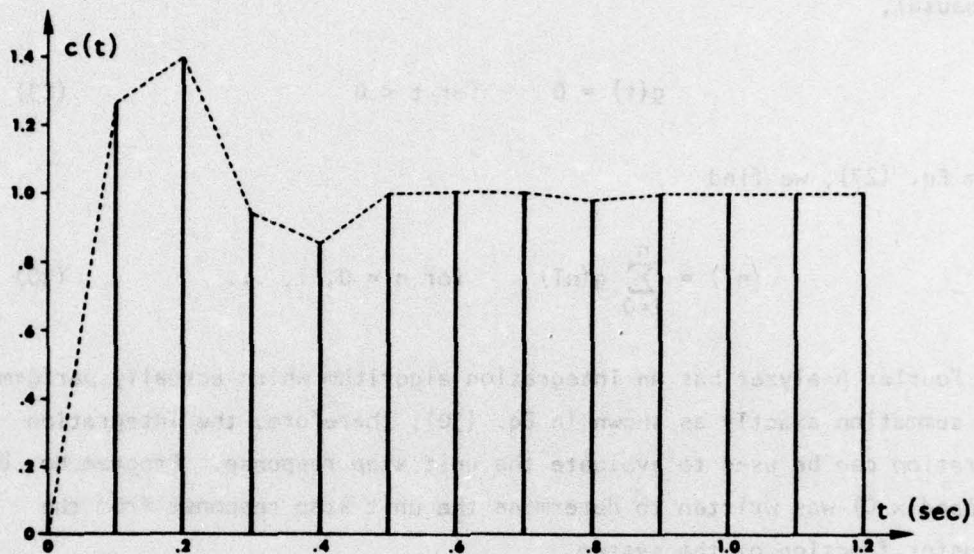


FIGURE 5-4. THE UNIT STEP RESPONSE OF EXAMPLE 3

**Example 4.** Find the unit impulse and unit step responses of the system with the transfer function

$$G(z) = \frac{1.5z(z+1)}{(z-1)(z^2-0.5z+0.5)} \quad (33)$$

and sampling period  $T = 0.1$  seconds.

**Solution.** First, define

$$G_1(z) = \frac{z-1}{z} \frac{1.5(z+1)}{z^2-0.5z+0.5} \quad (34)$$

The unit impulse response of  $G_1(z)$  is

$$\begin{aligned}
g_1(t) = & 1.501 \delta(t-0.1) + 2.25 \delta(t-0.2) \\
& + 0.0375 \delta(t-0.3) - 0.938 \delta(t-0.4) \\
& - 0.657 \delta(t-0.5) + 0.141 \delta(t-0.6) \\
& + 0.399 \delta(t-0.7) + 0.129 \delta(t-0.8) \\
& + 0.135 \delta(t-0.9) + 0.002 \delta(t-1.0) \\
& + 0.067 \delta(t-1.1) + \dots
\end{aligned} \tag{35}$$

From Eq. (30), the unit impulse response of  $G(z)$  is

$$\begin{aligned}
g(t) = & 1.501 \delta(t-0.1) + 3.751 \delta(t-0.2) \\
& + 4.126 \delta(t-0.3) + 3.188 \delta(t-0.4) \\
& + 2.532 \delta(t-0.5) + 2.673 \delta(t-0.6) \\
& + 3.071 \delta(t-0.7) + 3.200 \delta(t-0.8) \\
& + 3.065 \delta(t-0.9) + 2.933 \delta(t-1.0) \\
& + 2.935 \delta(t-1.1) + \dots
\end{aligned} \tag{36}$$

and the unit step response of  $G(z)$  is

$$\begin{aligned}
h(t) = & 1.51 \delta(t-0.1) + 5.26 \delta(t-0.2) \\
& + 9.38 \delta(t-0.3) + 12.57 \delta(t-0.4) \\
& + 15.10 \delta(t-0.5) + 17.77 \delta(t-0.6) \\
& + 20.85 \delta(t-0.7) + 24.05 \delta(t-0.8) \\
& + 27.11 \delta(t-0.9) + 30.04 \delta(t-1.0) \\
& + 32.98 \delta(t-1.1) + \dots
\end{aligned} \tag{37}$$

Both  $g(t)$  and  $h(t)$  are shown in Figures 5-5 and 5-6 respectively.

**Example 5.** Find the frequency, unit impulse, and unit step responses of the discrete-time system with the transfer function

$$G(z) = \frac{\sum_{i=0}^7 a_i z^i}{\sum_{i=0}^8 b_i z^i} \tag{38}$$

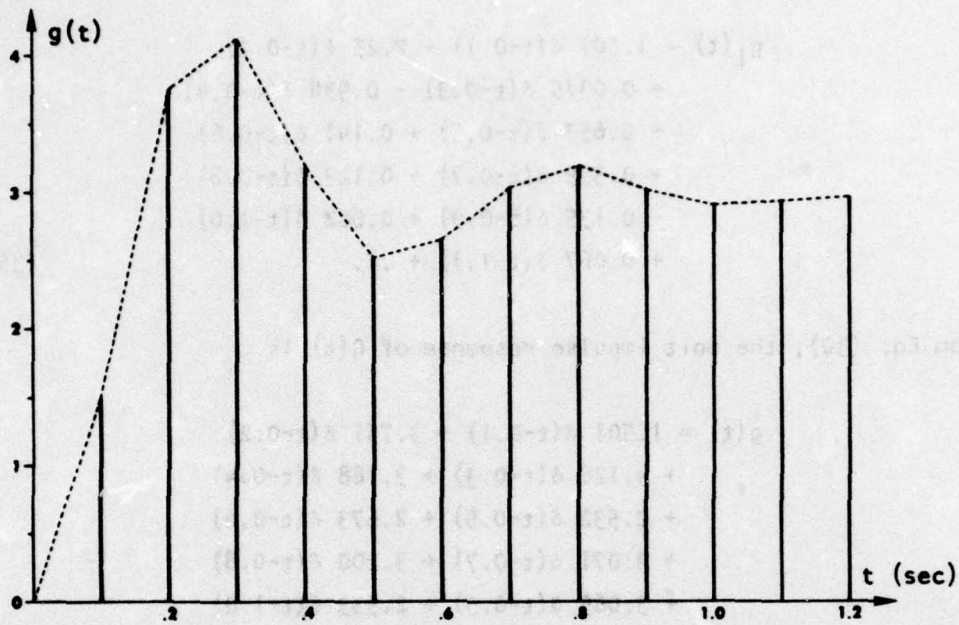


FIGURE 5-5. THE UNIT IMPULSE RESPONSE OF EXAMPLE 4

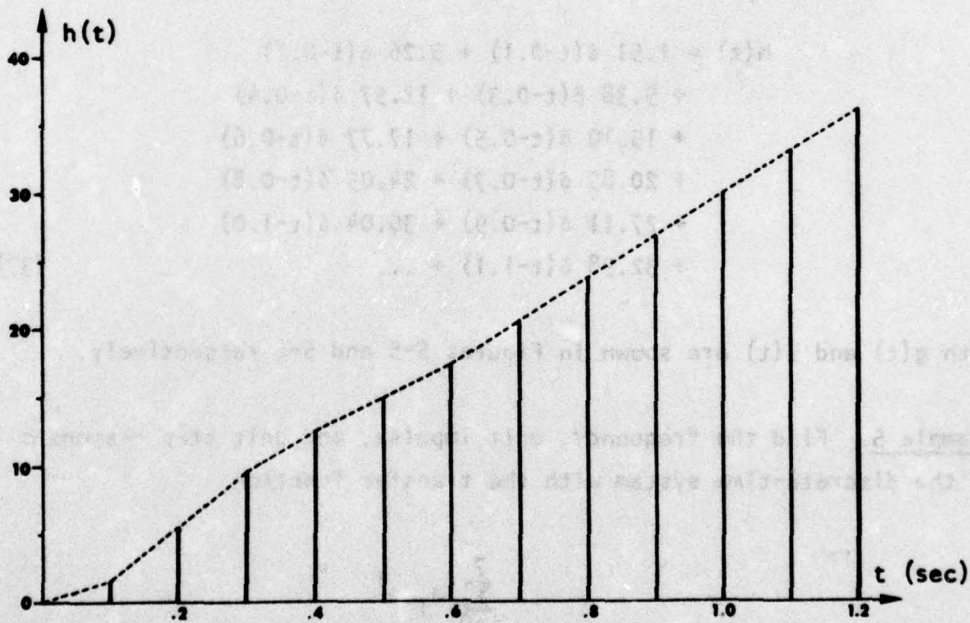


FIGURE 5-6. THE UNIT STEP RESPONSE OF EXAMPLE 4

where

$$\begin{aligned} a_0 &= -0.006 & b_0 &= 0.006 \\ a_1 &= 0.044 & b_1 &= -0.044 \\ a_2 &= -0.262 & b_2 &= 0.262 \\ a_3 &= -0.516 & b_3 &= 0.516 \\ a_4 &= 0.152 & b_4 &= -0.152 \\ a_5 &= -0.210 & b_5 &= 0.210 \\ a_6 &= 1.116 & b_6 &= -1.116 \\ a_7 &= 1.682 & b_7 &= -1.682 \\ & & b_8 &= 4.0 \end{aligned}$$

and sampling period  $T = 0.5$  seconds.

**Solution.** Utilize Program No. 8 (Appendix C) to find both frequency and transient responses of the system. Figure 5-7 shows the resulting frequency response. The unit impulse response is given by

$$\begin{aligned} g(t) &= 0.4205 \delta(t-0.5) + 0.4458 \delta(t-1.0) \\ &+ 0.2566 \delta(t-1.5) + 0.2510 \delta(t-2.0) \\ &+ 0.0403 \delta(t-2.5) - 0.0290 \delta(t-3.0) \\ &- 0.0797 \delta(t-3.5) - 0.0939 \delta(t-4.0) \\ &- 0.1035 \delta(t-4.5) - 0.0861 \delta(t-5.0) \\ &- 0.0597 \delta(t-5.5) - 0.0350 \delta(t-6.0) \\ &- 0.0139 \delta(t-6.5) + 0.0030 \delta(t-7.0) \\ &+ 0.0139 \delta(t-7.5) + 0.0185 \delta(t-8.0) \\ &+ 0.0186 \delta(t-8.5) + 0.0159 \delta(t-9.0) \\ &+ 0.0117 \delta(t-9.5) + 0.0070 \delta(t-10.0) + \dots \end{aligned} \quad (39)$$

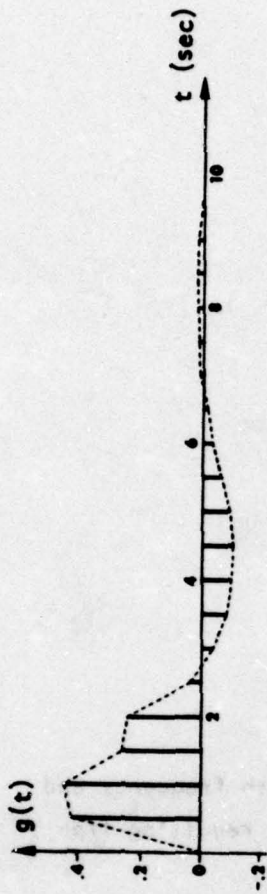


FIGURE 5-8. THE UNIT IMPULSE RESPONSE OF EXAMPLE 5

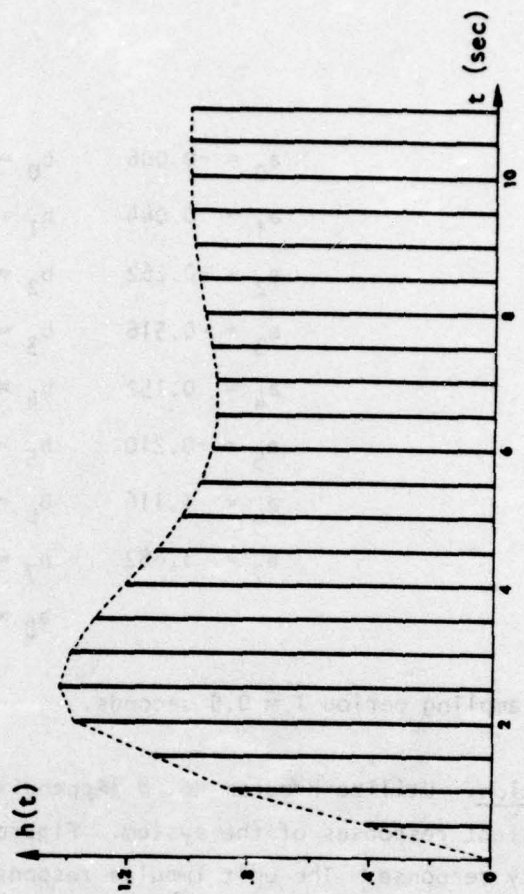


FIGURE 5-9. THE UNIT STEP RESPONSE OF EXAMPLE 5

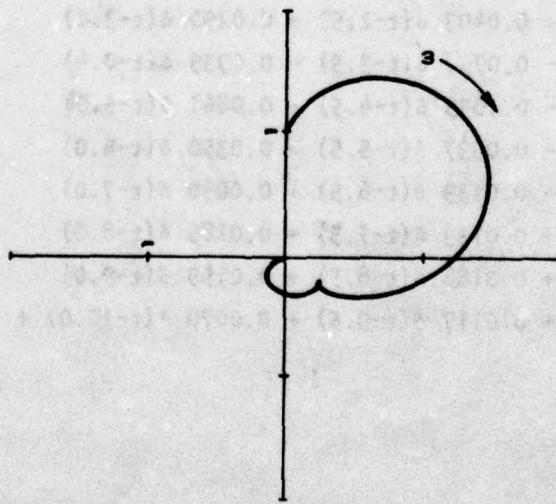


FIGURE 5-7. FREQUENCY RESPONSE OF EXAMPLE 5

and the unit step response is

$$\begin{aligned}
 h(t) = & 0.421 \delta(t-0.5) + 0.876 \delta(t-1.0) \\
 & + 1.133 \delta(t-1.5) + 1.384 \delta(t-2.0) \\
 & + 1.424 \delta(t-2.5) + 1.395 \delta(t-3.0) \\
 & + 1.315 \delta(t-3.5) + 1.222 \delta(t-4.0) \\
 & + 1.118 \delta(t-4.5) + 1.032 \delta(t-5.0) \\
 & + 0.973 \delta(t-5.5) + 0.939 \delta(t-6.0) \\
 & + 0.924 \delta(t-6.5) + 0.927 \delta(t-7.0) \\
 & + 0.941 \delta(t-7.5) + 0.959 \delta(t-8.0) \\
 & + 0.978 \delta(t-8.5) + 0.994 \delta(t-9.0) \\
 & + 1.005 \delta(t-9.5) + 1.012 \delta(t-10.0) + \dots \quad (40)
 \end{aligned}$$

Both  $g(t)$  and  $h(t)$  are shown in Figures 5-8 and 5-9, respectively.

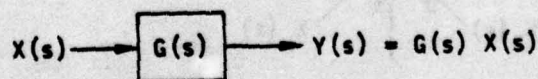
### 5.3 BLOCK DIAGRAM OPERATIONS FOR DISCRETE-TIME CONTROL SYSTEMS

To find the closed loop transfer function of a discrete-time system, we must first derive a set of block diagram operations for simplifying the system structure. The following outlines some elements and fundamental operations for simplifying the block diagram of a discrete-time system:

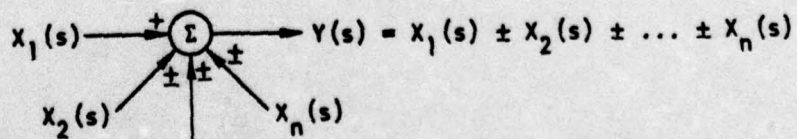
- The S-domain

- (1) Components

- (a) CC1 - Dynamic device



- (b) CC2 - Summing device.

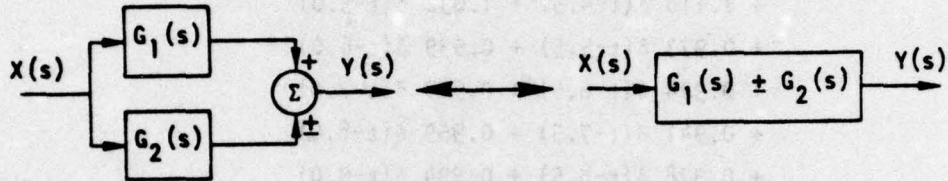


(2) Operations.

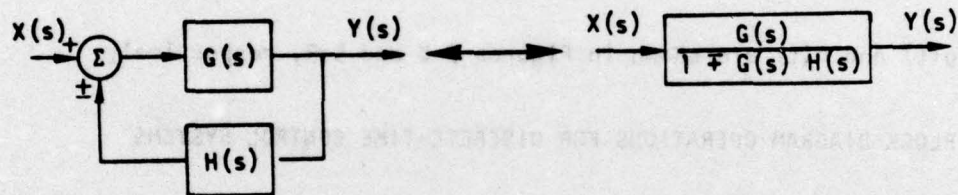
(a) C01 - Series operation.



(b) C02 - Parallel operation.



(c) C03 - Feedback operations.



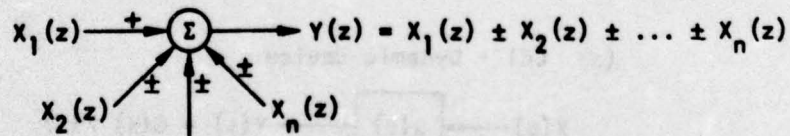
● The Z-domain.

(1) Components.

(a) DC1 - Dynamic device.



(b) DC2 - Summing device.

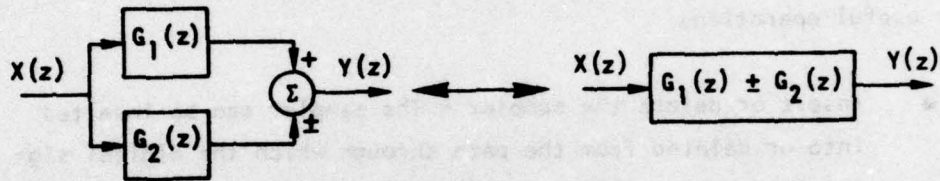


(2) Operations.

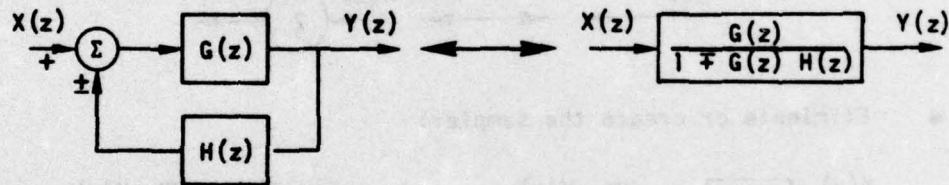
(a) D01 - Series operation.



(b) D02 - Parallel operation.



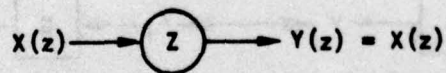
(c) D03 - Feedback operation.



• The hybrid domain.

(1) Component.

(a) HC1 - Sampler (discrete input).



(b) HC1 - Sampler (continuous input).



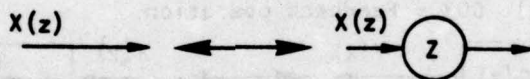
(2) Operation.

H01 - Ragazzini-Zadeh identity<sup>[21]</sup>.

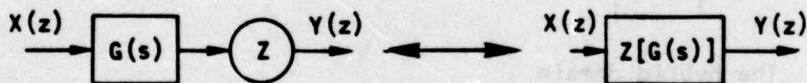


All of the previous operations are based on the linear graph theory with the exception of the Ragazzini-Zadeh identity. Through the use of these five components and seven fundamental operations, we can derive other useful operations:

- Insert or delete the sampler - The sampler can be inserted into or deleted from the path through which the digital signal is passed. This is based on the property of the sampler (HC1).

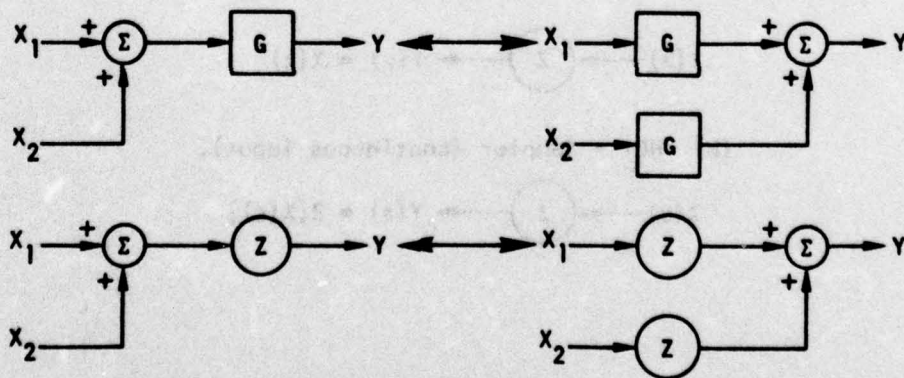


- Eliminate or create the sampler:

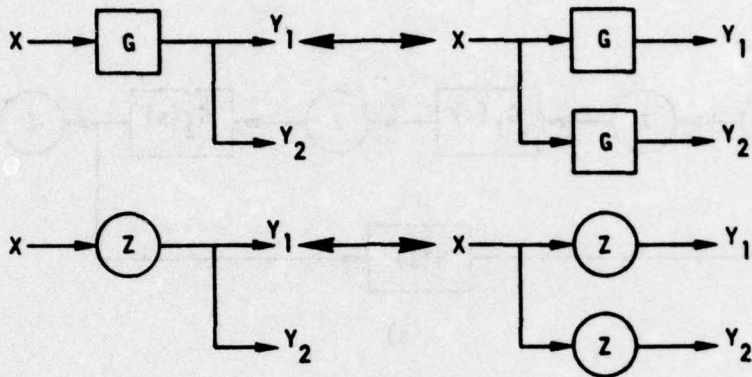


This operation results directly from Ragazzini-Zadeh identity.

- Moving a summing device beyond/ahead of devices or samplers.



- Moving the take-off point beyond/ahead of devices or samplers.



#### 5.4 CLOSED LOOP TRANSFER FUNCTION

The block diagram operations given in the previous section will be used to determine the closed loop transfer function of systems presented in this section. Consider the system shown in Figure 5-10(a); moving the summing device beyond the first sampler and the take-off point ahead of  $G_2(s)$ , the block diagram transforms into that shown in Figure 5-10(b). Next, using the Ragazzini-Zadeh Identity (Operation H01) to eliminate the samplers, we have Figure 5-10(c). Finally, applying the feedback operation D03 and the series operation D01, the transfer function can be expressed as

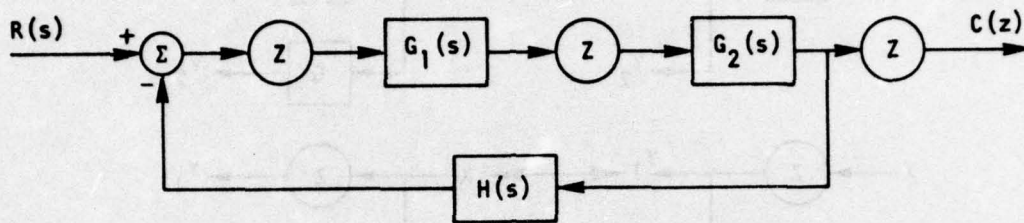
$$F(z) = \frac{C(z)}{R(z)} = \frac{G_1(z) G_2(z)}{1 + G_1(z) G_2 H(z)} \quad (41)$$

where

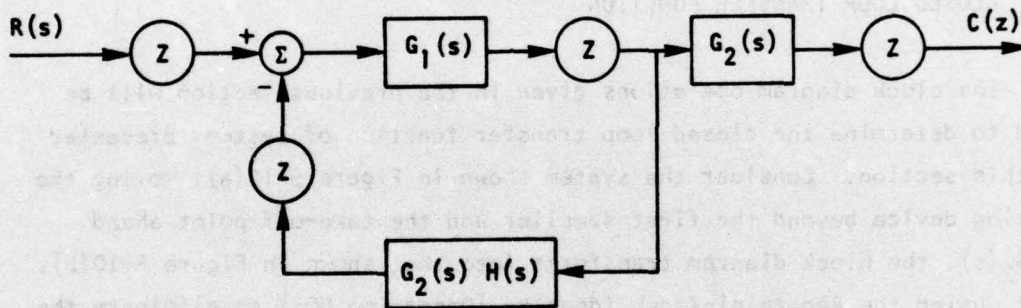
$$G_2 H(z) = Z[G_2(s) H(s)] \quad (42)$$

Consider the missile launching system with a digital controller as shown in Figure 5-11(a). The launcher dynamics are given by

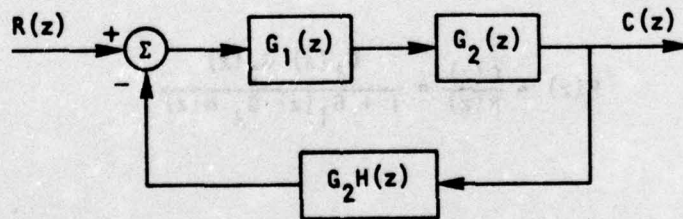
$$G_L(s) = \frac{50}{s(s+1)(s+2)} \quad (43)$$



(a)

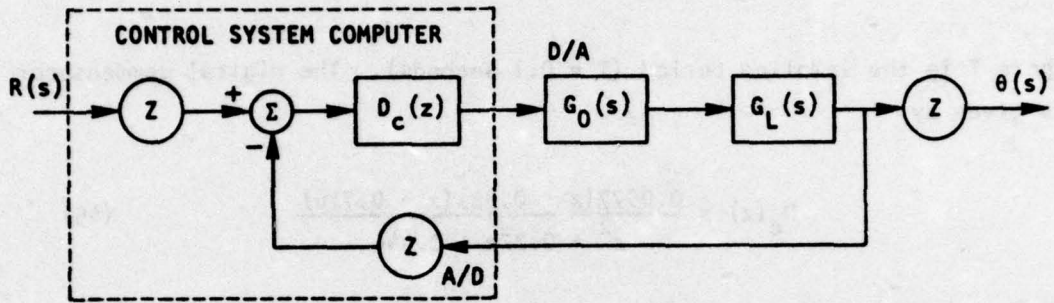


(b)

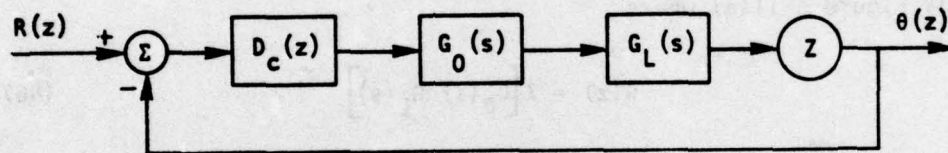


(c)

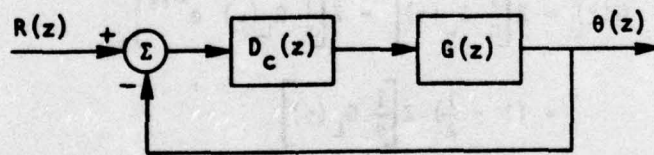
FIGURE 5-10. BLOCK DIAGRAM SIMPLIFICATION



(a) SYSTEM CONFIGURATION



(b) EQUIVALENT BLOCK DIAGRAM



(c) SIMPLIFIED SYSTEM

FIGURE 5-11. MISSILE LAUNCHING SYSTEM WITH DIGITAL CONTROLLER

The zero-order hold is

$$G_0(s) = \frac{1 - e^{-Ts}}{s} \quad (44)$$

where  $T$  is the sampling period ( $T = 0.1$  seconds). The digital compensator is given by

$$D_c(z) = \frac{0.0577(z - 0.92)(z - 0.716)}{z^2 + 0.22z + 0.446} \quad (45)$$

Moving the take-off point beyond the last sampler in the feed-forward path and eliminating the first sampler, the block diagram reduces to Figure 5-11(b). Applying the Ragazzini-Zadeh identity (Operation H01) yields Figure 5-11(a) where

$$G(z) = Z[G_0(s) G_L(s)] \quad (46)$$

Since  $G_0(s)$  is given in Eq. (44), we can express  $G(z)$  as

$$\begin{aligned} G(z) &= Z\left[\frac{1}{s} G_L(s)\right] - Z\left[\frac{1}{s} G_L(s) e^{-Ts}\right] \\ &= \left(1 - \frac{1}{z}\right) Z\left[\frac{1}{s} G_L(s)\right] \end{aligned} \quad (47)$$

In other words, we can write the zero-order hold as

$$G_0(s, z) = \frac{1 - z}{s} \quad (48)$$

If we replace  $G_0(s)$  in Eq. (46) by Eq. (48) and then apply the Ragazzini-Zadeh Identity, we can immediately obtain the result of Eq. (47). From Eq. (47) we have

$$G(z) = \frac{3.925 \times 10^{-4} (z + 3.35)(z + 0.26)}{(z - 1)(z - 0.9048)(z - 0.8187)} \quad (49)$$

Therefore, the closed loop transfer function is given by

$$\begin{aligned} F(z) &= \frac{D_c(z) G(z)}{1 + D_c(z) G(z)} \\ &= \frac{3.925 \times 10^{-4} (z + 3.35)(z + 0.26)(z - 0.92)(0.0577z - 0.403)}{z^2(z - 0.934)(z^2 - 1.508z + 0.6065)} \end{aligned} \quad (50)$$

### 5.5 STABILITY OF DISCRETE-TIME CONTROL SYSTEM

Numerous criteria, such as the Schur-Cohn criterion, the Inner theory, the Routh-Hurwitz criterion, the Nyquist criterion, etc., are available for testing the stability of discrete-time control systems. Most of these criteria, with the exception of the Nyquist criterion, are algebraic algorithms and are based on the closed loop characteristic equation. The original Nyquist criterion<sup>[1]</sup> is based on the encirclement of the frequency plot of the return ratio function of the closed loop system. Since the frequency response of the discrete-time control system can be found utilizing the FFT algorithm, it is evident that the Nyquist criterion can be an effective tool for stability testing via the FFT.

Recently, a generalized Nyquist criterion<sup>[28]</sup> based on the return difference rather than the return ratio has been derived and successfully used for testing the stability of lumped and distributed parameter continuous systems. Subsequently, we will derive its counterpart for discrete-time systems.

If a discrete-time control system has a feed-forward path transfer function  $G(z)$  and a feedback path transfer function  $H(z)$ , the closed loop system transfer function is given by

$$F(z) = \frac{G(z)}{1 + G(z) H(z)} \quad (51)$$

Similar to the definitions for continuous system, we can define the return ratio of the discrete-time system as

$$Q(z) = G(z) H(z) \quad (52)$$

and the return difference as

$$P(z) = 1 + Q(z) \quad (53)$$

Let us express the return ratio as

$$Q(z) = \frac{A(z)}{B(z)} \quad (54)$$

where  $A(z)$  and  $B(z)$  are relative prime polynomials, and the order of  $A(z)$  is not greater than that of  $B(z)$ . Substituting Eq. (54) into Eq. (51), yields

$$F(z) = \frac{G(z) B(z)}{A(z) + B(z)} \quad (55)$$

Assuming that there is no common factor between the denominator of  $G(z)$  and the numerator of  $H(z)$ , then  $G(z) B(z)$  in Eq. (55) is a polynomial;  $B(z)$  is the open loop characteristic function and  $A(z) + B(z)$  is the closed loop characteristic function  $A_1(z)$ . Thus the return difference becomes

$$\begin{aligned} P(z) &= \frac{A(z) + B(z)}{B(z)} = \frac{A_1(z)}{B(z)} \\ &= \frac{\text{closed loop characteristic function}}{\text{open loop characteristic function}} \quad (56) \end{aligned}$$

The original Nyquist criterion for discrete-time systems is to count the number of encirclements of the frequency response of the return ratio from  $\frac{\omega_s}{2}$  to  $-\frac{\omega_s}{2}$ , where  $\omega_s$  is the sampling frequency, about the critical point  $(-1 + j0)$ . The generalized Nyquist criterion considered here is to count the total phase change of the frequency response of the return difference from 0 to  $\frac{\omega_s}{2}$ ; therefore, the new criterion is much simpler than the original one.

Before proceeding any further, the following definitions are required:

- **Definition 1.** The open arc on the unit circle with the center at the origin of Z-plane, from  $\omega_i$  to  $\omega_{i+1}$  is the open segment of arc  $(e^{j\omega_i T}, e^{j\omega_{i+1} T})$ , where T is the sampling period.
- **Definition 2.** The phase angle change of the mapping of an open arc  $\ell(i) = (e^{j\omega_i T}, e^{j\omega_{i+1} T})$  by a certain complex function P(z) is defined by

$$\Delta\theta_{\ell(i)} = (\theta_{i+1}^-) - (\theta_i^+) \quad (57)$$

where

$$\theta_{i+1}^- = \lim_{\epsilon \rightarrow 0} \left\{ \text{ARG } P \left( e^{j(\omega_{i+1} T - \epsilon)} \right) \right\} \quad (58)$$

and

$$\theta_i^+ = \lim_{\epsilon \rightarrow 0} \left\{ \text{ARG } P \left( e^{j(\omega_i T + \epsilon)} \right) \right\} \quad (59)$$

- **Definition 3.** The total phase change of the mapping of all open arcs on the upper half of the unit circle by  $P(z)$  is defined as

$$\Delta\theta = \sum_{i=1}^n \Delta\theta_{\ell(i)} \quad (60)$$

where  $\Delta\theta_{\ell(i)}$  is the phase angle change due to the mapping of the  $i$ th open arc.

Assume that the return difference  $P(z)$  has the following properties:

- (1)  $P(e^{j\omega T}) \neq 0$  for  $0 \leq \omega \leq \frac{\omega_s}{2}$ .
- (2) There are  $\beta$  poles of  $P(z)$  on the unit circle and  $\gamma$  poles out of the unit circle, where  $\beta$  and  $\gamma$  are finite integers.
- (3)  $P^*(z) = P(z^*)$  where  $*$  means complex conjugate.

Consider the Nyquist contour for discrete-time system as shown in Figure 5-12. From the principle of argument, it is known that the total phase change of  $P(z)$  along the contour

$$\Gamma = \ell(-n) U_c(-n+1) \dots U_{\ell}(-1) U_c(0) U_{\ell}(1) U \dots \\ \dots U_{\ell}(n) U_c(n) \quad (61)$$

is given by

$$\Delta\theta_{\gamma} = 2\pi [(N_A - M) - (N_B - \gamma)] \quad (62)$$

where  $N_A$  is the order of  $A_1(z)$ ,  $N_B$  is the order of  $B(z)$ ,  $M$  is the number of closed loop characteristic roots out of the unit circle and  $\gamma$  is the number of open loop characteristic roots out of the unit circle. In detail, the total phase change of  $P(z)$  along  $\Gamma$  can be evaluated by the summation of individual phase changes along  $\ell(i)$ ,  $i = \pm 1, \pm 2, \dots, \pm n$  and semicircles  $c(i)$ ,  $i = 0, \pm 1, \pm 2, \dots, \pm(n-1), n$ . In other words

$$\Delta\theta_{\Gamma} = \sum_{i=1}^n \Delta\theta_{\ell(i)} + \Delta\theta_{\ell(-i)} - \sum_{i=-(n-1)}^n \Delta\theta_{c(i)} \quad (63)$$

Assume that

$$P(e^{j\omega T}) = U(\omega) + jV(\omega) \quad (64)$$

where  $U(\omega)$  and  $V(\omega)$  are real functions of  $\omega$ . From property (3), we have

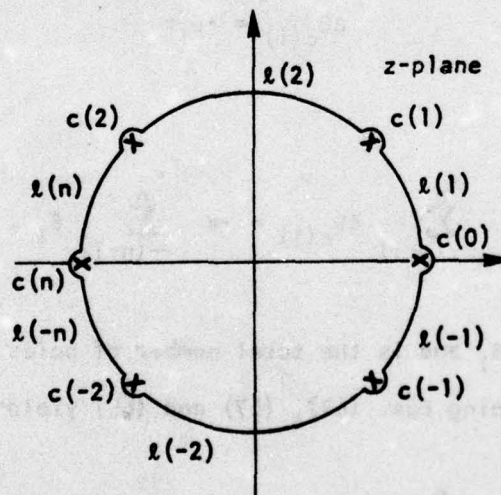


FIGURE 5-12. THE NYQUIST CONTOUR FOR DISCRETE-TIME CONTROL SYSTEMS

$$\begin{aligned}
P^*(e^{j\omega T}) &= U(\omega) - jV(\omega) \\
&= P(e^{-j\omega T}) \\
&= U(-\omega) + jV(-\omega)
\end{aligned} \tag{65}$$

Therefore, following the definition of the phase angle change, we have

$$\Delta\theta_{\ell}(i) = \Delta\theta_{\ell}(-i) \tag{66}$$

Substituting Eq. (66) into Eq. (63), yields

$$\Delta\theta_{\Gamma} = 2 \sum_{i=1}^n \Delta\theta_{\ell}(i) + \sum_{i=-(n-1)}^n \Delta\theta_{c}(i) \tag{67}$$

Next, consider the phase angle change along the semicircles  $c(i)$ . Assume that there are  $\beta_i$  poles of  $P(z)$  at  $z = e^{j\omega_i}$ , then

$$\Delta\theta_{c}(i) = -\beta_i \pi \tag{68}$$

Thus

$$\sum_{i=-(n-1)}^n \Delta\theta_{c}(i) = -\pi \sum_{i=-(n-1)}^n \beta_i \tag{69}$$

where  $\beta = \sum_{i=-(n-1)}^n \beta_i$  and is the total number of poles of  $P(z)$  on the unit circle. Combining Eqs. (62), (67) and (69) yields

$$\sum_{i=1}^n \Delta\theta_{\ell}(i) = \frac{\pi}{2} [2(\gamma - M - K) + \beta] \tag{70}$$

where

$$K = N_B - N_A \quad (71)$$

Now, we can state the generalized Nyquist criterion for discrete-time control systems, as follows:

If the return difference  $P(z)$  of the discrete-time system has the properties (1) through (3), the system is stable if and only if the total phase change along the open arcs  $\ell(i)$ ,  $i = 1, 2, \dots, n$ , is equal to  $\frac{\pi}{2} [2(\gamma - K) + \beta]$ .

Substituting  $M = 0$  into Eq. (70), we immediately prove the criterion. Program No. 9 (Appendix C) was written for use on the Fourier Analyzer to calculate and plot the phase angle of the return difference  $P(z)$  for  $0 < \omega < \frac{\omega_s}{2}$ .

**Example 6.** Consider the system with transfer functions

$$G(z) = \frac{-z^4 - 2z^3 + 0.7z^2 + 0.1z + 4}{(z^2 - 1)(z^2 + 4)} \quad (72)$$

$$H(z) = 1 \quad (73)$$

The return difference is given by

$$P(z) = \frac{z^3 + 0.7z^2 + 0.1z}{z^4 + 3z^2 - 4} \quad (74)$$

From Eqs. (72) and (74), we have

$$\beta = 2, \quad \gamma = 2, \quad K = 1$$

Therefore, the stability criterion is

$$\Delta\theta = \frac{\pi}{2} [2(\gamma-K) + \beta] = 2\pi$$

The phase plot of Eq. (74) is shown in Figure 5-13. The phase change is  $2\pi$ ; therefore, the system is stable.

Example 7. Consider the discrete-time system with transfer functions

$$G(z) = \frac{24z^4}{(z-3)(z+3)(z^2+1)} \quad (75)$$

$$H(z) = 1 \quad (76)$$

The return difference is given by

$$P(z) = \frac{25z^4 - 8z^2 - 9}{z^4 - 8z^2 - 9} \quad (77)$$

Examining Eqs. (75) and (77), yields

$$\beta = 2, \quad \gamma = 2, \quad K = 0$$

Thus, the stability criterion is

$$\begin{aligned} \Delta\theta &= \frac{\pi}{2} [2(\gamma-K) + \beta] \\ &= 3\pi \end{aligned}$$

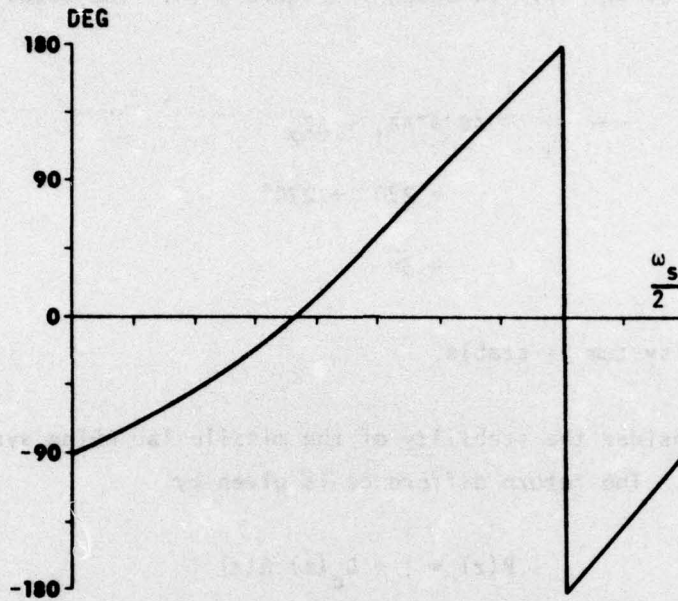


FIGURE 5-13. PHASE PLOT OF THE RETURN DIFFERENCE OF EXAMPLE 6

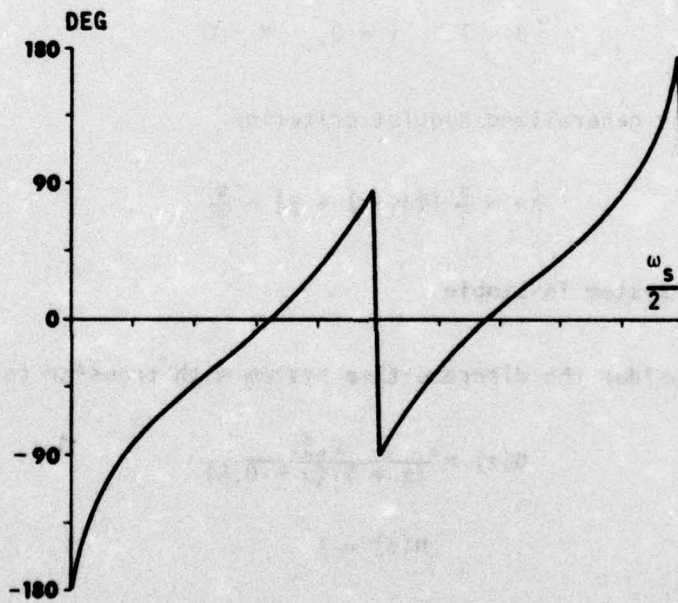


FIGURE 5-14. PHASE PLOT OF THE RETURN DIFFERENCE OF EXAMPLE 7

The phase plot of Eq. (77) is shown in Figure 5-14. The total phase change is

$$\begin{aligned}\Delta\theta &= \Delta\theta_1 + \Delta\theta_2 \\ &= 270^\circ + 270^\circ \\ &= 3\pi\end{aligned}$$

Therefore, the system is stable.

**Example 8.** Consider the stability of the missile launching system given in Section 5.4. The return difference is given by

$$P(z) = 1 + D_c(z) G(z)$$

Figure 5-15 shows the phase plot of the return difference; the phase change is  $\frac{\pi}{2}$ . From Eqs. (45) and (49), we have

$$\beta = 1, \quad \gamma = 0, \quad K = 0$$

According to the generalized Nyquist criterion

$$\Delta\theta = \frac{\pi}{2} [2(\gamma - K) + \beta] = \frac{\pi}{2}$$

Therefore, the system is stable.

**Example 9.** Consider the discrete-time system with transfer function

$$G(z) = \frac{0.5z}{(z+1)(z-0.5)} \quad (78)$$

$$H(z) = 1 \quad (79)$$

The return difference is given by

$$P(z) = \frac{z^2 + z - 0.5}{z^2 + 0.5z - 0.5} \quad (80)$$

Examining Eqs. (78) and (80), yields

$$\beta = 1, \quad \gamma = 0, \quad K = 0$$

Thus the stability criterion is  $\Delta\theta = \frac{\pi}{2}$ . The phase plot is shown in Figure 5-16; the phase angle change is  $-\frac{\pi}{2}$ . Therefore, the system is unstable.

#### 5.6 REMARKS

A unified approach to discrete-time control system analysis via the FFT algorithm has been established in this chapter. Even though only single-input/single-output systems were studied, it is evident that the approach can be easily extended to the multiple input/output case.

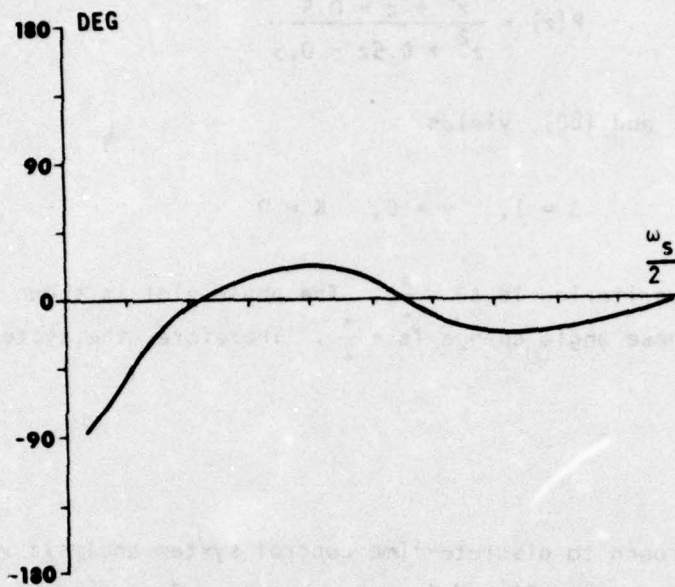


FIGURE 5-15. PHASE PLOT OF THE RETURN DIFFERENCE OF EXAMPLE 8

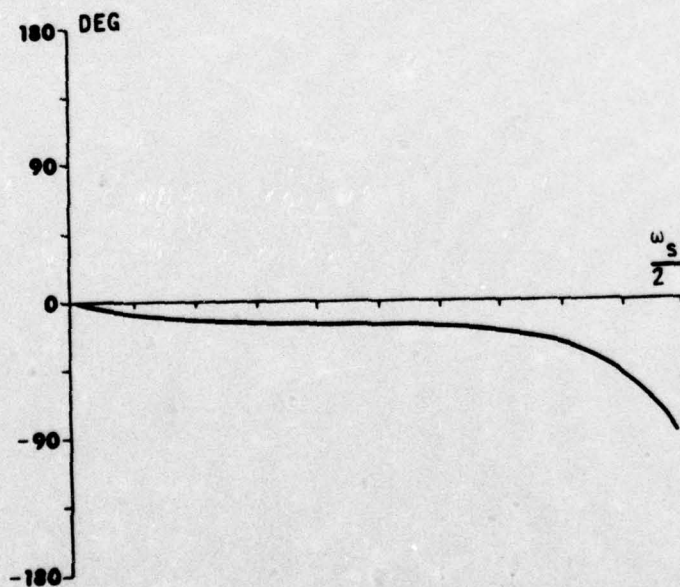


FIGURE 5-16. PHASE PLOT OF THE RETURN DIFFERENCE OF EXAMPLE 9

CHAPTER VI  
DESIGN OF DISCRETE-TIME CONTROL SYSTEMS

6.0 INTRODUCTION

A design procedure for discrete-time feedback control systems is presented in this chapter: (1) to study the closed loop specification by converting various requirements into a unified language which is manageable via the minicomputer; (2) to construct a reference model, for example, a required closed loop frequency response; (3) to search for the suitable frequency response of the compensator via the FFT algorithm; (4) to design a nonrecursive filter transfer function for the compensator using the window method; and (5) to verify the performance of the compensated system. Several design examples including type "0" and type "1" systems are developed for illustration.

6.1 FREQUENCY DOMAIN APPROACH FOR DISCRETE-TIME CONTROL SYSTEM DESIGN

Consider a basic configuration of a direct digital control (DDC) system as shown in Figure 6-1.  $G_p(s)$  is the plant;  $H(s)$  is the feedback device; and  $G_o(s)$  is the holding circuit or D/A converter. Usually the zero order hold is taken to be

$$G_o(s) = \frac{1 - e^{-sT}}{s} \quad (1)$$

where  $T$  is the sampling period.  $D_c(z)$  is the digital compensator and  $Z$  is the sampler or A/D converter.

Using the block diagram operations described in Chapter V, a simplified block diagram in the  $z$ -domain is obtained and is shown in Figure 6-2, where

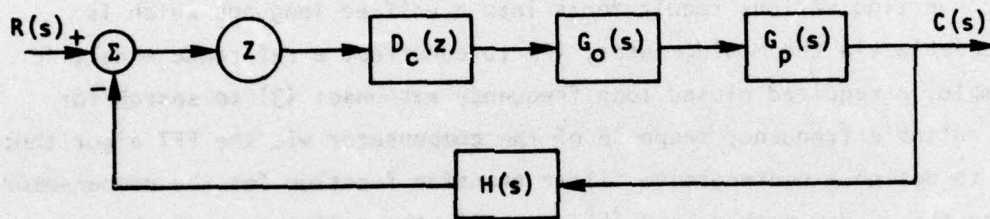


FIGURE 6-1. BASIC CONFIGURATION OF DIRECT DIGITAL CONTROL SYSTEM

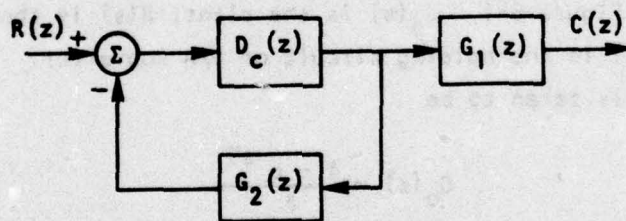


FIGURE 6-2. SIMPLIFIED BLOCK DIAGRAM IN THE Z-DOMAIN

$$G_1(z) = Z[G_p(s) G_o(s)] \quad (2)$$

and

$$G_2(z) = Z[G_o(s) G_p(s) H(s)] \quad (3)$$

Therefore, the closed loop transfer function is given by

$$F(z) = \frac{C(z)}{R(z)} = \frac{D_c(z) G_1(z)}{1 + D_c(z) G_2(z)} \quad (4)$$

The design problem is to find the compensator  $D_c(z)$  such that the characteristics of the compensated system match the required specifications.

If  $G_1(z)$  and  $G_2(z)$  are given, from Eq. (4) we have

$$D_c(z) = \frac{F(z)}{G_1(z) - G_2(z) F(z)} \quad (5)$$

In other words, if the closed loop transfer function  $F(z)$  is specified, the compensator  $D_c(z)$  is given by Eq. (5). However, there are some problem areas:

- (1) The analytic form of the specific closed loop transfer function is necessary.
- (2) The compensator  $D_c(z)$  determined by Eq. (5) is in recursive form and since the characteristics of a recursive filter are very sensitive to its coefficients, high accuracy in determining coefficients is necessary. Therefore the microcomputer, which usually has a data word length of less than 16 bits, is not always suitable to be employed as a recursive digital compensator.
- (3) The compensator determined by Eq. (5) may be unstable.

In order to avoid the disadvantages of the design method in z-domain, we will develop a frequency domain approach. The frequency response of  $D_c(z)$  is given by

$$D_c(e^{j\omega T}) = \frac{F(e^{j\omega T})}{G_1(e^{j\omega T}) - G_2(e^{j\omega T}) F(e^{j\omega T})} \quad (6)$$

If  $G_1(z)$  and  $G_2(z)$  are given, the frequency response  $G_1(e^{j\omega T})$  and  $G_2(e^{j\omega T})$  can be found using the FFT algorithm as described in Chapter V. The required information concerning the closed loop characteristics is the frequency response  $F(e^{j\omega T})$ . Therefore,  $F(z)$  can be specified either in analytic form or by the time or frequency domain characteristics from which an approximate frequency response can be found. If we take the inverse Fourier Transform of  $D_c(e^{j\omega T})$ , we can easily find the non-recursive filter form for  $D_c(z)$ . In other words, the window method for nonrecursive digital filter design as given in Chapter IV can be used to design a discrete-time control system.

## 6.2 SPECIFYING THE FREQUENCY RESPONSE OF CLOSED LOOP SYSTEMS

Many approaches are available for specifying the closed loop frequency response to match the required specifications. Two of these approaches are discussed in the ensuing paragraphs.

### (1) The Required Specification is Given In The Continuous Time Domain or The Frequency Domain

When the output of the discrete-time control system is continuous in time, we can specify the closed loop transfer function in the s-domain according to the required specifications and then find its transfer function in z-domain. For example, if we need the closed loop system which has

$$\zeta = 0.7$$

$$\omega_d = 5$$

$$K_v = 20$$

then, by the use of the multi-dimensional Newton-Raphson method<sup>[27]</sup> the required closed loop transfer function can be determined and is given by

$$F_1(s) = \frac{4.350s + 12.674}{s^2 + 4.984s + 12.674} \quad (7)$$

Assuming the sampling period of the system is  $T = 0.1$  seconds; the z-transform of  $F(s)$  is given by

$$F(z) = \frac{4.350z^2 - 3.140z}{z^2 - 1.5087z + 0.6075} \quad (8)$$

Using the FFT algorithm, the frequency response of the closed loop transfer function can be easily found.

## (2) The Specification is Given by The Discrete Transient Response

If the impulse response of the closed loop is specified, the frequency response can be obtained by taking the inverse Fourier Transform of the impulse response. Sometimes, the step response, instead of the impulse response, of the closed loop is specified. In this case, we need to find the impulse response first. Since the step response is

$$C_u(z) = F(z) \frac{z}{z-1} \quad (9)$$

the impulse response is given by

$$\begin{aligned}
 C_{\delta}(z) &= C_u(z) \frac{z^{-1}}{z} \\
 &= C_u(z) (1 - z^{-1})
 \end{aligned}
 \tag{10}$$

In the time domain, we have

$$C_{\delta}(t) = C_u(t) - C_u(t-T) \tag{11}$$

The Fourier Analyzer contains a differentiator which is actually an operator with transfer function  $1 - z^{-1}$ ; therefore, the impulse response can be found from the step response using the differentiator. Once the impulse response is obtained, the frequency response of the closed loop can be found easily. Program No. 10 (Appendix C) can be used to find the frequency response from the step response.

For example, the required unit step response is listed in Table 6-1 and the sampling period is  $T = 0.1$  seconds. The transient response for  $0 \leq t \leq 5.0$  is plotted in Figure 6-3(a). Using Program No. 10 (Appendix C), the impulse response was obtained and is shown in Figure 6-3(b) and listed in Table 6-1. The frequency response is shown in Figures 6-3(c) and 6-3(d).

TABLE 6-1

REQUIRED UNIT STEP AND IMPULSE RESPONSES

t	$C_u(t)$	$C_{\delta}(t)$	t	$C_u(t)$	$C_{\delta}(t)$
0	0	0	0.9	0.985	0.005
0.1	0.280	0.280	1.0	0.995	0.010
0.2	0.850	0.570	1.1	1.010	0.015
0.3	1.050	0.200	1.2	1.005	-0.005
0.4	1.100	0.050	1.3	0.998	-0.007
0.5	1.070	-0.030	1.4	0.999	0.001
0.6	1.030	-0.040	1.5	1.000	0
0.7	0.990	-0.040	.	1.000	0
0.8	0.980	-0.010	.	1.000	0
			$\infty$	1.000	0

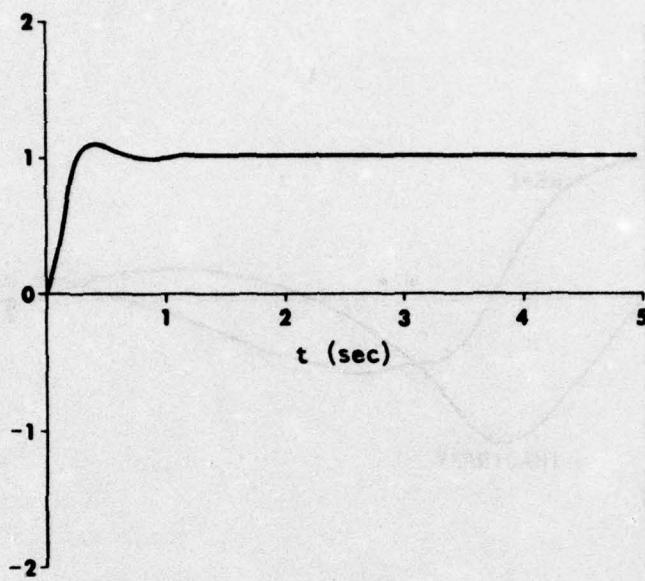


FIGURE 6-3(a). REQUIRED UNIT STEP RESPONSE

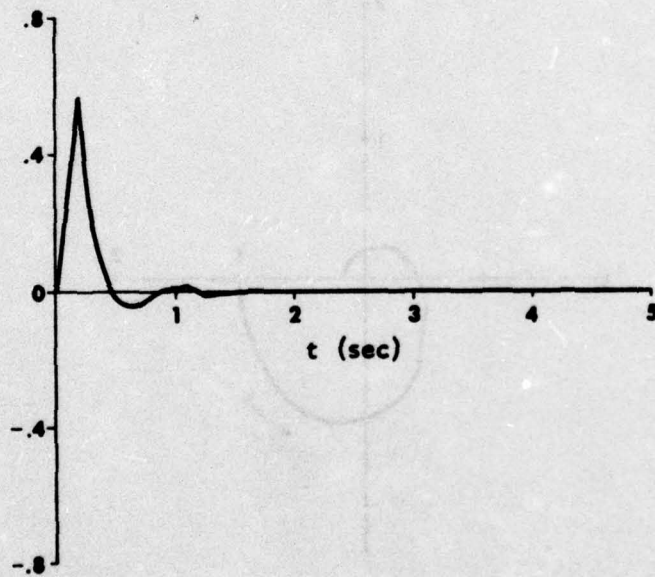


FIGURE 6-3(b). UNIT IMPULSE RESPONSE

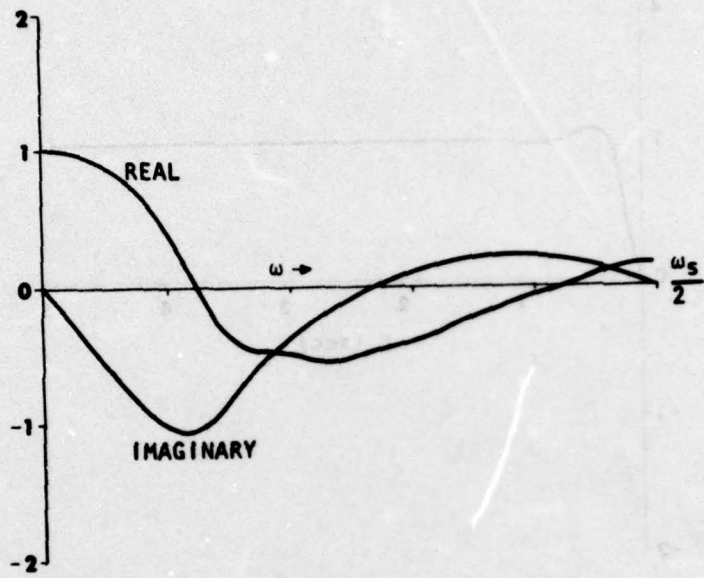


FIGURE 6-3(c). FREQUENCY RESPONSE (RECTANGULAR)

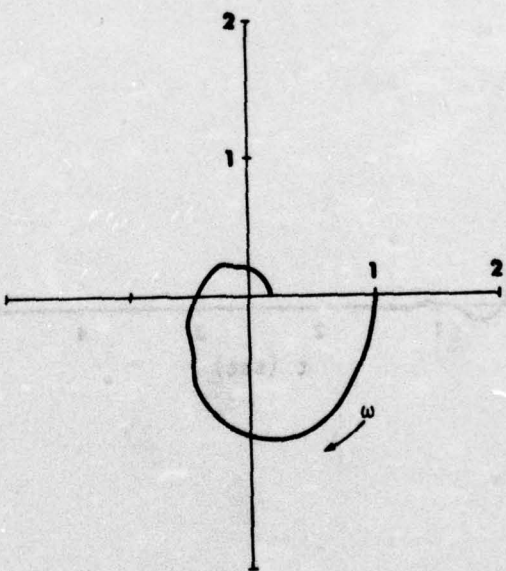


FIGURE 6-3(d). FREQUENCY RESPONSE (POLAR)

### 6.3 THE STEADY STATE ERROR AT THE SAMPLING INSTANTS

Consider the unit feedback system as shown in Figure 6-4. The system error is defined as

$$\begin{aligned} E(z) &= R(z) - C(z) \\ &= \frac{R(z)}{1 + G(z)} \end{aligned} \quad (12)$$

where  $R(z)$  is the input and  $C(z)$  is the output. From the Final Value theorem, the steady state error is given by

$$\begin{aligned} e_{ss} &= \lim_{t \rightarrow \infty} e(t) \\ &= \lim_{z \rightarrow 1} \frac{z-1}{z} E(z) \\ &= \lim_{z \rightarrow 1} \frac{(z-1) E(z)}{z[1 + G(z)]} \end{aligned} \quad (13)$$

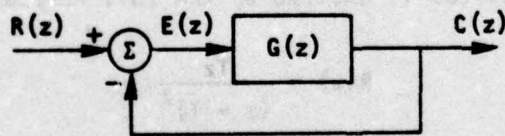


FIGURE 6-4. THE UNIT FEEDBACK SYSTEM

The following three kinds of steady state errors are most important in considering the closed loop specifications:

(1) Position errors.

The position error  $e_p$  is defined as the steady state error when the input is the unit step function

$$R(z) = \frac{z}{z-1} \quad (14)$$

From Eq. (13), we have

$$e_p = \lim_{z \rightarrow 1} \frac{1}{1+G(z)} = \frac{1}{1+G(1)} = \frac{1}{K_p} \quad (15)$$

where

$$K_p = 1 + G(1) \quad (16)$$

is called the position error constant. For type "0" systems, the position error  $e_p$  is finite; for type "1" or higher systems, the position error  $e_p$  is zero.

(2) Velocity errors.

The velocity error  $e_v$  is defined as the steady state error when the system is excited by the unit ramp signal

$$R(z) = \frac{Tz}{(z-1)^2} \quad (17)$$

Thus, from Eq. (13) we have

$$e_v = \lim_{z \rightarrow 1} \frac{T}{(z-1)[1+G(z)]} \quad (18)$$

$$= \frac{1}{K_v} \quad (19)$$

where

$$K_v = \frac{1}{T} \lim_{z \rightarrow 1} (z - 1) G(z) \quad (20)$$

is called the velocity error constant. For type "0" systems  $e_v = \infty$ ; for type "1" systems  $e_v$  is finite; and for type "2" or higher systems  $e_v = 0$ .

### (3) Acceleration errors.

The acceleration error  $e_a$  is defined as the steady state error when the system is excited by the unit parabolic signal

$$r(t) = \frac{1}{2} t^2 \quad (21)$$

or

$$R(z) = \frac{T^2(z+1)z}{2(z-1)^2} \quad (22)$$

Therefore, from Eq. (13) we have

$$\begin{aligned} e_a &= \lim_{z \rightarrow 1} \frac{T^2}{(z-1)^2 [1 + G(z)]} \\ &= \frac{1}{K_a} \end{aligned} \quad (23)$$

where

$$K_a = \frac{1}{T^2} \lim_{z \rightarrow 1} (z-1)^2 G(z) \quad (24)$$

is called the acceleration error constant. For type "0" and type "1" systems,  $e_a = \infty$ ; for type "2" systems  $e_a$  is finite; for type "3" or higher systems  $e_a = 0$ .

If the open loop transfer function  $G(z)$  is given, it is straightforward to find the error constants  $K_p$ ,  $K_v$  and  $K_a$ . If only the closed loop transfer function  $F(z)$  is given, we have to find the open loop transfer function

$$G(z) = \frac{F(z)}{1 - F(z)} \quad (25)$$

and then find the error constants. However, if only the frequency response of the closed loop is specified as described in Section 6.2, we do not have the analytic form for  $F(z)$ , and must find the error constants from the frequency response.

Substituting Eq. (25) into Eq. (16), yields

$$K_p = \lim_{z \rightarrow 1} \left[ 1 + \frac{F(z)}{1 - F(z)} \right] \quad (26)$$

Since  $z = e^{j\omega T}$ ,  $z \rightarrow 1$  corresponds to  $\omega \rightarrow 0$ . Thus, in the frequency domain Eq. (26) becomes

$$K_p = \lim_{\omega \rightarrow 0} \frac{1}{1 - F(e^{j\omega T})} \quad (27)$$

Similarly, from Eqs. (20) and (24), we have

$$K_v = \lim_{\omega \rightarrow 0} \frac{F(e^{j\omega T})(e^{j\omega T} - 1)}{T[1 - F(e^{j\omega T})]} \quad (28)$$

and

$$K_a = \lim_{\omega \rightarrow 0} \frac{F(e^{j\omega T})(e^{j\omega T} - 1)}{T^2[1 - F(e^{j\omega T})]} \quad (29)$$

Most servo systems or autopilot systems are type "1", and the velocity error is important; therefore, we will discuss the velocity error constant  $K_v$  in detail. For the type 1 system, the open loop transfer function can be rewritten as

$$G(z) = \frac{1}{z-1} X(z) \quad (30)$$

where  $X(1)$  is nonzero finite. Thus, the closed loop transfer function is given by

$$F(z) = \frac{G(z)}{1 + G(z)} = \frac{X(z)}{(z-1) + X(z)} \quad (31)$$

and

$$F(1) = 1 \quad (32)$$

In other words,  $F(z) - 1$  has a factor  $(z - 1)$ . From Eq. (31), we have

$$\frac{dF(z)}{dz} = \frac{(z-1)\frac{dX(z)}{dz} - X(z)}{[(z-1) + X(z)]^2} \quad (33)$$

Therefore, we have

$$F'(1) = -\frac{1}{X(1)} \quad (34)$$

Since  $X(1)$  is nonzero finite, we conclude that  $F'(1) \neq 0$  and  $z = 1$  is a simple root of  $F(z) - 1 = 0$  or

$$Y(z) \triangleq \frac{F(z) - 1}{z - 1} \quad (35)$$

is nonzero finite as  $z \rightarrow 1$ .

If we define

$$D(z) = \frac{F(z)}{\frac{z}{z-1} - \frac{z}{z-1} F(z)} \quad (36)$$

then  $z = 1$  is the simple root of  $F(z) - 1 = 0$ , and the denominator of Eq. (36) is nonzero finite as  $z \rightarrow 1$ . From Eq. (28) we have

$$K_V = \frac{1}{T} D(e^{j\omega T}) \Big|_{\omega = 0} \quad (37)$$

Another approach to finding  $K_V$  is to first find the error response  $E(z)$ . From Eq. (12), the error response of the unit ramp input is

$$\begin{aligned} E(z) &= \frac{\frac{Tz}{(z-1)^2}}{1 + \frac{F(z)}{1-F(z)}} \\ &= Tz^{-1} \left[ \frac{z}{z-1} - \frac{z}{z-1} F(z) \right] \end{aligned} \quad (38)$$

Since  $\frac{z}{z-1} F(z)$  is the unit step response of the closed loop,  $\frac{z}{z-1} - \frac{z}{z-1} F(z)$  is the error response of the unit step input. If the closed loop characteristic is specified by its unit step response, the error response of the unit step input in the time domain

$$e_u(t) = Z^{-1} \left[ \frac{z}{z-1} - \frac{z}{z-1} F(z) \right] \quad (39)$$

can be found easily. Then, the error response of the unit ramp in the time domain

$$e_r(t) = Z^{-1}[E(z)] \quad (40)$$

can be obtained by integrating  $(\frac{z}{z-1})$  and the right shifting ( $Z^{-1}$ ) of  $E_u(t)$ . Once  $e_r(t)$  is found, the velocity error is

$$e_v = \lim_{t \rightarrow \infty} [t - e_r(t)] \quad (41)$$

and

$$K_v = \frac{1}{e_v} \quad (42)$$

The entire procedure for finding the frequency response and analyzing the velocity error from the specified step response of the closed loop is included in Program No. 11 (Appendix C).

For the system with closed loop step response shown in Figure 6-3(a), the frequency response of  $D(z)$  [Eq. (36)] is shown in Figure 6-4(a). From Figure 6-4(a), we have  $D(e^{j\omega T}) = 0.604$  when  $\omega = 0$ ; therefore,

$$K_v = \frac{D(1)}{T} = 6.04 \quad (43)$$

The error response of the unit ramp input is shown in Figure 6-4(b). The steady state error is approximately 0.1654; thus,

$$K_v = \frac{1}{e_v} = 6.04595 \quad (44)$$

and the results of Eqs. (43) and (44) are consistent.

#### 6.4 CALCULATION OF THE FREQUENCY RESPONSE OF REQUIRED COMPENSATOR

The basic formula for finding the frequency response of the required compensator is given by Eq. (6). For computing advantages, we need to study the following system categories:

(1) Type "0" systems.

For the type "0" system, no pole occurs at  $z = 1$  for both  $G_1(z)$  and  $G_2(z)$ ; therefore, Eq. (6) can be used without difficulty. In the unit feedback system as shown in Figure 6-4,  $G(z) \triangleq G_1(z) = G_2(z)$ ; therefore, we have

$$D_c(e^{j\omega T}) = \frac{F(e^{j\omega T})}{G(e^{j\omega T})[1 - F(e^{j\omega T})]} \quad (45)$$

When  $\omega = 0$ , or  $e^{j\omega T} = 1$ , we have

$$D_c(1) = \frac{F(1)}{G(1)[1 - F(1)]} \quad (46)$$

From Eq. (27) we have

$$K_p = \frac{1}{1 - F(1)} \quad (47)$$

and

$$F(1) = 1 + \frac{1}{K_p} \quad (48)$$

Thus, we have

$$D_c(1) = \frac{1 + K_p}{G(1)} \quad (49)$$

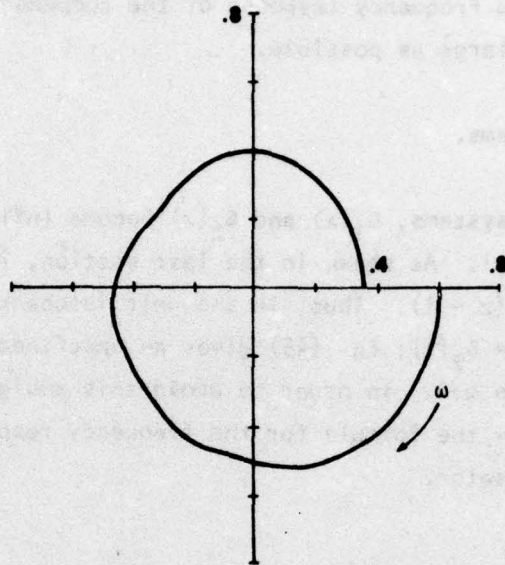


FIGURE 6-4(a). FREQUENCY RESPONSE OF  $D(z)$

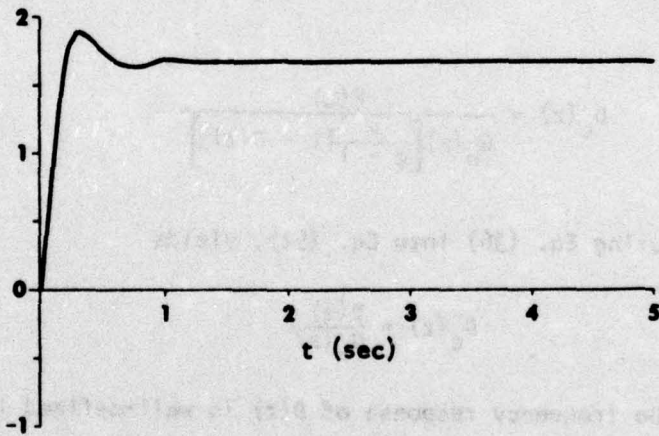


FIGURE 6-4(b). ERROR RESPONSE OF THE UNIT RAMP INPUT

When a small position error or a large position error constant ( $K_p$ ) is required, Eq. (49) indicates that the dc gain of the frequency response of the compensator should be as large as possible.

(2) Type "1" systems.

For type "1" systems,  $G_1(z)$  and  $G_2(z)$  become infinite when  $\omega \rightarrow 0$  or  $z \rightarrow 1$ . As shown in the last section,  $[1 - F(z)]$  has a factor  $(z - 1)$ . Thus, in the unit feedback system,  $G(z) \triangleq G_1(z) = G_2(z)$ ; Eq. (45) gives an undefined value for  $D_c(z)$  when  $\omega \rightarrow 0$ . In order to avoid this ambiguity, we must modify the formula for the frequency response of the compensator.

Assume that

$$G(z) = \frac{z}{z-1} G_n(z) \quad (50)$$

when  $G_n(z)$  has no pole or zero at  $z = 1$ . From Eq. (45), we have

$$D_c(z) = \frac{F(z)}{G_n(z) \left[ \frac{z}{z-1} [1 - F(z)] \right]} \quad (51)$$

Substituting Eq. (36) into Eq. (51), yields

$$D_c(z) = \frac{D(z)}{G_n(z)} \quad (52)$$

Since the frequency response of  $D(z)$  is well-defined for  $0 \leq \omega \leq \omega_s$ , the frequency response of the required compensator is given by

$$D_c(e^{j\omega T}) = \frac{D(e^{j\omega T})}{G_n(e^{j\omega T})} \quad (53)$$

From Eq. (37), we see that

$$D(1) = TK_v \quad (54)$$

When  $\omega = 0$ , we have

$$D_c(1) = \frac{TK_v}{G_n(1)} \quad (55)$$

Eq. (55) indicates that the dc gain of the frequency response of the compensator is proportional to the velocity error constant  $K_v$ .

#### 6.5 GENERAL PROCEDURE FOR DESIGNING NONRECURSIVE COMPENSATORS BY THE WINDOW METHOD

Once the frequency response of the required compensator is found, the frequency response can be expanded as a Fourier series in the frequency domain and then truncated through the use of windows to construct a nonrecursive compensator of the proper order. The basic principle is the same as the window method for nonrecursive digital filter design.

As pointed out in Chapters II and III, the effects of windowing are: (1) to reduce or to eliminate the Gibbs' phenomenon in the frequency domain and (2) to improve the damping rate of the side lobes of the rectangular window which corresponds to the truncation of the Fourier series. In most cases, we do not have a point of discontinuity in the frequency response of the compensator; therefore, the principal effect of windowing in nonrecursive compensator design is the latter. In fact, this effect smooths the frequency response of the compensator.

The general procedure for nonrecursive compensator design by the window method can be outlined as follows:

- (1) Specify the closed loop characteristics; such as the overshoot, the rise time, the settling time, the velocity error, the position error, etc.
- (2) Find the frequency response of the closed loop matching the required specifications.
- (3) Calculate the frequency response of the required compensator from the frequency responses of the open loop and the closed loop.
- (4) Construct the transfer function of the compensator from its frequency response by the window method and determine the compensator in nonrecursive form.
- (5) Check the closed loop characteristics of the compensated system; such as the frequency response, the impulse response, the step response, etc.

The whole procedure can be performed using the FFT algorithm. Following this procedure, the Fourier Analyzer becomes a power tool for discrete-time control system design.

Since there are some differences in computation of the frequency responses of the compensator for type "0" and type "1" systems, two separate programs were prepared for the design of each type. Program No's 12 and 13 (Appendix C) were written for type "0" and type "1" system designs respectively.

## 6.6 TYPE "0" SYSTEM DESIGN

Example 1. Consider the dynamic system as shown in Figure 6-5. The required specifications are as follows:

- (1) The rise time is less than  $4T$ ,  $T = 0.2$  seconds,
- (2) The overshoot is less than 15%, and
- (3) The position error constant  $K_p = 5$ .

The open loop transfer function in the  $z$ -domain is given by

$$\begin{aligned} G(z) &= z \left[ G_p(s) \frac{1 - z^{-1}}{s} \right] \\ &= \frac{0.4487z + 0.2962}{z^2 - 0.5564z + 0.3012} \end{aligned} \quad (56)$$

The open loop frequency response is shown in Figure 6-6. The step response as shown in Figure 6-7(a) is the specified model of the required closed loop, and matches all the specifications given by (1) through (3). The frequency response of the closed loop, based on the step response in Figure 6-7(a), is shown in Figure 6-7(b) and the frequency response of the required compensator is shown in Figure 6-7(c).

The coefficients of nonrecursive compensators obtained by different windows are shown in Table 6-2. Figures 6-8(a), (b) and (c) show the frequency response of  $D_1(z)$  obtained using the rectangular window, the corresponding system frequency response, and the unit step response of the compensated closed loop system with compensator  $D_1(z)$ , respectively. From Figure 6-8 we see that both the frequency response and the transient response have too many ripples; therefore, this compensator is not suitable. Figures 6-9(a), (b) and (c) show the frequency response of

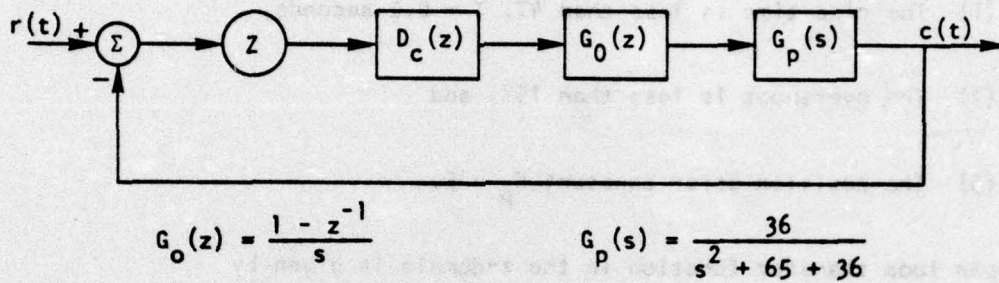


FIGURE 6-5. A TYPE "0" DYNAMIC SYSTEM

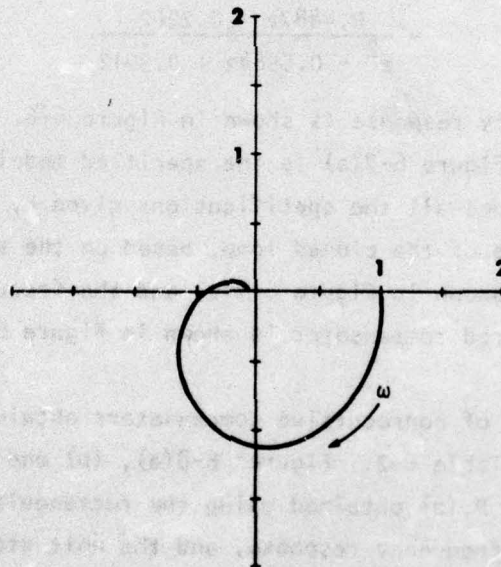
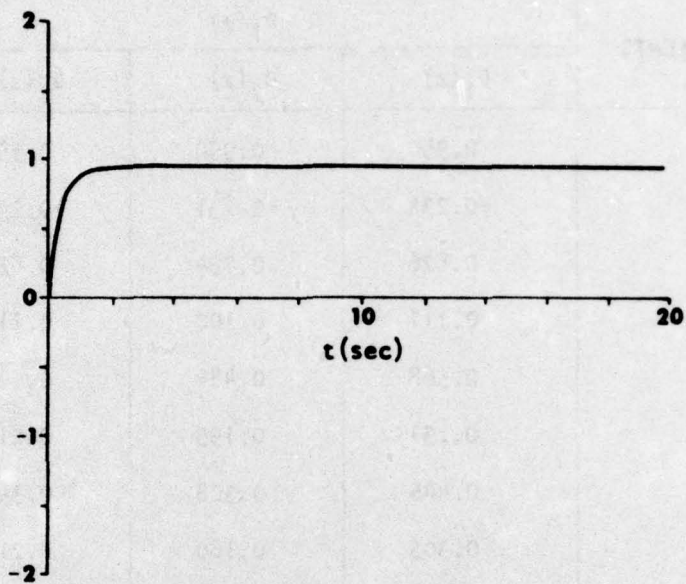
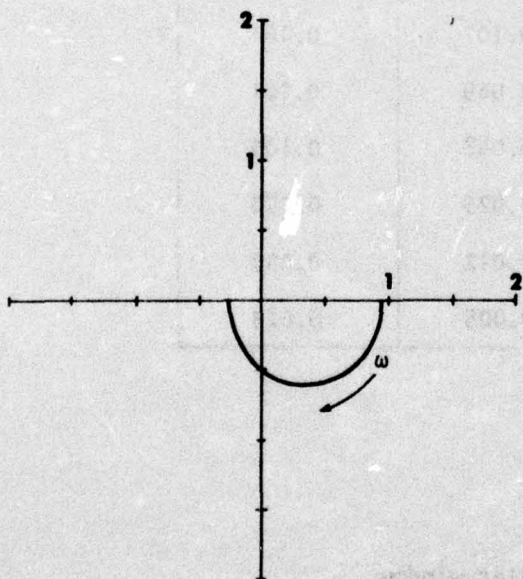


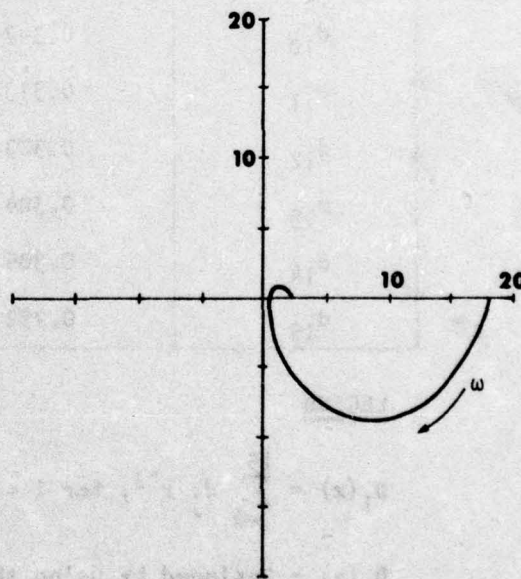
FIGURE 6-6. OPEN LOOP FREQUENCY RESPONSE



(a) REQUIRED UNIT STEP RESPONSE



(b) REQUIRED CLOSED LOOP  
FREQUENCY RESPONSE



(c) FREQUENCY RESPONSE OF  
THE REQUIRED COMPENSATOR

FIGURE 6-7. DESIGN MODELS OF EXAMPLE 1

TABLE 6-2  
COMPENSATORS FOR EXAMPLE 1

COEFFICIENTS	$D_i(z)$		
	$D_1(z)$	$D_2(z)$	$D_3(z)$
$d_0$	0.950	0.950	0.950
$d_1$	-0.234	-0.231	-0.234
$d_2$	0.826	0.794	0.826
$d_3$	0.111	0.102	0.111
$d_4$	0.568	0.484	0.524
$d_5$	0.251	0.195	0.212
$d_6$	0.446	0.308	0.343
$d_7$	0.303	0.180	0.210
$d_8$	0.383	0.192	0.236
$d_9$	0.316	0.127	0.170
$d_{10}$	0.347	0.107	0.161
$d_{11}$	0.313	0.069	0.121
$d_{12}$	0.323	0.048	0.100
$d_{13}$	0.304	0.025	0.070
$d_{14}$	0.305	0.012	0.047
$d_{15}$	0.292	0.005	0.023

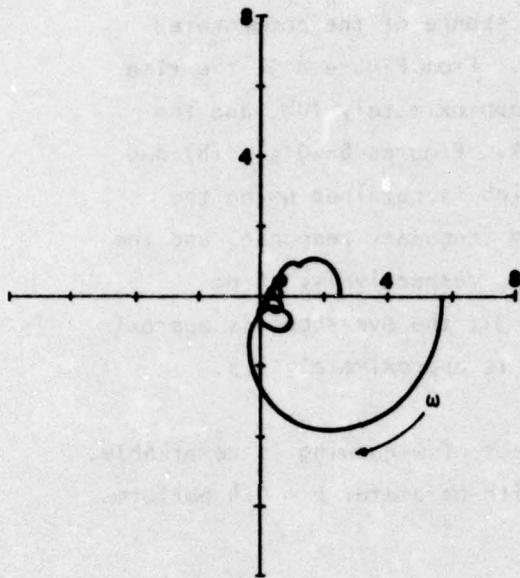
**LEGEND**

$$D_i(z) = \sum_{j=0}^{15} d_j z^{-j}, \text{ for } i = 1, 2, 3.$$

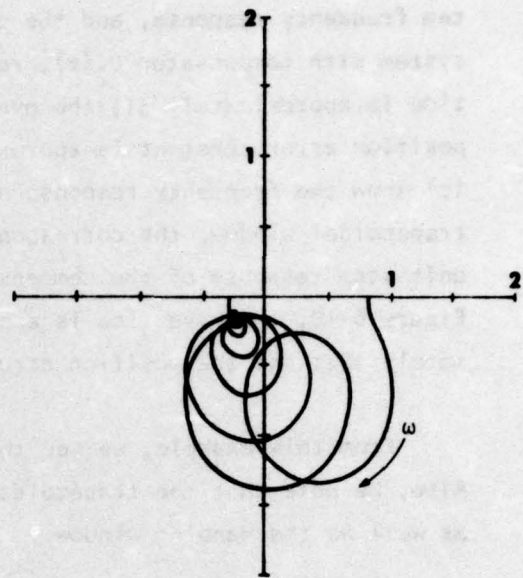
$D_1(z)$  - Designed by using the rectangular window.

$D_2(z)$  - Designed by using the Hanning window.

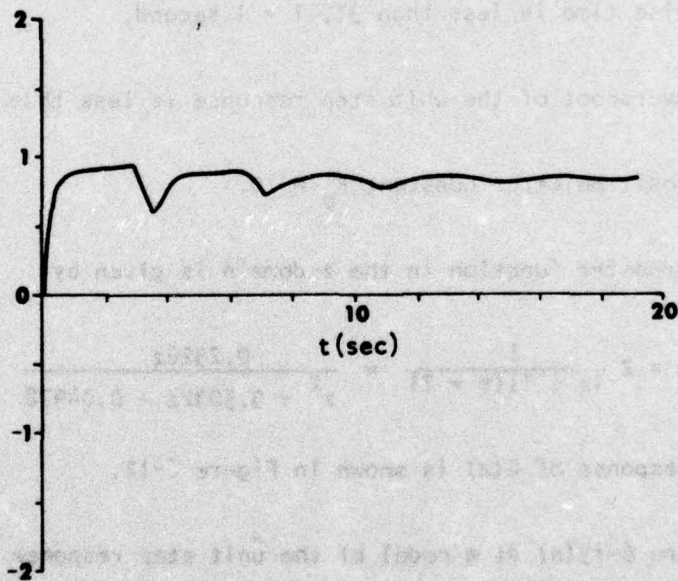
$D_3(z)$  - Designed by using the trapezoidal window,  $b = 0.4$ .



(a) FREQUENCY RESPONSE OF THE COMPENSATOR  $D_1(z)$



(b) FREQUENCY RESPONSE OF THE COMPENSATED SYSTEM



(c) UNIT STEP RESPONSE OF THE COMPENSATED SYSTEM

FIGURE 6-8. PERFORMANCE OF THE SYSTEM COMPENSATED WITH  $D_1(z)$

$D_2(z)$  which is obtained using the Hanning window, the corresponding system frequency response, and the unit step response of the compensated system with compensator  $D_2(z)$ , respectively. From Figure 6-9, the rise time is approximately  $3T$ ; the overshoot is approximately 10%, and the position error constant is approximately 4.4. Figures 6-10(a), (b) and (c) show the frequency response of  $D_3(z)$  which is obtained using the trapezoidal window, the corresponding system frequency response, and the unit step response of the compensated system, respectively. From Figure 6-10, the rise time is approximately  $3T$ ; the overshoot is approximately 12%; and the position error constant is approximately 4.9.

From this example, we see that the effect of windowing is remarkable. Also, we note that the trapezoidal window with parameter  $b = 0.4$  performs as well as the Hanning window.

**Example 2.** Consider the system as shown in Figure 6-11. The required specifications are as follows:

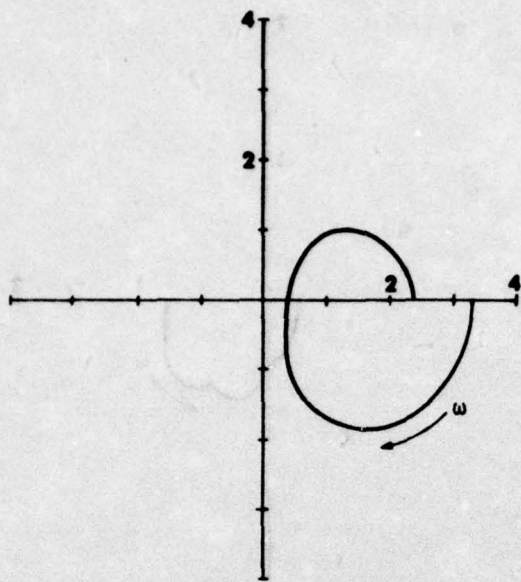
- (1) The rise time is less than  $3T$ ,  $T = 1$  second,
- (2) The overshoot of the unit step response is less than 30%, and
- (3) The position error constant  $K_p = 10$ .

The open loop transfer function in the  $z$ -domain is given by

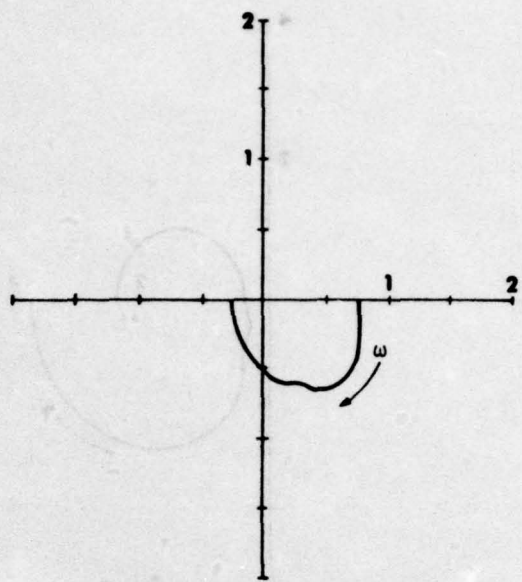
$$G(z) = Z \frac{1}{(s+1)(s+2)} = \frac{0.2326z}{z^2 - 0.5032z + 0.04978} \quad (57)$$

The frequency response of  $G(z)$  is shown in Figure 6-12.

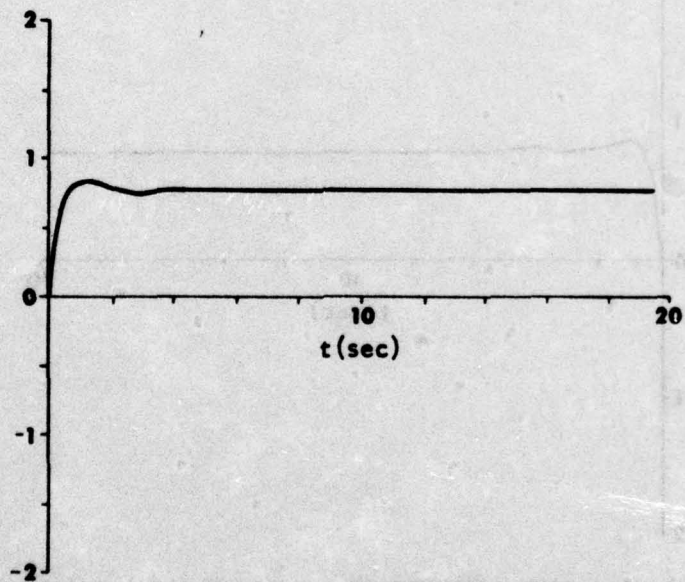
Using Figure 6-13(a) as a model of the unit step response for the compensated closed loop system, the required frequency response is shown



(a) FREQUENCY RESPONSE OF THE COMPENSATOR  $D_2(z)$

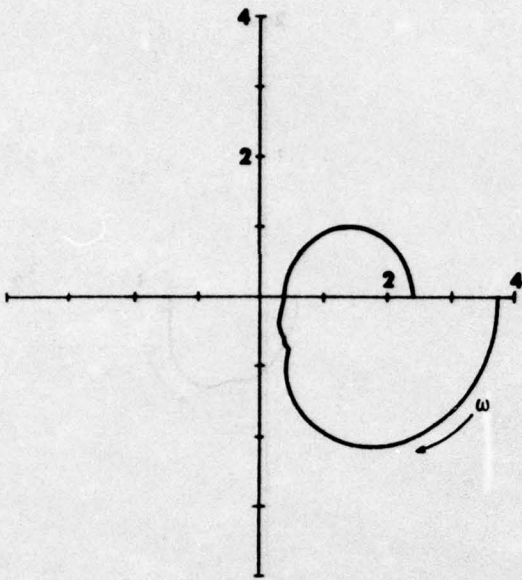


(b) FREQUENCY RESPONSE OF THE COMPENSATED SYSTEM

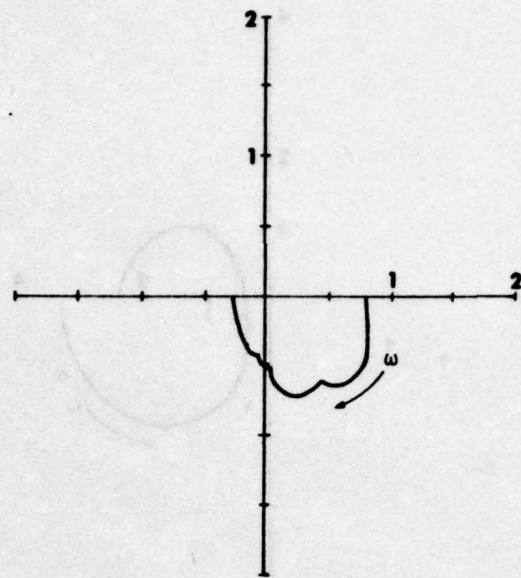


(c) UNIT STEP RESPONSE OF THE COMPENSATED SYSTEM

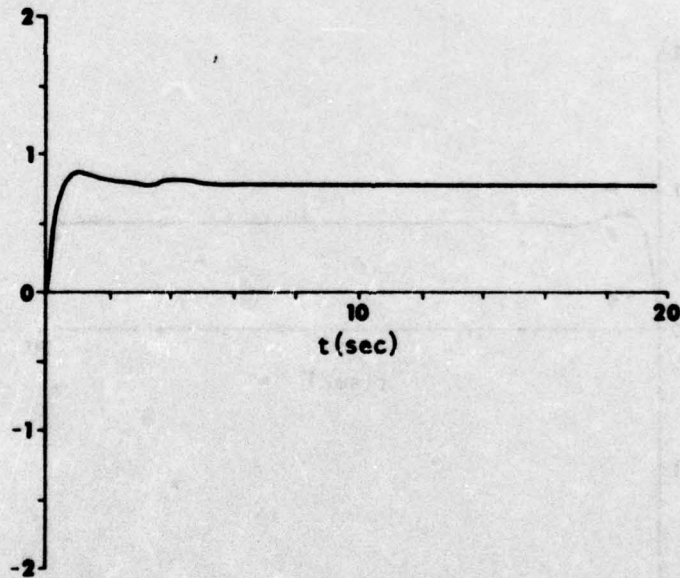
FIGURE 6-9. PERFORMANCE OF THE SYSTEM COMPENSATED WITH  $D_2(z)$



(a) FREQUENCY RESPONSE OF THE COMPENSATOR  $D_3(z)$



(b) FREQUENCY RESPONSE OF THE COMPENSATED SYSTEM



(c) UNIT STEP RESPONSE OF THE COMPENSATED SYSTEM

FIGURE 6-10. PERFORMANCE OF THE SYSTEM COMPENSATED WITH  $D_3(z)$

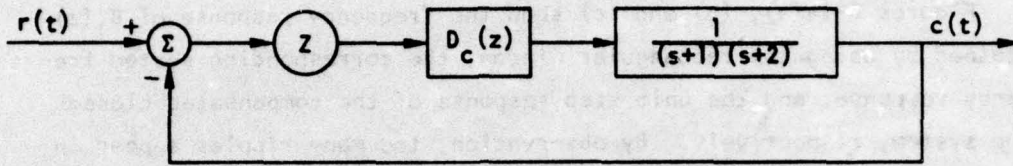


FIGURE 6-11. A TYPE "0" SYSTEM WITH DIGITAL CONTROLLER

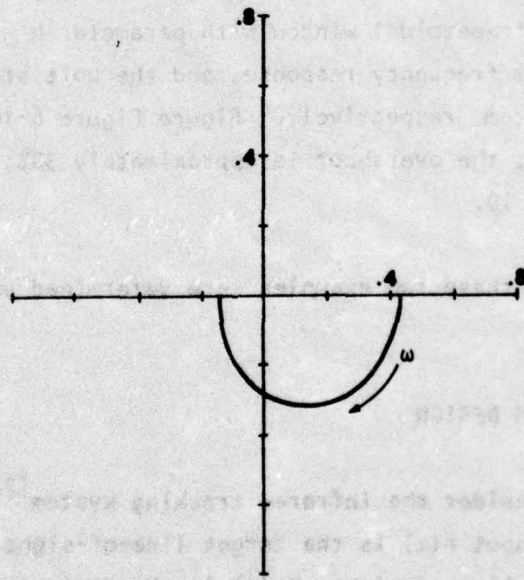


FIGURE 6-12. OPEN LOOP FREQUENCY RESPONSE

in Figure 6-13(b). The frequency response of the compensator is shown in Figure 6-13(c). The coefficients of nonrecursive compensators obtained using various windows are listed in Table 6-3.

Figures 6-14(a), (b) and (c) show the frequency response of  $D_1(z)$  obtained by using the rectangular window, the corresponding system frequency response, and the unit step response of the compensated closed loop system, respectively. By observation, too many ripples appear in the closed loop frequency response and too many wavelets in the transient response; therefore, this compensator is not acceptable.

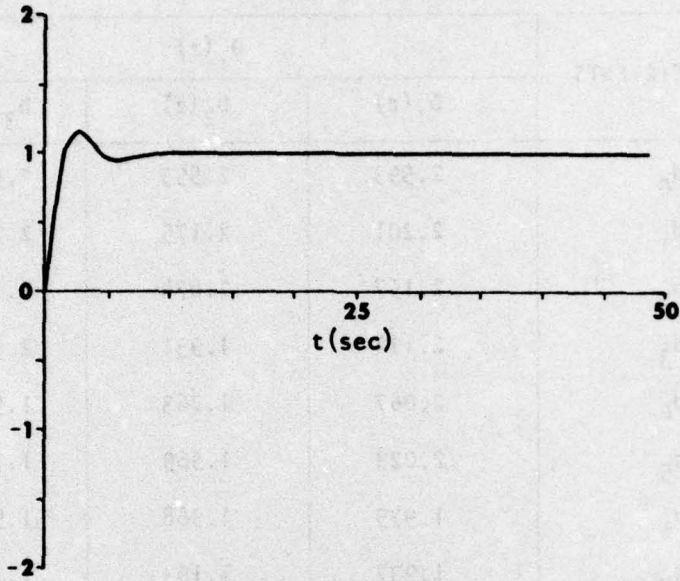
Figures 6-15(a), (b) and (c) show the frequency response of  $D_2(z)$  obtained using the Hanning window, the corresponding system frequency response and the unit step response of the compensated system respectively. From Figure 6-15, the rise time is approximately  $2T$ ; the overshoot is approximately 28%; and the position error constant  $K_p \cong 9$ .

Figures 6-16(a), (b) and (c) show the frequency response of  $D_3(z)$  obtained using the trapezoidal window with parameter  $b = 0.4$ , the corresponding system frequency response, and the unit step response of the compensated system, respectively. Figure Figure 6-16, the rise time is approximately  $2T$ ; the overshoot is approximately 30%; and the position error constant  $K_p \cong 10$ .

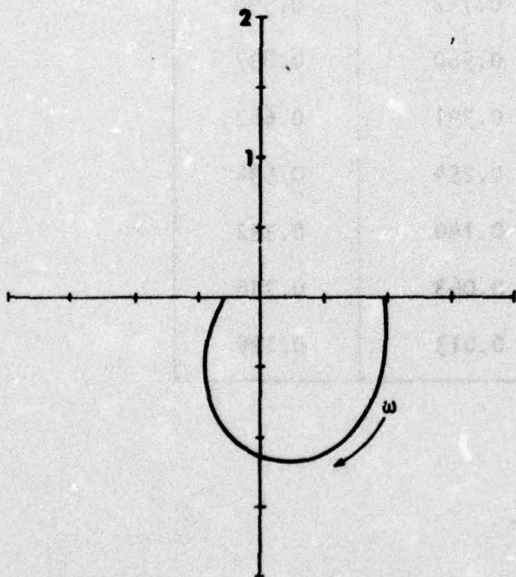
The results of these two examples were determined using Program No. 12 (Appendix C).

## 6.7 TYPE "I" SYSTEM DESIGN

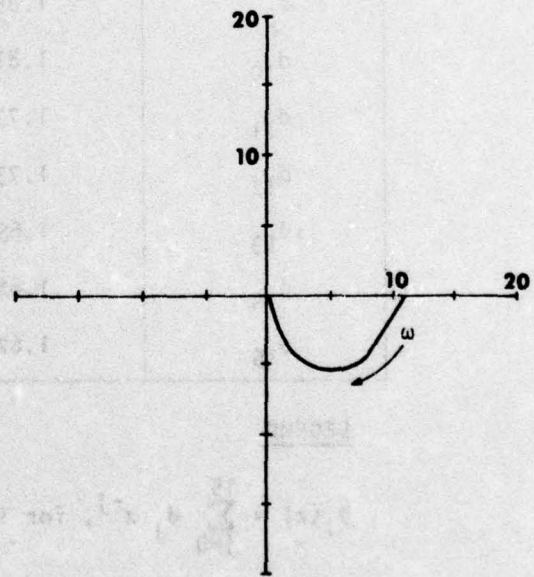
Example 3. Consider the infrared tracking system<sup>[22]</sup> as shown in Figure 6-17. The input  $r(t)$  is the target line-of-sight; the output  $c(t)$  is the tracker line-of-sight;  $D_c(z)$  is the digital compensator and  $G_0(s)$  is the zero order hold given by



(a) REQUIRED UNIT STEP RESPONSE



(b) REQUIRED CLOSED LOOP  
FREQUENCY RESPONSE



(c) FREQUENCY RESPONSE OF  
THE REQUIRED COMPENSATOR

FIGURE 6-13. DESIGN MODELS OF EXAMPLE 2

TABLE 6-3

## COMPENSATORS FOR EXAMPLE 2

COEFFICIENTS	$D_i(z)$		
	$D_1(z)$	$D_2(z)$	$D_3(z)$
$d_0$	2.593	2.593	2.593
$d_1$	2.201	2.175	2.201
$d_2$	2.157	2.074	2.157
$d_3$	2.114	1.931	2.114
$d_4$	2.067	1.763	1.908
$d_5$	2.023	1.569	1.712
$d_6$	1.979	1.368	1.522
$d_7$	1.937	1.153	1.341
$d_8$	1.894	0.947	1.166
$d_9$	1.853	0.742	0.998
$d_{10}$	1.813	0.560	0.837
$d_{11}$	1.774	0.391	0.682
$d_{12}$	1.735	0.254	0.534
$d_{13}$	1.697	0.140	0.392
$d_{14}$	1.660	0.063	0.256
$d_{15}$	1.623	0.013	0.125

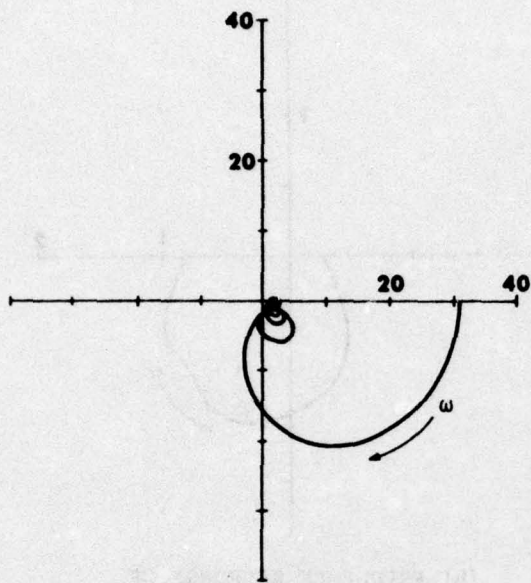
LEGEND

$$D_i(z) = \sum_{j=0}^{15} d_j z^{-j}, \text{ for } i = 1, 2, 3.$$

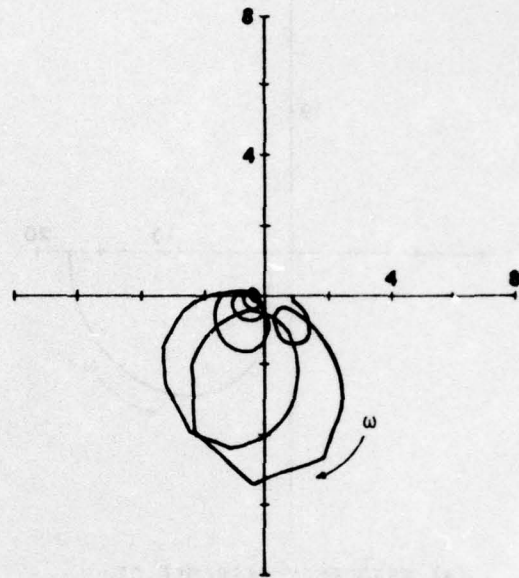
$D_1(z)$  - Designed by using the rectangular window.

$D_2(z)$  - Designed by using the Hanning window.

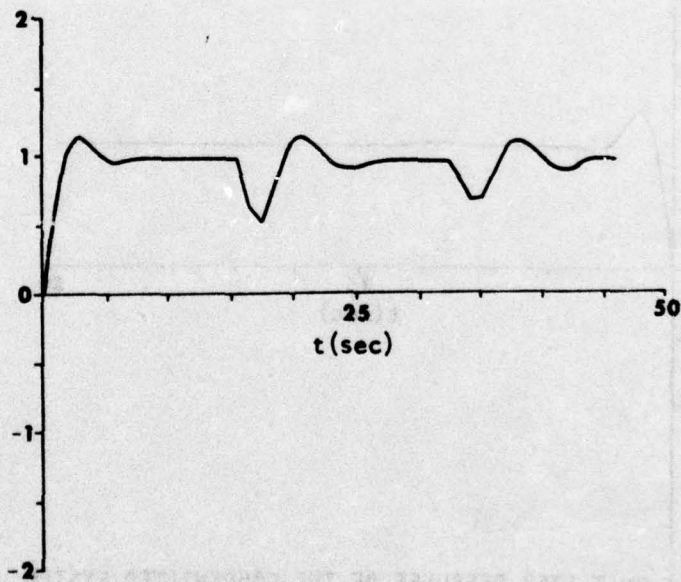
$D_3(z)$  - Designed by using the trapezoidal window,  $b = 0.4$ .



(a) FREQUENCY RESPONSE OF THE COMPENSATOR  $D_1(z)$

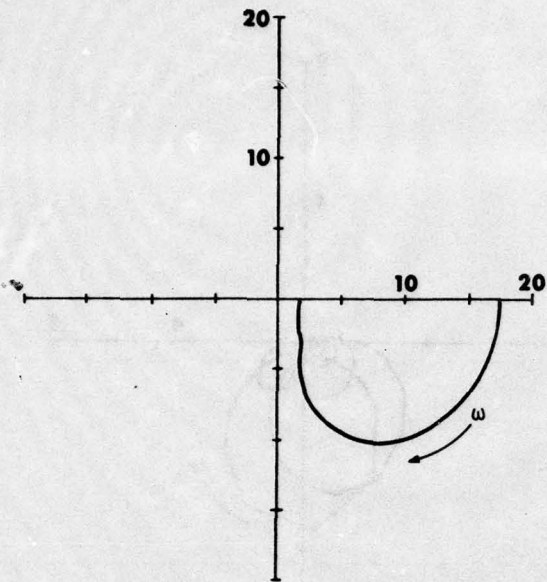


(b) FREQUENCY RESPONSE OF THE COMPENSATED SYSTEM

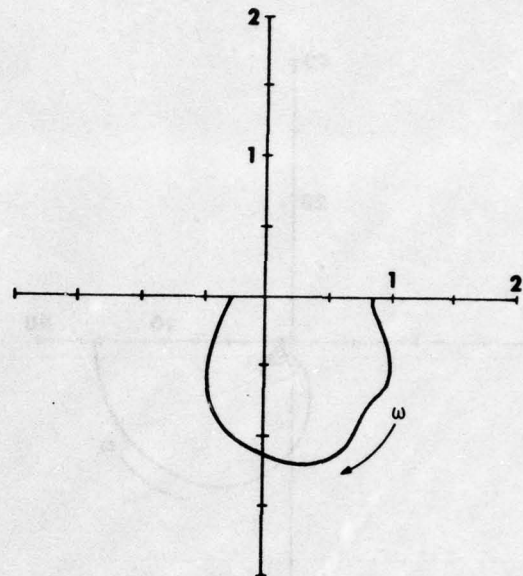


(c) UNIT STEP RESPONSE OF THE COMPENSATED SYSTEM

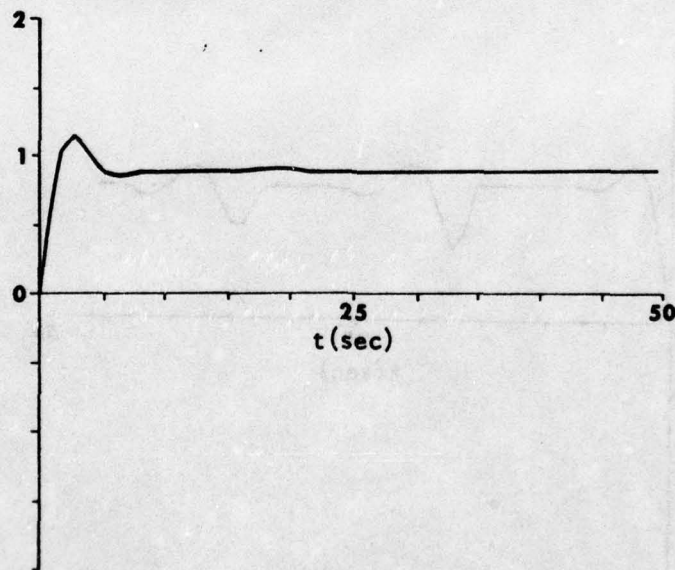
FIGURE 6-14. PERFORMANCE OF THE SYSTEM COMPENSATED WITH  $D_1(z)$



(a) FREQUENCY RESPONSE OF THE COMPENSATOR  $D_2(z)$

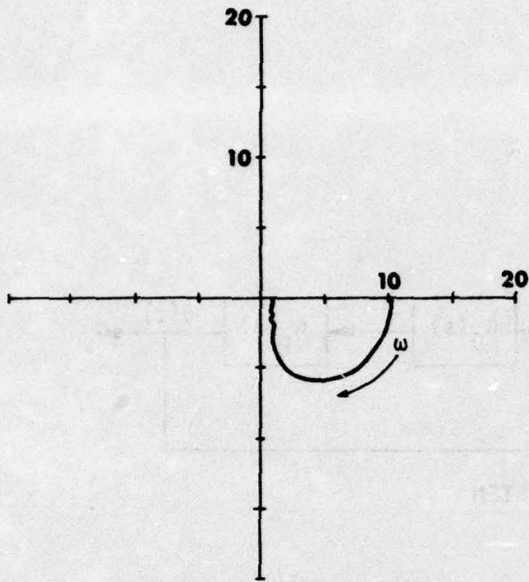


(b) FREQUENCY RESPONSE OF THE COMPENSATED SYSTEM

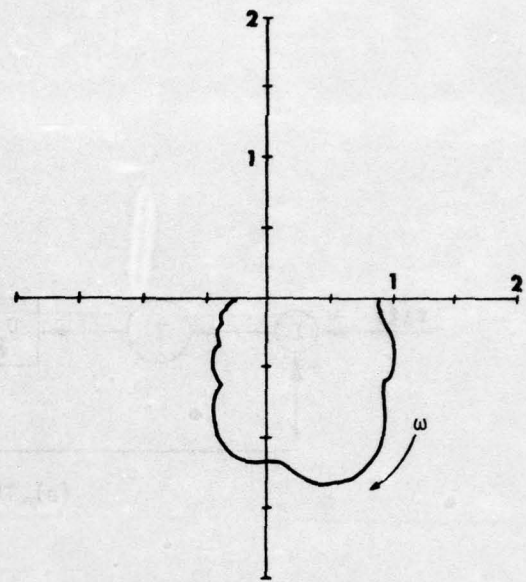


(c) UNIT STEP RESPONSE OF THE COMPENSATED SYSTEM

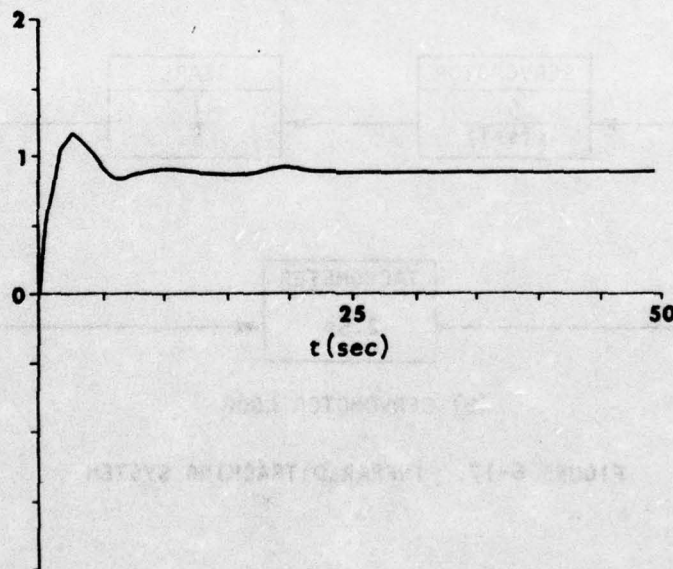
FIGURE 6-15. PERFORMANCE OF THE SYSTEM COMPENSATED WITH  $D_2(z)$



(a) FREQUENCY RESPONSE OF THE COMPENSATOR  $D_3(z)$

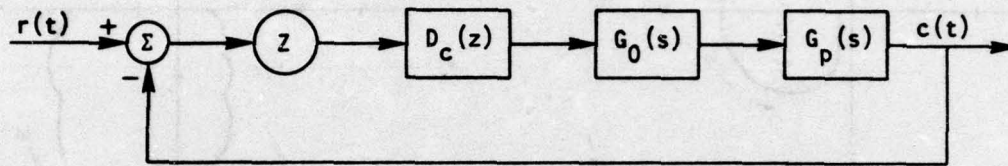


(b) FREQUENCY RESPONSE OF THE COMPENSATED SYSTEM

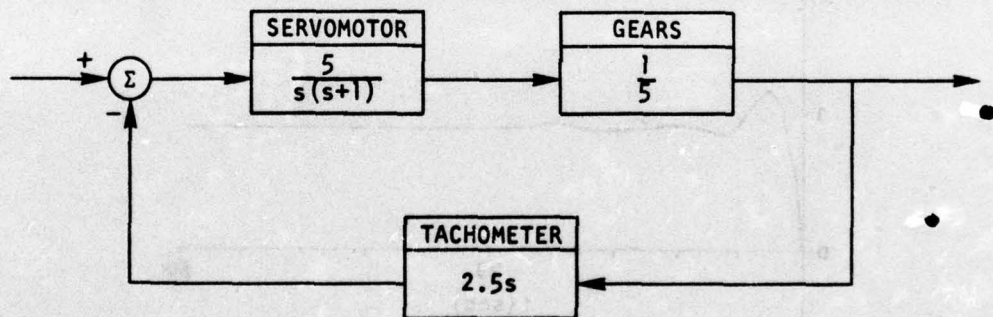


(c) UNIT STEP RESPONSE OF THE COMPENSATED SYSTEM

FIGURE 6-16. PERFORMANCE OF THE SYSTEM COMPENSATED WITH  $D_3(z)$



(a) TRACKING SYSTEM



(b) SERVO MOTOR LOOP

FIGURE 6-17. INFRARED TRACKING SYSTEM

$$G_0(s) = \frac{1 - e^{-sT}}{s} \quad (58)$$

The transfer function of the servomotor loop is

$$G_p(s) = \frac{1}{s(s + 3.5)} \quad (59)$$

The required specifications of the IR tracking system are as follows:

- (1) The overshoot is less than 25%,
- (2) The rise time is less than  $3T$ ,
- (3) The settling time is less than  $15T$ ,
- (4) The velocity error constant is greater than  $10 \text{ sec}^{-1}$ , and
- (5) The bandwidth is greater than  $6.28 \text{ rad/sec}$ .

According to Eq. (5), we must choose the sampling frequency,  $\omega_s > 2\omega_b = 4\pi$ . Thus, the sampling frequency should be greater than 2 Hz. Let us choose  $f_s = 10 \text{ Hz}$ , or a sampling period of  $T = 0.1 \text{ seconds}$ .

The open loop transfer function, in the z-domain, of the tracking loop is given by

$$\begin{aligned} G(z) &= Z[G_0(s) G_p(s)] \\ &= \frac{0.00446(z + 0.8903)}{(z - 1)(z - 0.7047)} \quad (60) \end{aligned}$$

Using Figure 6-18(a) as the model of the unit step response for the compensated closed loop matching specifications (1) through (4), the

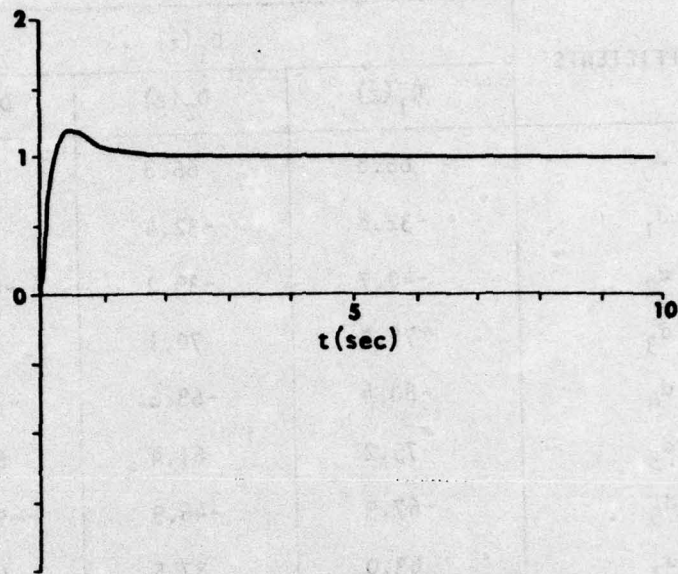
corresponding closed loop frequency response is shown in Figure 6-18(b). The frequency response of the required compensator is shown in Figure 6-18(c). The coefficients of nonrecursive compensators obtained using various windows are listed in Table 6-4.

Figures 6-19(a), (b) and (c) show the frequency response of  $D_1(z)$  obtained using the rectangular window, the corresponding system frequency response and the unit step response of the compensated system respectively. By observation, too many ripples appear in the closed loop frequency response and too many small wavelets in the transient response; therefore, this compensator is not suitable.

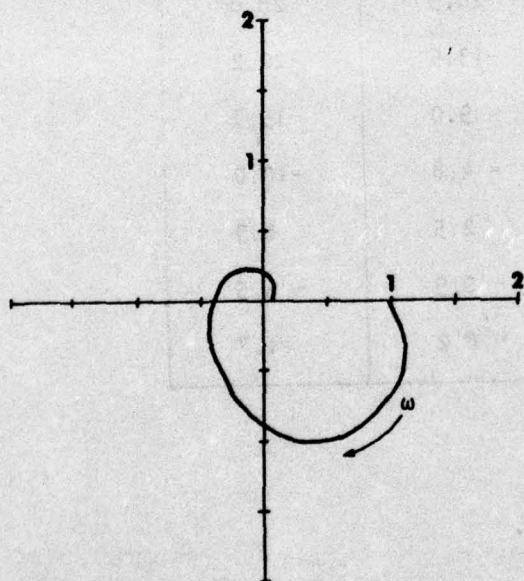
Figures 6-20(a), (b) and (c) show the frequency response of  $D_2(z)$  obtained using the Hanning window, the corresponding system frequency response and the unit step response of the compensated system respectively. From Figure 6-20 we find: (1) the overshoot is 20%, (2) the rise time is  $2T$ , (3) the settling time is  $10T$ , and (4) the velocity error constant is  $K_V = 9.97$ .

Figures 6-21(a), (b) and (c) show the frequency response of  $D_3(z)$  obtained using the trapezoidal window with the parameter  $b = 0.4$ , the corresponding system frequency response and the unit step response of the compensated system respectively. From Figure 6-21 we find: (1) the overshoot is 22%, (2) the rise time is  $2T$ , (3) the settling time is  $10T$ , and (4) the velocity error constant is  $K_V = 11.2$ .

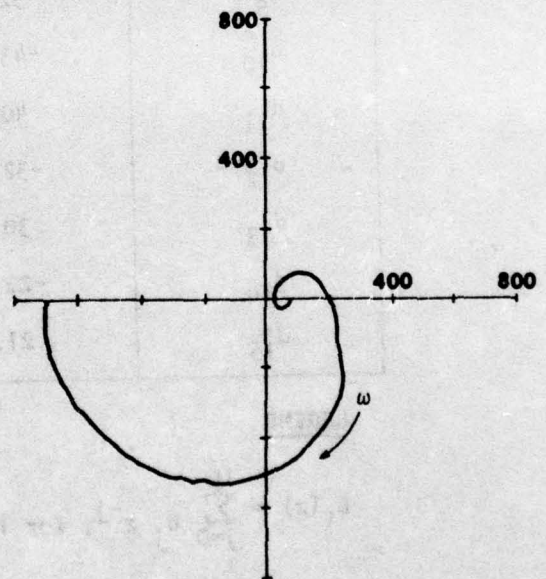
Comparing Figure 6-21 with Figure 6-20, we note that the trapezoidal window performs even better than the Hanning window and yields a larger velocity error constant.



(a) REQUIRED UNIT STEP RESPONSE



(b) REQUIRED CLOSED LOOP  
FREQUENCY RESPONSE



(c) FREQUENCY RESPONSE OF  
THE REQUIRED COMPENSATOR

FIGURE 6-18. DESIGN MODELS OF EXAMPLE 3

TABLE 6-4  
COMPENSATORS FOR EXAMPLE 3

COEFFICIENTS	$D_i(z)$		
	$D_1(z)$	$D_2(z)$	$D_3(z)$
$d_0$	66.8	66.8	66.8
$d_1$	-32.8	-32.4	-32.8
$d_2$	-40.7	-39.2	-40.7
$d_3$	76.7	70.1	76.7
$d_4$	-80.4	-68.6	-74.2
$d_5$	79.2	61.4	67.0
$d_6$	-67.9	-46.9	-52.0
$d_7$	63.0	37.5	43.6
$d_8$	-54.2	-27.1	-33.4
$d_9$	52.1	20.9	28.0
$d_{10}$	-43.9	-13.5	-20.2
$d_{11}$	40.8	9.0	15.7
$d_{12}$	-32.6	- 4.8	-10.0
$d_{13}$	30.0	2.5	6.9
$d_{14}$	-22.85	- 0.9	- 3.5
$d_{15}$	21.4	0.2	1.7

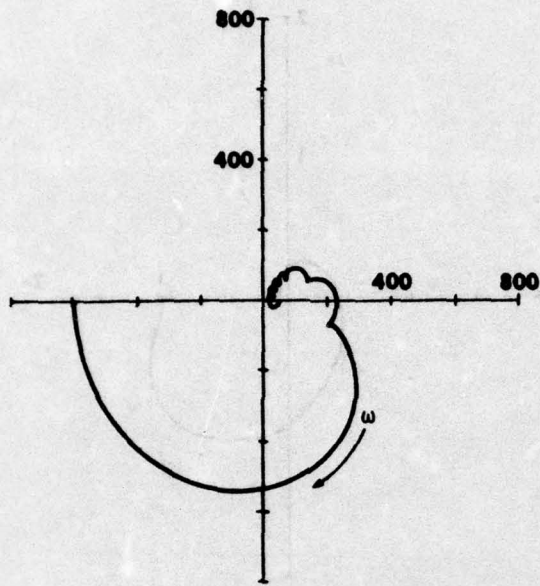
**LEGEND**

$$D_i(z) = \sum_{j=0}^{15} d_j z^{-j}, \text{ for } i = 1, 2, 3.$$

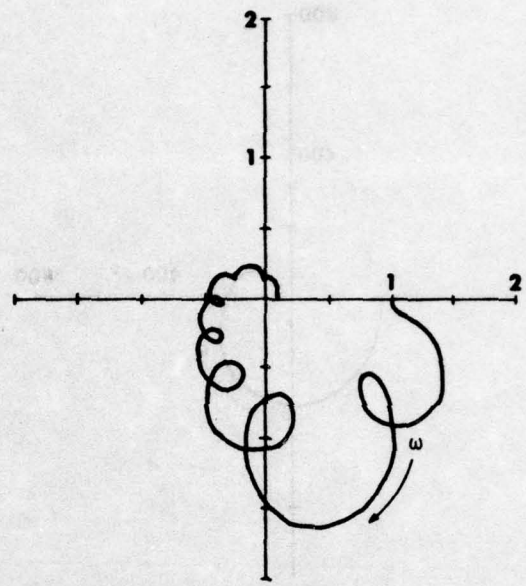
$D_1(z)$  - Designed by using the rectangular window.

$D_2(z)$  - Designed by using the Hanning window.

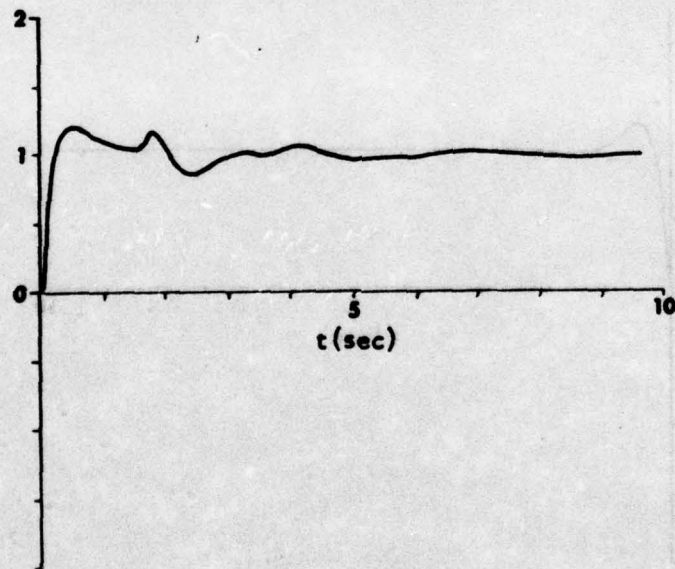
$D_3(z)$  - Designed by using the trapezoidal window,  $b = 0.4$ .



(a) FREQUENCY RESPONSE OF THE COMPENSATOR  $D_1(z)$

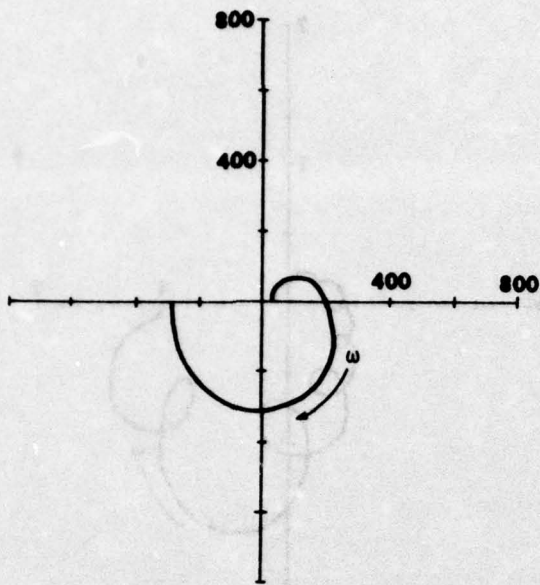


(b) FREQUENCY RESPONSE OF THE COMPENSATED SYSTEM

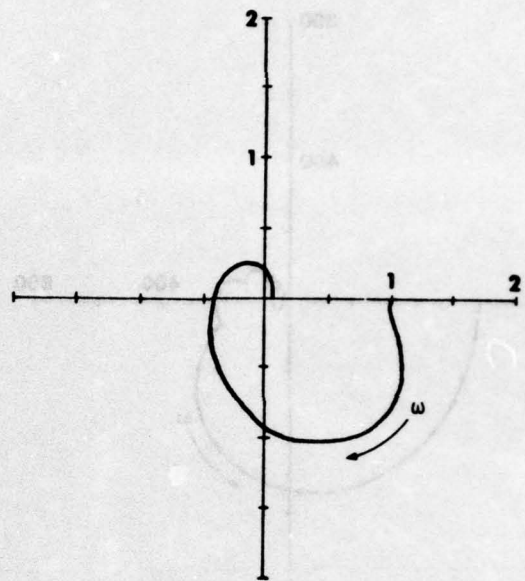


(c) UNIT STEP RESPONSE OF THE COMPENSATED SYSTEM

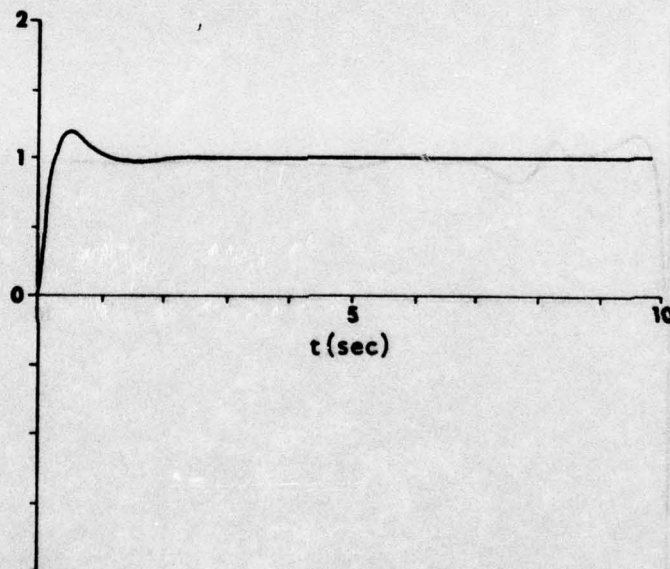
FIGURE 6-19. PERFORMANCE OF THE SYSTEM COMPENSATED WITH  $D_1(z)$



(a) FREQUENCY RESPONSE OF THE COMPENSATOR  $D_2(z)$

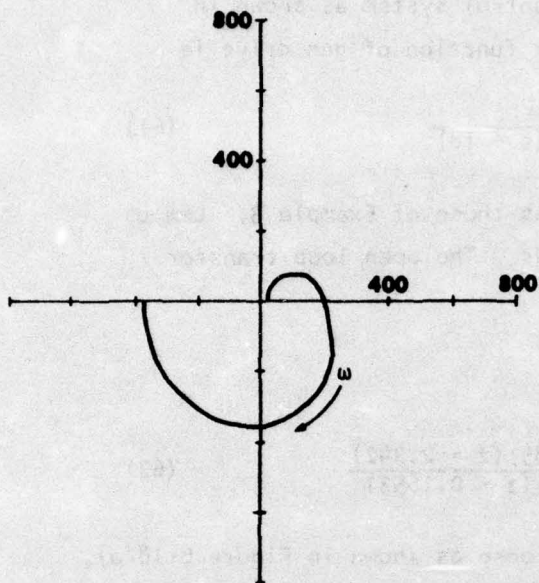


(b) FREQUENCY RESPONSE OF THE COMPENSATED SYSTEM

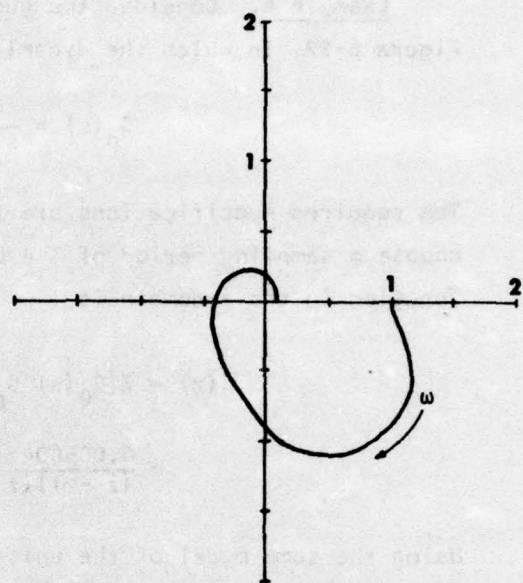


(c) UNIT STEP RESPONSE OF THE COMPENSATED SYSTEM

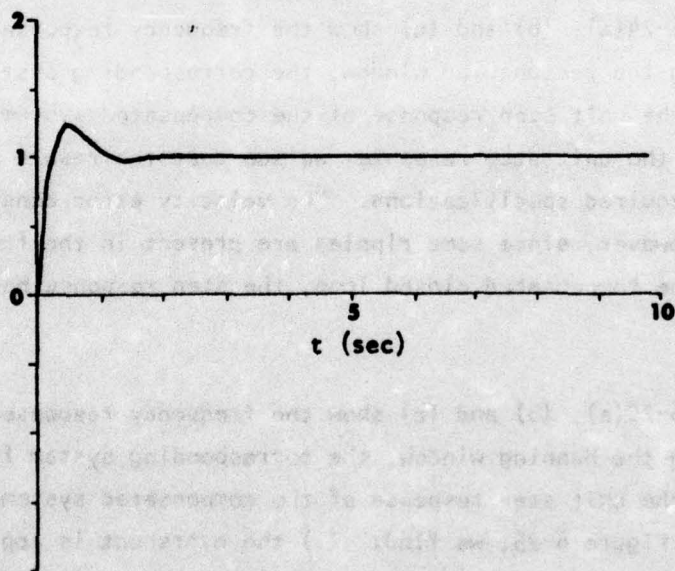
FIGURE 6-20. PERFORMANCE OF THE SYSTEM COMPENSATED WITH  $D_2(z)$



(a) FREQUENCY RESPONSE OF THE COMPENSATOR  $D_3(z)$



(b) FREQUENCY RESPONSE OF THE COMPENSATED SYSTEM



(c) UNIT STEP RESPONSE OF THE COMPENSATED SYSTEM

FIGURE 6-21. PERFORMANCE OF THE SYSTEM COMPENSATED WITH  $D_3(z)$

Example 4. Consider the gun drive control system as shown in Figure 6-22, in which the dynamic transfer function of gun drive is

$$G_p(s) = \frac{55}{s(s + 3.5)(s + 18)} \quad (61)$$

The required specifications are the same as those of Example 3. Let us choose a sampling period of  $T = 0.1$  seconds. The open loop transfer function in the  $z$ -domain is

$$\begin{aligned} G(z) &= Z[G_0(s) G_p(s)] \\ &= \frac{0.005604z(z = 0.1489)(z = 2.342)}{(z - 1)(z - 0.7047)(z - 0.1653)} \end{aligned} \quad (62)$$

Using the same model of the unit step response as shown in Figure 6-18(a), the frequency response of the required compensator is shown in Figure 6-23. The coefficients of nonrecursive compensators obtained using various windows are listed in Table 6-5.

Figures 6-24(a), (b) and (c) show the frequency response of  $D_1(z)$  obtained using the rectangular window, the corresponding system frequency response and the unit step response of the compensated system respectively. From the unit step response, we see that the result almost matches the required specifications. The velocity error constant is  $K_v = 18.9$ . However, since some ripples are present in the frequency response of the compensated closed loop, the step response has a small wavelet.

Figures 6-25(a), (b) and (c) show the frequency response of  $D_2(z)$  obtained using the Hanning window, the corresponding system frequency response and the unit step response of the compensated system respectively. From Figure 6-25, we find: (1) the overshoot is approximately 20%, (2) the rise time is  $2T$ , (3) the settling time is  $7T$ , and (4) the velocity error constant is 14.0. The unit step response is smoother than that in Figure 6-24.

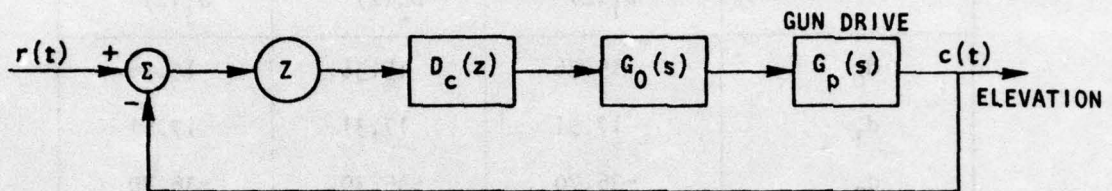


FIGURE 6-22. GUN DRIVE CONTROL SYSTEM

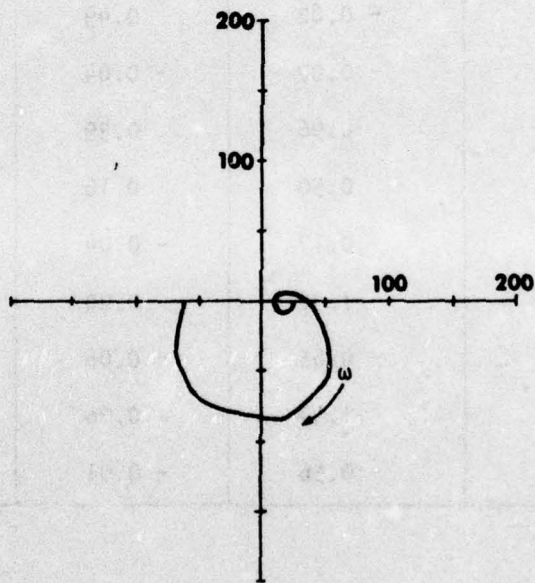


FIGURE 6-23. FREQUENCY RESPONSE OF THE REQUIRED COMPENSATOR

TABLE 6-5

## COMPENSATORS FOR EXAMPLE 4

COEFFICIENTS	$D_i(z)$		
	$D_1(z)$	$D_2(z)$	$D_3(z)$
$d_0$	15.36	15.36	15.36
$d_1$	17.51	17.31	17.51
$d_2$	-36.70	-35.30	-36.70
$d_3$	26.36	24.08	26.36
$d_4$	-11.64	- 9.93	-10.74
$d_5$	4.93	3.82	4.17
$d_6$	- 0.59	- 0.41	- 0.46
$d_7$	- 0.82	0.49	0.57
$d_8$	- 0.07	- 0.04	- 0.05
$d_9$	0.96	0.39	0.52
$d_{10}$	0.50	0.16	0.23
$d_{11}$	- 0.17	- 0.04	- 0.07
$d_{12}$	1.36	0.20	0.42
$d_{13}$	- 0.65	- 0.06	- 0.16
$d_{14}$	1.47	0.06	0.23
$d_{15}$	- 0.56	- 0.01	- 0.05

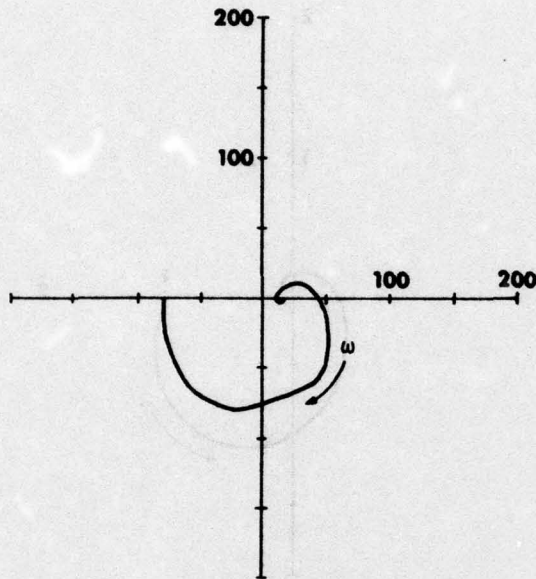
LEGEND

$$D_i(z) = \sum_{j=0}^{15} d_j z^{-j}, \text{ for } i = 1, 2, 3.$$

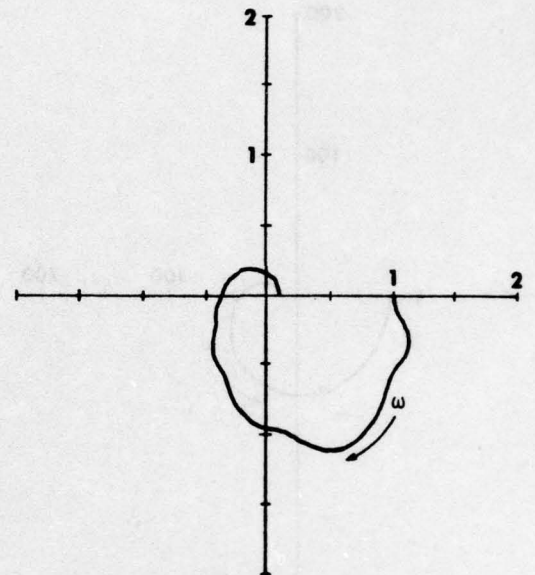
$D_1(z)$  - Designed by using the rectangular window.

$D_2(z)$  - Designed by using the Hanning window.

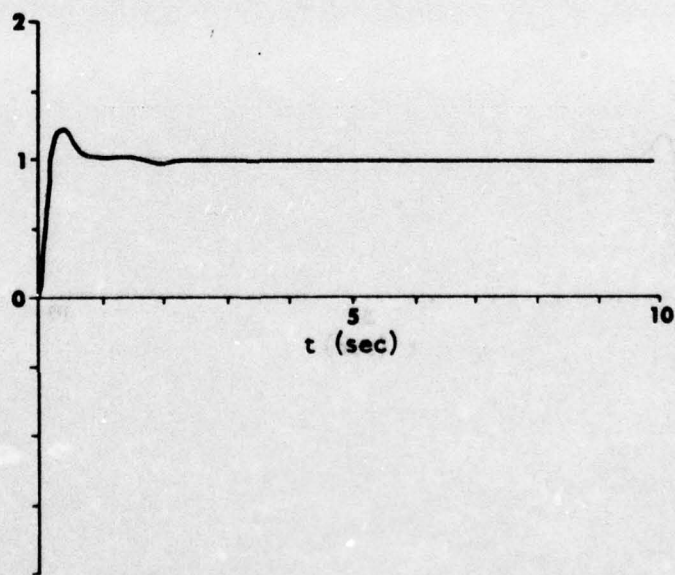
$D_3(z)$  - Designed by using the trapezoidal window,  $b = 0.4$ .



(a) FREQUENCY RESPONSE OF THE COMPENSATOR  $D_1(z)$



(b) FREQUENCY RESPONSE OF THE COMPENSATED SYSTEM



(c) UNIT STEP RESPONSE OF THE COMPENSATED SYSTEM

FIGURE 6-24. PERFORMANCE OF THE SYSTEM COMPENSATED WITH  $D_1(z)$

AD-A034 027

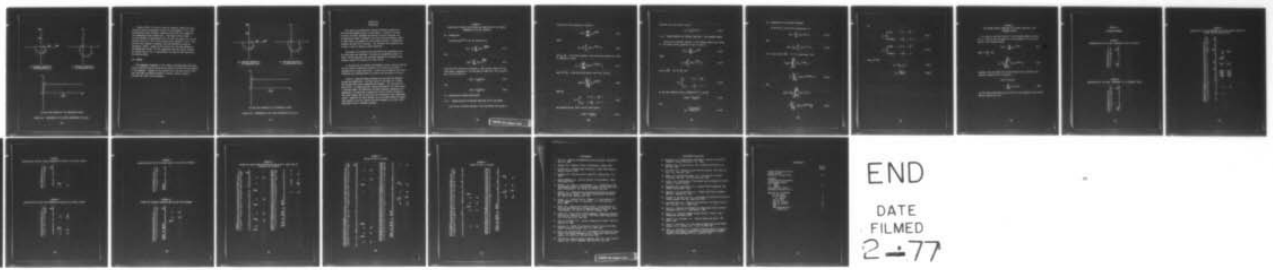
ARMY MISSILE RESEARCH DEVELOPMENT AND ENGINEERING LAB--ETC F/O 9/4  
ANALYSIS AND DESIGN OF DIGITAL CONTROL SYSTEMS. PART II. PRINCI--ETC(U)  
OCT 76 R E YATES, Y T TSAY, C F CHEN

UNCLASSIFIED

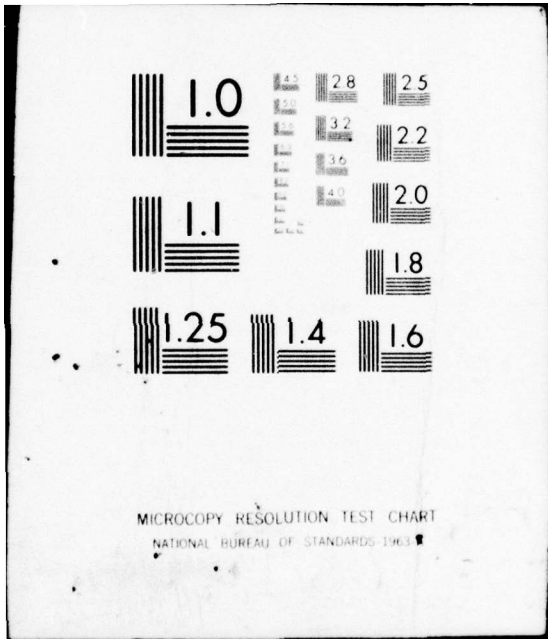
RG-77-3

NL

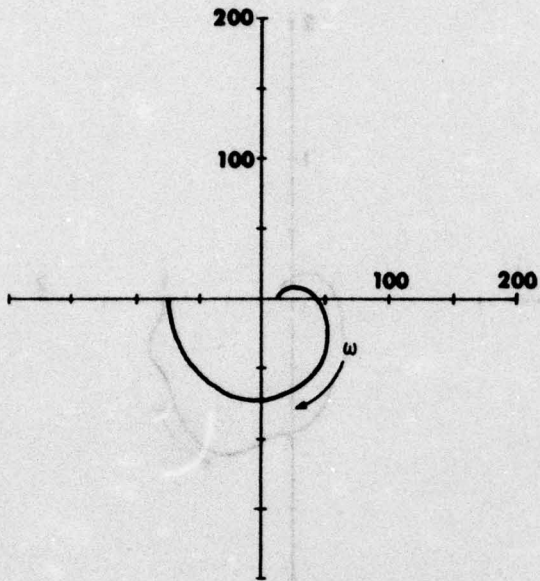
3 of 3  
AD  
A034027



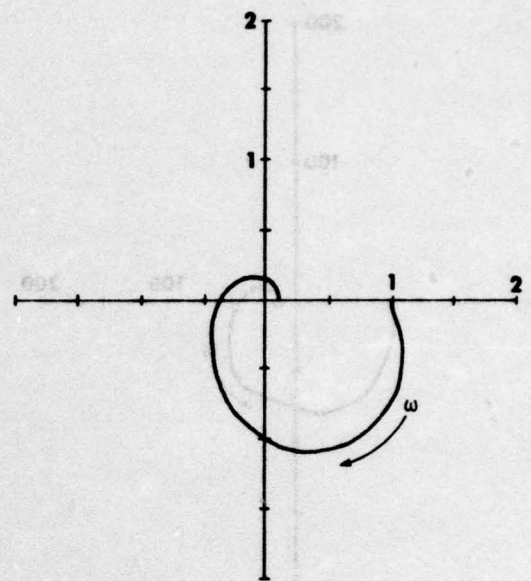
END  
DATE  
FILMED  
2-77



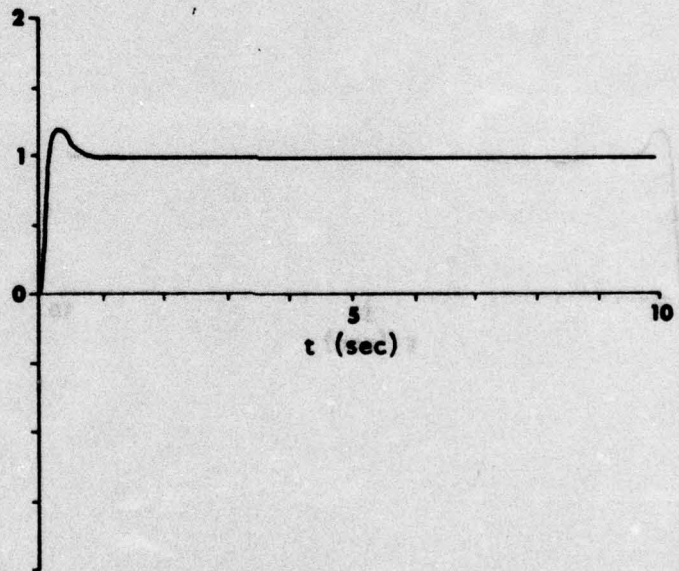
MICROCOPY RESOLUTION TEST CHART  
NATIONAL BUREAU OF STANDARDS-1963-A



(a) FREQUENCY RESPONSE OF THE COMPENSATOR  $D_2(z)$



(b) FREQUENCY RESPONSE OF THE COMPENSATED SYSTEM



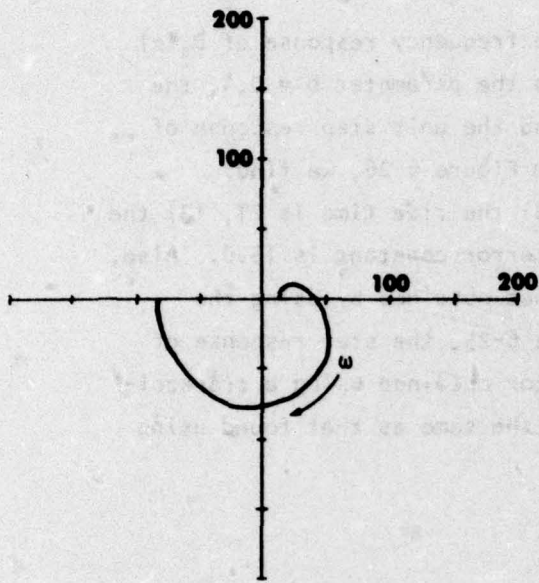
(c) UNIT STEP RESPONSE OF THE COMPENSATED SYSTEM

FIGURE 6-25. PERFORMANCE OF THE SYSTEM COMPENSATED WITH  $D_2(z)$

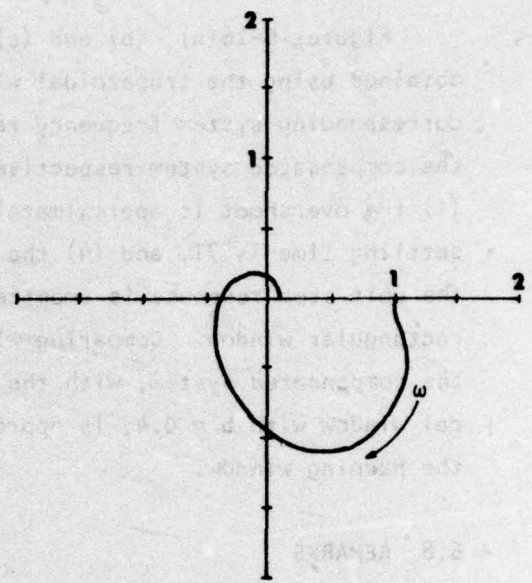
Figures 6-26(a), (b) and (c) show the frequency response of  $D_3(z)$  obtained using the trapezoidal window with the parameter  $b = 0.4$ , the corresponding system frequency response and the unit step response of the compensated system respectively. From Figure 6-26, we find: (1) the overshoot is approximately 21%, (2) the rise time is  $2T$ , (3) the settling time is  $7T$ , and (4) the velocity error constant is 15.0. Also, the unit step response is smoother than that obtained by using the rectangular window. Comparing with Figure 6-25, the step response of the compensated system, with the compensator obtained using a trapezoidal window with  $b = 0.4$ , is approximately the same as that found using the Hanning window.

#### 6.8 REMARKS

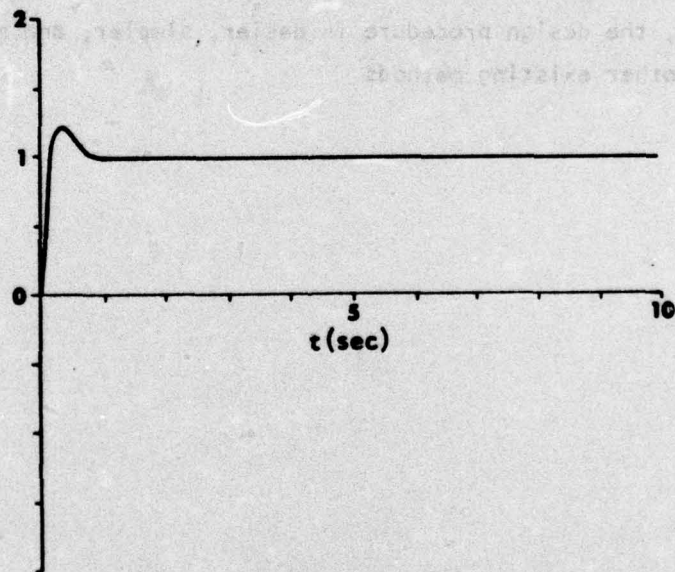
The compensators designed in this chapter are associated with direct digital controllers which can be easily realized using on-line minicomputer or microcomputer. Because of the availability of the Fast Fourier Transform algorithm, the design procedure is easier, simpler, and more accurate than other existing methods.



(a) FREQUENCY RESPONSE OF THE COMPENSATOR  $D_3(z)$



(b) FREQUENCY RESPONSE OF THE COMPENSATED SYSTEM



(c) UNIT STEP RESPONSE OF THE COMPENSATED SYSTEM

FIGURE 6-26. PERFORMANCE OF THE SYSTEM COMPENSATED WITH  $D_3(z)$

## CHAPTER VII CONCLUSIONS

This report has established a general windowing procedure for discrete-time feedback control system design. Initially, the basic principle of Gibbs' phenomena was derived; and then developed into the generalized Gibbs' phenomena in both the time and frequency domain. In other words, the reasons for using window functions in compensator synthesis has been fully explored. The rationale were presented step by step in order to develop a sound foundation.

The process for nonrecursive filter design was presented and two new techniques were developed. One used the trapezoidal windows to offer a unified approach, and the other extended the frequency transformation method for nonrecursive filter design.

In the analysis of discrete-time feedback systems, we mainly applied the Fast Fourier Transform to evaluate the transient and frequency responses and to study stabilities. A new criterion based on the return difference was formulated which is simpler than the Nyquist criterion.

Finally, a detailed design procedure for discrete-time feedback systems was established. Two kinds (type "0" and type "1") of feedback systems were used as demonstration examples. The five steps for design were: (1) Specifying the required performance; (2) Constructing a reference model; (3) Computing a suitable frequency response of the compensator; (4) Designing a nonrecursive filter transfer function by the window method; and (5) Verifying the performance of the compensated system. Compared with other methods, this new window method for compensator design is not only simpler and more systematic, but also a fast algorithmic which is computer-oriented.

APPENDIX A  
EVALUATION OF FOURIER COEFFICIENTS AND COMPUTATION OF THE FOURIER  
TRANSFORM VIA THE FFT ALGORITHM

A.0 INTRODUCTION

The definitions<sup>[5]</sup> of the FFT algorithm are

$$X(n) = \frac{1}{N} \sum_{m=0}^{N-1} x(m) e^{-j2\pi nm/N} \quad (A-1)$$

and

$$x(m) = \sum_{n=0}^{N-1} X(n) e^{j2\pi mn/N} \quad (A-2)$$

where  $X(n)$  and  $x(m)$  are the sequences in the frequency domain and the time domain, respectively. For the sake of simplicity, let us rewrite Eqs. (A-1) and (A-2) as

$$X(n) = FF_{Nn}[x(m)] \quad (A-3)$$

and

$$x(m) = FF_{Nm}^{-1}[X(n)] \quad (A-4)$$

A.1 EVALUATION OF FOURIER COEFFICIENTS

A.1.1 FOURIER ANALYSIS OF PERIODIC FUNCTIONS IN THE TIME DOMAIN

Let  $f(t)$  be a periodic function in the time domain with period  $T$ .

The Fourier series expansion is given by

$$f(t) = \sum_{n=-\infty}^{\infty} a_n e^{jn\omega_0 t} \quad (\text{A-5})$$

where

$$a_n = \frac{1}{T} \int_0^T f(t) e^{-jn\omega_0 t} dt \quad (\text{A-6})$$

and  $\omega_0 = \frac{2\pi}{T}$ . If we take  $N$  samples in one period and evaluate Eq. (A-6) by summation, we have

$$a_n = \frac{1}{T} \sum_{m=0}^{N-1} f(m\Delta t) e^{-jn\omega_0 m\Delta t} \Delta t \quad (\text{A-7})$$

where  $\Delta t = \frac{T}{N}$ . Write the finite partial sum of Eq. (A-5) as

$$f(m\Delta t) = \sum_{n=-\frac{N}{2}}^{\frac{N}{2}-1} a_n e^{jn\omega_0 m\Delta t} \quad (\text{A-8})$$

Defining

$$b_n = \begin{cases} a_n & n = 0, \dots, \frac{N}{2} - 1 \\ a_{n-N} & n = \frac{N}{2}, \dots, N - 1 \end{cases} \quad (\text{A-9})$$

and substituting Eq. (A-9) into Eq. (A-8) yields

$$f(m\Delta t) = FF_{Nm}^{-1}[b_n] \quad (\text{A-10})$$

From Eqs. (A-7) and (A-8), we have

$$b_n = \text{FF}_{Nn} [f(n\Delta t)] \quad (\text{A-11})$$

### A.1.2 FOURIER ANALYSIS OF PERIODIC FUNCTIONS IN THE FREQUENCY DOMAIN

Let  $G(\omega)$  be a periodic function in the frequency domain with period  $P$ . The Fourier series expansion of  $G(\omega)$  is given by

$$G(\omega) = \sum_{n=-\infty}^{\infty} A_n e^{-jn\omega P} \quad (\text{A-12})$$

where

$$A_n = \frac{1}{P} \int_0^P G(\omega) e^{jnt_0\omega} d\omega \quad (\text{A-13})$$

and  $t_0 = \frac{2\pi}{P}$ . Let  $\Delta\omega = \frac{P}{N}$ , and

$$B_n = \begin{cases} A_n & n = 0, \dots, \frac{N}{2} - 1 \\ A_{n-N} & n = \frac{N}{2}, \dots, N - 1 \end{cases} \quad (\text{A-14})$$

By the same reasoning used in subsection A.1.1, we have

$$G(m\Delta\omega) = \text{FF}_{Nm} [B_n] N \quad (\text{A-15})$$

and

$$B_n = \frac{\text{FF}_{Nn}^{-1} [G(m\Delta\omega)]}{N} \quad (\text{A-16})$$

## A.2 COMPUTATION OF THE FOURIER TRANSFORM

By definition, the Fourier Transform pair is

$$F(\omega) = \int_{-\infty}^{\infty} f(t) e^{j\omega t} dt \quad (\text{A-17})$$

and

$$f(t) = \frac{1}{2\pi} \int_{-\infty}^{\infty} F(\omega) e^{-j\omega t} d\omega \quad (\text{A-18})$$

Let  $t = \frac{T}{N} n$ , and  $\Delta\omega = \frac{2\pi}{T}$ . If  $T$  is large enough, then

$$\begin{aligned} F(n\Delta\omega) &\approx \int_{-\frac{T}{2}}^{\frac{T}{2}} f(t) e^{-jn\Delta\omega t} dt \\ &\approx \sum_{m=-\frac{N}{2}}^{\frac{N}{2}-1} f(m\Delta t) e^{-jnm\Delta\omega\Delta t} \Delta t \end{aligned} \quad (\text{A-19})$$

and

$$\begin{aligned} f(m\Delta t) &\approx \frac{1}{2\pi} \int_{-\frac{\pi}{T}}^{\frac{\pi}{T}} F(\omega) e^{j\omega m\Delta t} d\omega \\ &\approx \sum_{n=-\frac{N}{2}}^{\frac{N}{2}-1} F(n\Delta\omega) e^{jnm\Delta\omega\Delta t} \frac{\Delta\omega}{2\pi} \end{aligned} \quad (\text{A-20})$$

Let

$$F_n = \begin{cases} F(n\Delta\omega) & n = 0, \dots, \frac{N}{2} - 1 \\ F(\overline{n-N}\Delta\omega) & n = \frac{N}{2}, \dots, N - 1 \end{cases} \quad (\text{A-21})$$

$$f_m = \begin{cases} f(m\Delta t) & m = 0, \dots, \frac{N}{2} - 1 \\ f(\overline{m-N}\Delta t) & m = \frac{N}{2}, \dots, N - 1 \end{cases} \quad (\text{A-22})$$

Then, we have

$$F_n = FF_{Nn} f_m T \quad (\text{A-23})$$

$$f_m = \frac{FF^{-1}}{T} F_n \quad (\text{A-24})$$

APPENDIX B  
THE INVERSE FOURIER TRANSFORM OF A PERIODIC FUNCTION IN THE  
FREQUENCY DOMAIN

Let  $C(\omega)$  be a periodic function in the frequency domain with period  $\omega_s$ . From Eq. (34) of Chapter II, we can expand  $C(\omega)$  as a Fourier series in the frequency domain,

$$C(\omega) = \sum_{k=-\infty}^{\infty} A_k e^{-jkT\omega} \quad (B-1)$$

where  $T = \frac{2\pi}{\omega_s}$ , and

$$A_k = \frac{1}{\omega_s} \int_{-\frac{\omega_s}{2}}^{\frac{\omega_s}{2}} C(x) e^{-jkTx} dx \quad (B-2)$$

Therefore, from the definition of the inverse Fourier Transform, the inverse transform of  $C(\omega)$  is given by

$$\begin{aligned} c(t) &\triangleq F^{-1}[C(\omega)] \\ &= \sum_{k=-\infty}^{\infty} A_k \delta(t-kT) \end{aligned} \quad (B-3)$$

and the Fourier coefficients ( $A_k$ 's) form the time sequence of the inverse Fourier Transform of  $C(\omega)$ .

APPENDIX C

KEYBOARD PROGRAMS

PROGRAM 1

DEMONSTRATION OF THE GIBBS' PHENOMENON IN THE TIME DOMAIN

1	L	0
4	BS	4096
7	L	1
10	CL	0
13	X<	3
16	D	0
19	F	
21	D	0
24	F	
26	Y	807
29	Y	807
32	.	

PROGRAM 2

DEMONSTRATION OF THE GIBBS' PHENOMENON IN THE FREQUENCY DOMAIN

1	L	0
4	BS	4096
7	L	1
10	CL	0
13	X<	3
16	D	0
19	F	
21	D	0
24	F	
26	D	0
29	TP	0
32	D	0
35	Y	807
38	Y	807
41	.	

PROGRAM 3

EVALUATION OF THE TIME RESPONSES OF THE TIME DOMAIN TRAPEZOIDAL  
WINDOWS AND THE WINDOW EFFECTS

1	L	0		
4	BS	128		
7	CL	0		
10	CL	1		
13	D	0		
16	J	10		
22	CL	1		
25	BS	4096		
28	CL	0	51	2048
33	:	0	64	
37	F	0		
40	:	0	64	
44	-	0	2048	
48	D	0		
51	Y	807		
54	W	0	2036	2067
59	S	0		
62	D	0		
65	Y	807		
68	W	0	2095	2126
73	W	0	2180	2211
78	W	0	1895	1926
83	W	0	1960	1991
88	J	99		
91	L	10		
94	X	1		
97	X>	2		
100	X	1		
103	S	1	0	50
108	D	1		
111	X	1		
114	A-	2		
117	*	0	-1	
121	A+	1		
124	<			
126	L	99		
129	.			

PROGRAM 4

EVALUATION OF THE FREQUENCY RESPONSE OF THE FREQUENCY DOMAIN TRAPEZOIDAL  
WINDOWS AND THE WINDOW EFFECTS

1	L	0		
4	BS	256		
7	CL	0		
10	CL	1		
13	D	0		
16	J	10		
19	D	0		
22	CL	1		
25	BS	4096		
28	CL	0	201	4095
33	-	0	100	
37	F	0		
40	W	0	0	3
45	D	0		
48	D	0	0	500
53	Y	807		
56	D	0		
59	X>	1		
62	TL	1		
65	D	1	0	500
70	Y	807		
73	D	1	0	160
78	J	99		
81	L	10		
84	X	1		
87	X>	2		
90	X	1		
93	S	1	0	100
98	D	1		
101	X	1		
104	A-	2		
107	*	0	-1	
111	A+	1		
114	X>	1		
117	A-	50		
120	*	0	-1	
124	D	0		
127	CL	0	0	155
132	A+	1		
135	-	0	156	
139	<			
141	L	99		
144	.			

PROGRAM 5  
DESIGN OF NONRECURSIVE FILTERS

1 L	0			65 X	1		
4 BS	4096			68 X>	2		
7 CL	0			71 X	1		
10 D	0			74 S	1	0	8
13 F	0			79 D	1		
16 :	0	4096		82 X	1		
20 W	0	0	9	85 A-	2		
25 D	0			88 *	0	-1	
28 -	0	4088		92 A+	1		
32 D	0			95 X>	1		
35 F	0			98 A-	3		
38 *	0	4096		101 *	0	-1	
42 TL	0			105 D	0		
45 D	0			108 CL	0	0	55
48 Y	807			113 A+	1		
51 D	0			116 -	0	56	
54 Y	807			120 D	0		
57 D	0			123 <			
60 <				125 .			
62 L	30						

PROGRAM 6  
EVALUATION OF THE FREQUENCY RESPONSE OF DISCRETE-TIME CONTROL SYSTEMS

1 L	0
4 D	0
7 CL	0
10 CL	1
13 D	0
16 F	0
19 F	1
22 :	1
25 D	0
28 Y	810
31 Y	807
34 Y	809
37 D	0
40 Y	807
43 D	0
46 Y	810
49 Y	807
52 Y	809
55 .	

PROGRAM 7

EVALUATION OF THE UNIT IMPULSE RESPONSE OF DISCRETE-TIME CONTROL SYSTEMS

1	L	0		
4	BS	1024		
7	CL	0		
10	CL	1		
13	D	0		
16	F	0		
19	F	1		
22	:	1		
25	D	0		
28	F	0		
31	:	0	1024	
35	W	0	0	63
40	.			

PROGRAM 8

EVALUATION OF THE UNIT STEP RESPONSE OF DISCRETE-TIME CONTROL SYSTEMS

1	L	0		
4	BS	1024		
7	CL	0		
10	CL	1		
13	D	0		
16	W	0	0	10
21	V	1	0	10
26	F	0		
29	F	1		
32	:	1		
35	D	0		
38	F	0		
41	:	0	1024	
45	W	0	0	63
50	S	0		
53	V	0	0	63
58	.			

PROGRAM 9  
 CALCULATION AND PLOT OF THE PHASE ANGLE OF THE RETURN DIFFERENCE

1	L	0
4	CL	0
7	CL	1
10	D	0
13	F	0
16	F	1
19	:	1
22	D	0
25	TP	0
28	D	0
31	Y	807
34	Y	810
37	Y	809
40	.	

PROGRAM 10  
 FINDING THE FREQUENCY RESPONSE FROM THE UNIT STEP RESPONSE

1	L	0		
4	BS	1024		
7	D	0		
10	V	0	0	63
15	D	0		
18	X	0		
21	W	0	0	63
26	F	0		
29	*	0	1024	
33	D	0		
36	Y	807		
39	Y	810		
42	Y	809		
45	D	0		
48	Y	807		
51	D	0		
54	Y	807		
57	Y	810		
60	Y	809		
63	.			

PROGRAM 11

FINDING THE DESIGN MODEL AND ANALYZING THE VELOCITY ERROR FROM THE SPECIFIED STEP RESPONSE

1	L	0			116	CL	0	0	
4	BS	1024			120	X>	9		
7	CL	0			123	W	0	0	63
10	D	0			128	D	0		
13	V	0	0	63	131	X<	12		
18	D	0			134	CL	0	0	0
21	X>	15			139	:	0	10	
24	*	0	-1		143	S	0	0	100
28	A+	12			148	W	0	0	63
31	X>	10			153	X>	8		
34	F				156	D	0		
36	*	0	1024		159	A-	9		
40	X>	5			162	W	0	0	63
43	X<	15			167	X>	7		
46	X	0			170	D	0		
49	X>	14			173	L	10		
52	W	0	0	63	176	D	0		
57	D	0			179	Y	807		
60	F	0			182	Y	810		
63	*	0	1024		185	Y	809		
67	X>	13			188	<			
70	D	0			190	L	20		
73	:	5			193	D	0		
76	X>	6			196	Y	807		
79	W	0	0	31	199	Y	810		
84	D	0			202	Y	809		
87	F	0			205	D	0		
90	:	0	1024		208	Y	807		
94	W	0	0	63	211	D	0		
99	D	0			214	Y	807		
102	X<	10			217	Y	810		
105	:	0	10		220	Y	809		
109	S	0			223	<			
112	-	0	1023		225	.			

PROGRAM 12  
DESIGN OF TYPE "O" SYSTEMS

1 L	0			155 X>	8		
4 BS	1024			158 V	0	0	31
7 CL	0			163 A+	11		
10 D	0			166 X>	4		
13 V	0	0	63	169 X<	8		
18 D	0			172 :	4		
21 X>	15			175 X>	6		
24 *	0			178 D	0		
27 X>	14			181 D	0		
30 V	0	0	63	184 L	40		
35 D	0			187 F	0		
38 F	0			190 :	0	1024	
41 *	0	1024		194 W	0	0	63
45 X>	13			199 D	0		
48 D	0			202 L	50		
51 A-	11			205 S	0		
54 *	0	-1		208 W	0	0	63
58 X>	5			213 D	0		
61 X<	12			216 L	60		
64 A-	15			219 S	0	0	400
67 D	0			224 -	0	1023	
70 CL	0			228 D	0		
73 CL	1			231 CL	0	0	0
76 D	0			236 V	0	0	63
79 F	0			241 D	0		
82 F	1			244 L	10		
85 :	1			247 D	0		
88 X>	10			250 Y	807		
91 *	5			253 Y	810		
94 X>	1			256 Y	809		
97 X<	13			259 <			
100 :	1			261 L	20		
103 D	0			264 D	0		
106 F	0			267 Y	807		
109 :	0	1024		270 Y	810		
113 X>	9			273 Y	809		
116 V	0	0	63	276 D	0		
121 D	0			279 Y	807		
124 L	30			282 D	0		
127 V	0	0	63	285 Y	807		
132 F	0			288 Y	810		
134 *	0	1024		291 Y	809		
138 D	0			294 <			
141 X>	1			296 .			
144 V	1	0	31				
149 X<	1						
152 *	10						

PROGRAM 13  
DESIGN OF TYPE "I" SYSTEMS

1 L	0			124 D	0		
4 CL	0			127 D	0		
7 CL	1			130 L	40		
10 D	0			133 F	0		
13 F	0			136 :	0	1024	
16 F	1			140 W	0	0	63
19 :	1			145 D	0		
22 X>	10			148 L	50		
25 *	5			151 S	0		
28 X>	1			154 W	0	0	63
31 X<	13			159 D	0		
34 :	1			162 L	60		
37 D	0			165 S	0	0	400
40 F	0			170 -	0	1023	
43 :	0	1024		174 D	0		
47 X>	9			177 CL	0	0	0
50 W	0	0	63	182 W	0	0	63
55 D	0			187 D	0		
58 L	30			190 L	10		
61 W	0	0	63	193 D	0		
66 F	0			196 Y	807		
68 *	0	1024		199 Y	810		
72 X>	1			202 Y	809		
75 W	1	0	31	205 <			
80 D	0			207 L	20		
83 X<	10			210 D	0		
86 X>	2			213 Y	807		
89 D	0			216 Y	810		
92 X<	1			219 Y	809		
95 *	2			222 D	0		
98 D	0			225 Y	807		
101 X>	8			228 D	0		
104 W	0	0	31	231 Y	807		
109 A+	7			234 Y	810		
112 X>	4			237 Y	809		
115 X<	8			240 <			
118 :	4			242 .			
121 X>	6						

#### BIBLIOGRAPHY

1. Tou, J.T., "Digital and Sampled-Data Control Systems," McGraw-Hill, New York, 1959.
2. AcKroyd, M.H., "Digital Filters," Butterworths, London, 1973.
3. William, D.S., "Digital Signal Processing," Reston Publishing Co., Reston, Virginia, 1975.
4. Brigham, D.O., "The Fast Fourier Transform," Prentice Hall, N.J., 1974.
5. Hewlett-Packard, Inc., "Fourier Analyzer Training Manual," Application Note 140-0.
6. Rabiner, L.R., Gold, B., and McGonegal, C.A., "An Approach To The Approximation Problem for Nonrecursive Digital Filter," IEEE Trans. Audio Electroacoust., Vol. AU-18, pp. 83-105, June 1970.
7. Rabiner, L.R., "Techniques for Designing Finite-Duration Impulse-Response Digital Filters," IEEE Trans. Communication Technology, Vol. COM-19, pp. 188-195, April 1971.
8. Kaiser, J.F., "Digital Filters," Chapter 7 in System Analysis by Digital Computers, Kuo, F.F. and Kaiser, J.F., Eds. New York: Wiley, 1966.
9. Helms, H.D., "Nonrecursive Digital Filters: Design Methods for Achieving Specifications on Frequency Response," IEEE Trans. Audio Electroacoust., Vol. AU-16, pp. 336-342, September 1968.
10. Helms, H.D., "Fast Fourier Transform Method of Computing Difference Equations and Simulating Filters," IEEE Trans. Audio Electroacoust., Vol. AU-15, pp. 85-90, June 1967.
11. Gold, B. and Rader, C.M., "Digital Processing of Signals," New York: McGraw-Hill, 1969.
12. Herrmann, O., "Design of Nonrecursive Digital Filters with Linear Phase," Electronics Letters, Vol. 6, p. 328, 1970.
13. Parks, T.W. and McClellan, J.H., "A Program for The Design of Linear Phase Finite Impulse Response Filters," IEEE Trans. Audio Electroacoust., Vol. AU-20, pp. 195-199, August 1972.
14. IEEE Special issues on Digital Filtering, IEEE Trans. Audio Electroacoust., Vols. AU-16, September 1968 and AU-18, June 1970.

#### BIBLIOGRAPHY (Continued)

15. Carslaw, H.S., "Introduction to The Theory of Fourier's Series and Integrals," Dover Publications, Inc., 1930.
16. Edwards, R.E., "Fourier Series," Holt, Rinehard and Winston, Inc., New York, 1967.
17. Guillemin, E.A., "Theory of Linear Physical Systems," John Wiley and Sons, Inc., New York, 1963.
18. Bogner, R.E. and Constantinides, A.G., "Introduction to Digital Filtering," New York: John Wiley and Sons, 1975.
19. Potter, R.W., "Compilation of Time Windows and Line Shapes for Fourier Analysis," Hewlett Packard.
20. Oppenheim, A.V. and Schaffer, R.W., "Digital Signal Processing," New Jersey, Prentice-Hall, 1975.
21. Ragazzini, J.R. and Franklin, G.F., "Sampled Data Control Systems," New York: McGraw-Hill, 1958.
22. Saucedo, R. and Schiring, E.E., "Introduction to Continuous and Digital Control Systems," New York, Macmillan, 1958.
23. Constantinides, A.G., "Spectral Transformations for Digital Filters," Proc. IEE, Vol. 117, p. 1585, 1970.
24. Kuo, B.C., "Analysis and Synthesis of Sampled-Data Control Systems," Englewood Cliffs, N.J.: Prentice-Hall, 1963.
25. Smith, C.L., "Digital Computer Process Control," London, Intext Educational Publishers, 1972.
26. Rabiner, L.R. and Rader, C.M., "Digital Signal Processing," IEEE Press, 1972.
27. Chen, C.F. and Shieh, L.S., "An Algebraic Method for Control System Design," Int. J. Control, Vol. 11, pp. 717-739, 1970.
28. Chen, C.F. and Tsay, U.T., "A General Frequency Stability Criterion for Multi-Input-Output, Lumped-and Distributed-Parameter Feedback Systems," to be published in Int. J. Control, 1975.

DISTRIBUTION

	<u>No. of Copies</u>
Defense Documentation Center Cameron Station Alexandria, Virginia 22314	12
Commander US Army Materiel Development and Readiness Command Attn: DRCRD DRCDL 5001 Eisenhower Avenue Alexandria, Virginia 22333	1 1
DRSMI-FR, Mr. Strickland	1
-LP, Mr. Voigt	1
-R, Dr. McDaniel	1
Dr. Kobler	1
-RG, Mr. Huff	1
-RGC, Mr. Griffith	1
-RGT, Mr. Leonard	15
-RBD	3
-RPR (Reference Set)	1
(Record Set)	1